STRUCTURAL AND CATALYTIC PROPERTIES OF DNA/RNA-HEME COMPLEXES

by

Lester Chi-Heng Poon
B.Sc., University of British Columbia 2008

THESIS
SUBMITTED IN PARTIAL FULFILLMENT OF
THE REQUIREMENTS FOR THE DEGREE OF

MASTER OF SCIENCE

In the
Department of Molecular Biology and Biochemistry

SIMON FRASER UNIVERSITY

Summer 2011

Approval

Name: **Lester Chi-Heng Poon**

Degree: **Master of Science**

Title of Thesis: **Structural and catalytic properties of DNA/RNA-heme complexes**

Examining Committee:

Chair: **Dr. Mark Brockman**
Associate Professor of Molecular Biology and Biochemistry, SFU

_____

Dr. Dipankar Sen
Senior Supervisor
Professor of Molecular Biology and Biochemistry, SFU

_____

Dr. Lisa Craig
Supervisor
Associate Professor of Molecular Biology and Biochemistry, SFU

_____

Dr. Erika Plettner
Supervisor
Associate Professor of Chemistry, SFU

_____

Dr. Peter Unrau
Internal Examiner
Associate Professor of Molecular Biology and Biochemistry, SFU

Date Defended/Approved: 26 May 2011

Declaration of
Partial Copyright Licence

Abstract

DNA and RNA G-quadruplexes have been shown to catalyze 1-electron oxidation reactions when bound to heme. In this work, we set out to explore the fundamental nature of G-quadruplexes that allow for heme binding, and the potential of nucleoheme complexes in catalyzing other heme-related enzymatic reactions. A combination of spectroscopic and gel-based tools was used to observe structural features of nucleoheme complexes. We determined that the *in vitro* selected heme apatamer, PS2.M, is highly polymorphic and predominantly parallel-stranded. The ability of many parallel G-quadruplexes to bind heme and perform peroxidase reactions led us to believe that some nucleoheme complexes may be capable of catalyzing oxygen transfer or 2-electron oxidation reactions. By using gas chromatography and high performance liquid chromatography analysis, we determined that nucleoheme complexes were capable of oxidizing electron-rich substrates: thioanisole, indole, and styrene. This discovery has expanded our understanding of the catalytic repertoire of nucleic acids, which leads to questions about the consequences and potential of this catalytic ability.

Keywords: Guanine (G)-quadruplex; Heme; Oxidation reaction; DNAzyme; Ribozyme

To my loving family and Iris for your unflinching support. I will always be grateful for all the sacrifices all of you have made. To Nancy, Lucy and Sammy for being the greatest piggies a person could ever want.

Acknowledgements

I would like to express my deepest gratitude to Dr. Dipankar Sen for his support, guidance, and inspiration over the years. I thank my supervisory committee members, Dr. Lisa Craig and Dr. Erika Plettner for their advice and valuable insight. I thank Dr. Peter Unrau for being my internal examiner and for his well-timed humour. I thank Dr. Mark Brockman for taking the time from his busy schedule to chair my defence.

I would like to express my special gratitude to all past, present, and honoury members of the Sen laboratory. I shall always be grateful for your friendship.

I would like to thank all members of the CTEF group for their help and friendship throughout the years. I would like to specifically thank Dr. Neil Branda and Dr. Byron Gates for their mentorship. I owe a substantial portion of my research to the CTEF group.

I would like to thank Dr. Andrew Bennet and Dr. Frédéric Pio for their helpful collaborations. I wish to thank Dr. Regine Gries and Hongwen Chen for their time and expertise. I would also like to extend thanks to the laboratories of Dr. Gerhard Gries, Dr. Robert Britton and Dr. Robert Young.

Special thanks to friends and staff in the MBB and Chemistry departments for the helpful hallway discussions and their support.

Finally, I would like to thank my family for their committment, support and patience.

Table of Contents

List of Figures

List of Tables

List of Abbreviations

A	Adenosine
ABTS	2,2’-azinobis(3-ethylbenzothiozoline)-6-sulfonic acid
ATP	Adenosine triphosphate
bp	Base pair
C	Cytidine
CD	Circular dichroism
Cs	Cesium
DMF	Dimethyl formamide
DMS	Dimethylsulfate
DMSO	Dimethylsulfoxide
DNA	Deoxyribonucleic acid
ds (prefix)	Double stranded
EDTA	Ethylenediaminetetraacetate
Fe	Iron
FID	Flame ionization detector
G	Guanine
GC	Gas chromatography
H-bonding	Hydrogen-bonding
HEPES	4-(2-hydroxyethyl)-1-piperazineethanesulfonic acid

HPLC	High performance liquid chromatography
KCl	Potassium chloride
LC	Liquid chromatography
Li	Lithium
MS	Mass spectrometer
NaCl	Sodium chloride
NH_4OH	Ammonium hydroxide
NMM	N-methyl mesoporphrin IX
OAc	Acetate
P450	Cytochrome P450 monooxygenase
r (prefix)	RNA
RNA	Ribonucleic acid
SELEX	Systematic evolution of ligands by exponential enrichment
T	Thymidine
TE	Tris-EDTA
TEMED	Tetramethylethylenediamine
Tris	Tris(hydroxymethyl)aminomethane
UV	Ultraviolet

1: Introduction

1.1 Nucleic acids

In the age of genomics, sometimes it is easy to forget that the complexities of genetics are the result of a simple code composed of four chemical building blocks. Prior to the understanding that nucleic acids, specifically deoxyribonucleic acids (DNA), were responsible for housing genetic information, it was thought that nucleic acids were too chemically simple to serve as genetic material. Since the chemical diversity of nucleic acids derives from only a few canonical nitrogenous bases, it was postulated that protein was the polymer that stored genetic information [1]. Proteins in contrast to nucleic acids contain a wealth of chemical functionalities which allow proteins to be efficient catalysts, but would this complexity make protein the ideal carrier of genetic material?

The extensive amount of functionalities that proteins provide makes them an ideal building block for enzyme creation. Despite the diversity of functionalities that proteins exhibit, they lack the key chemical stability and simplicity seen in nucleic acids. DNA is an ideal chemical vessel to house the genetic code because it is chemically stable and has only four different building blocks, which make DNA much simpler to replicate with high fidelity and high frequency.

The fact that DNA was the biopolymer that stored genetic information was not always evident. Individuals in the scientific community believed that the genetic code was fabricated by amino acids until the Avery–MacLeod–McCarty experiment. In the

late 1930's and early 1940's, it was discovered that bacterial virulence was able to be transferred from one strain of bacteria to another [2]. Avery and colleagues took this discovery a step further and attempted to discover the biopolymer that was responsible for the transformation; thus, this would also show the identity of the biopolymer responsible for containing the genetic code. Through careful purification and preparation, Avery and colleagues were able to separate DNA from the other contents of the bacteria. They found that the DNA alone from infectious strains of bacteria was capable of transforming non-infectious bacterial strains to infectious bacterial strains [3].

1.1.1 Fundamentals of guanine-quadruplexes

Around this time, there was a lot of momentum building for research in the field of nucleic acids, as the structure of double stranded DNA was recently determined to be a right-handed double helix [4]. The discovery of the DNA double helix was a major milestone in science, specifically for nucleic acids research. The structural determination of DNA has not only inspired researchers, but has permeated the public consciousness. As a result, when we think about DNA, we typically think about the B-type helix of DNA and none of the other secondary and tertiary structures that DNA also forms. However, as the field of molecular biology matured, there has been an increased interest in the minute structural fluctuations along the double helix and the other structures formed by nucleic acids.

Recently, a bright light has been shone on one specific DNA formation known as telomeres. The 2009 Nobel Prize in Physiology or Medicine was awarded to Dr. Elizabeth Blackburn, Dr. Carol Greider, and Dr. Jack Szostak for their discovery and characterization of telomeres and telomerase, the enzyme that adds the telomeric

sequence to the ends of chromosomes [5]. Telomeres are structures that serve as the caps at the ends of the chromosomes that keep the integrity of the chromosomes intact [6]. Telomeres have also been associated with the aging process and the longevity of cells [7]. The length of the telomere shortens with each successive cell division, acting like an internal clock for the cell [7]. Shortening of the telomeres to a critical length results in cell death [7]. The sequence of the telomeres from different organisms have shown a large abundance of guanines, which has major implications on the folding of the secondary structure of the telomeric ends [6]. These higher ordered structures are thought to be guanine-quadruplexes (G-quadruplexes), as determined by *in vitro* studies [8, 9].

More recently, non-telomeric sequences that may form G-quadruplexes have been of increasing interest for researchers [10, 11]. Huppert and Balasubramanian showed that there are close to 400,000 putative G-quadruplex sequences in the human genome, which is roughly 1 in every 10,000 bases [12]. The prevalence of possible G-quadruplex-forming sequences is even more striking in promoter regions of the human genome, with over 40% of promoter regions containing sequences that could form G-quadruplexes [10]. In addition, some of the promoters that have been postulated to contain putative G-quadruplex sequences have also been identified to control the expression of proto-oncogenes, like the promoter of *c-MYC* and *BCL-2* [13]. Hurley and colleagues suppressed the expression of *c-MYC* with a known G-quadruplex-stabilizing porphyrin-derivative, 5,10,15,20-tetrakis(*N*-methyl-4-pyridyl)-porphyrin [13]. These results by Hurley and colleagues have ignited interest in developing therapeutics for cancer treatment with compounds that interact with G-quadruplexes [11].

The G-quadruplex is a structure formed by multiple guanine-quartets (G-quartets). Gellert et al. used crystallographic methods to demonstrate that guanosine monophosphate monomers were capable of self assembly to form a tetrameric arrangement that they called G-quartets, depicted in Figure 1.1 [14]. There have been a variety of techniques used to detect and analyze G-quadruplexes, ranging from circular dichroism, infrared, and nuclear magnetic resonance spectroscopy to X-ray fiber and crystal diffraction studies [15-18].

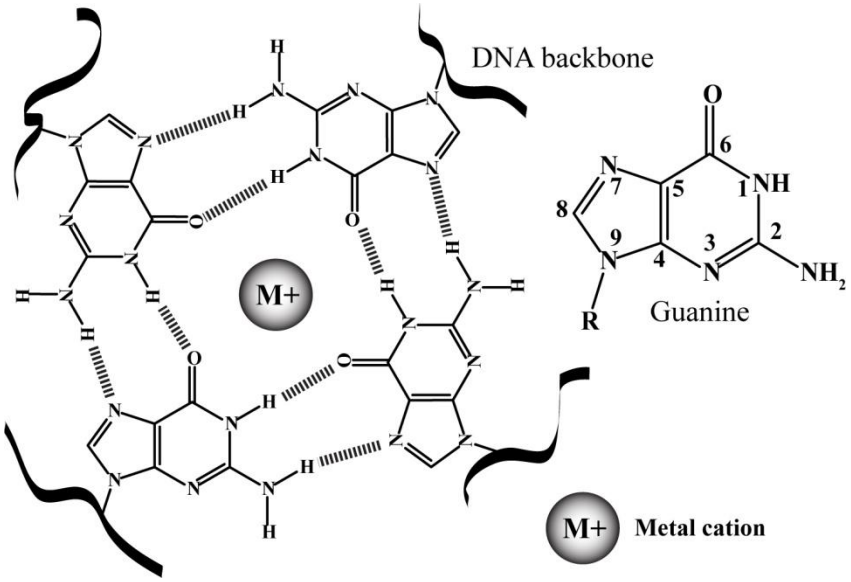

Figure 1.1: The key stabilizing and bonding features of a guanine-quartet.

1.1.2 Factors that stabilize G-quadruplexes

The factors that stabilize G-quadruplexes are similar to those that stabilize DNA duplexes, such as base stacking and hydrogen bonding (H-bonding). A G-quadruplex is a highly stable structure formed from multiple G-quartets stacked upon each other. The "stacking force" that is vital in both duplex and quadruplex formation is a summation of several forces. Since the bases of nucleic acids are non-polar entities, they will self-associate to limit their interaction with water. The stability of the association of nuclear

bases with each other is the result of hydrophobic, electrostatic, and van der Waals forces [19, 20].

Not unlike the stacking observed between adjacent bases in DNA duplexes, the geometry of G-quartet stacks are heterogeneous along the length of the G-quadruplex [21]. The G-quartets at the two ends of the quadruplex exhibit the greatest degree of geometric heterogeneity as compared to the uniform quartets in the middle of the G-quadruplex. The linker regions, the nucleotides between the tracts of guanines involved in G-quartet formation, restrict the position of the guanosines which causes the G-quartets at both ends of the stacks to tilt from the core of the G-quadruplex. As a result; the linkers between guanine tracts play an important role in determining the positioning of the G-quartets [21]. In addition, the G-quartets at the core of the quadruplex tend to be more planar and are less heterogeneous [21].

Within the G-quartets are four guanines Hoogsteen hydrogen (H)-bonded to each other, as depicted in Figure 1.1 [22]. This involves the N1 position acting as a hydrogen bond donor to the exocyclic oxygen at the sixth position of the adjacent guanine in the quartet. Also, the exocyclic amino group at the C2 position acts as a hydrogen bond donor to the nitrogen at the seventh position of the adjacent base. Since these interactions repeat around the quartet, there is a total of eight H-bonds. The eight H-bonds between four guanines give greater stability than the three H-bonds between a guanine-cytosine base pair, as there are 2 H-bonds per base in a G-quartet compared to 1.5 H-bonds per base in a GC base pair.

Aside from the number of H-bonds per base between a duplex and quadruplex, the individual H-bonds between these two motifs are different. Each H-bond in a G-

quadruplex is about double the energy of an H-bond in a duplex [23]. Simulation studies showed that a guanine-guanine paired through Hoogsteen H-bonding causes a redistribution of electron density that strengthens additional H-bonds [23]. This cooperative behavior of H-bonding is called resonance-assisted hydrogen-bonding [23].

This energy of bonding is further increased with the addition of metal cations in the centre of the G-quartet [15]. Since the G-quartet brings several oxygen atoms within close proximity of each other, a cation is needed to stabilize the electronically unfavourable cyclic arrangement of oxygens through cation-dipole interactions between the cation and the C6 exocyclic oxygen atoms of guanines [24]. The cations can be either monovalent or divalent; the stability of the G-quadruplex due to cation interactions is dependent on the radii of the ion and its hydration sphere [25]. As a result, lithium (Li^+) is too small and cesium (Cs^+) is too large to stabilize the negative polarity at the core of a G-quadruplex [24]. The two most studied cations for G-quadruplex stabilization are potassium (K^+) and sodium (Na^+) ions because they tend to cause the greatest stability in G-quadruplexes [25].

As depicted in Figure 1.2, the K^+ ions are larger than the Na^+ ions and fit in between two G-quartets, while Na^+ ions fit much closer to the plane of a G-quartet. K^+ ions have been experimentally demonstrated to have a greater stabilizing effect on G-quadruplexes than Na^+ ions. The stability that K^+ ions afford G-quadruplexes as compared to Na^+ ions can be seen in the difference in melting temperature between K^+ and Na^+ stabilized G-quadruplexes, 8ºC for the oligomer derived from the human telomeric sequence and 30ºC for the thrombin aptamer [26]. This higher stability afforded by K^+ ions is primarily driven by the relative ease of dehydrating K^+ ions as

compared to Na^+ ions [27]. The combination of H-bonding, base stacking and cation interactions help guanine-rich DNA and RNA form stable G-quadruplex structures.

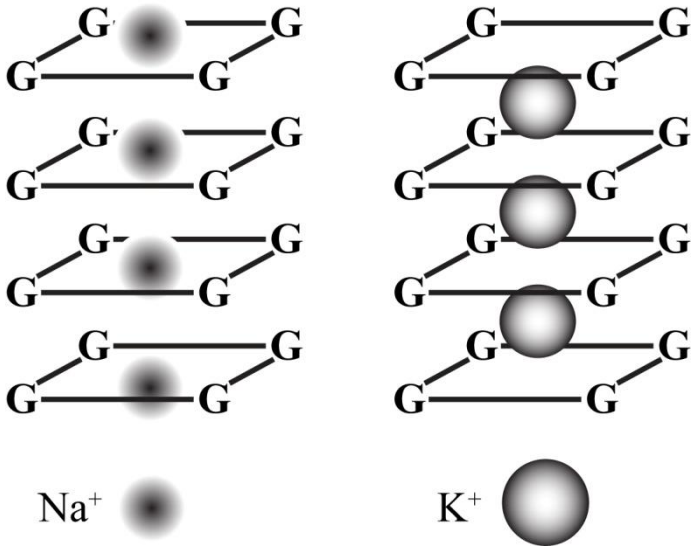

Figure 1.2: Cation localization within a guanine-quadruplex.

1.2 Peroxidases and monooxygenases: enzymes that catalyze oxidation reactions

Heme is a ubiquitous cofactor found in enzymes that have a wide variety of functions. Heme-enzymes have abilities ranging from diatomic gas sensing to reduction-oxidation reactions. The heme-enzymes that perform reduction-oxidation reactions are some of the most widely studied and characterized enzymes [28]. Even within this group of enzymes that perform redox reactions there are multiple subgroups that span a wide range of oxidative functions. However, despite the wealth of knowledge accumulated for these enzymes, there are still many unresolved mysteries. Two closely related groups of heme-containing enzymes are the peroxidases, which perform 1-electron oxidation reactions and the monooxygenases, which perform 2-electron oxidations [29]. The 1-electron oxidation reactions involve a single electron abstraction from the reducing substrate, while the 2-electron oxidation reactions involve an oxygen atom insertion into the substrate.

Even though there is a difference of oxidative power between the two groups of oxidative enzymes, the reactive intermediate with a high oxidation-potential for both groups of enzymes is the same. The famed Compound I intermediate is believed to be the reactive species for both peroxidases and monooxygenases. At the heart of peroxidases and monooxygenases lies a heme cofactor, protoporphyrin IX containing ferric iron (3+ oxidation state). Ferric heme is oxidized by peroxides in the case of peroxidases and by molecular oxygen in the case of monoxygenases, to a higher oxidized species called Compound I. In the case of P450 monooxygenases, several accessory proteins are needed to transfer electrons to aid in the formation of Compound I. As depicted in Figure 1.3, first there is an 1-electron reduction of Fe(III) heme to Fe(II)

heme that allows for dioxygen association. After the association of dioxygen with ferrous heme an additional electron is transferred to the dioxygen-heme complex to allow for heterolytic cleavage to take place.

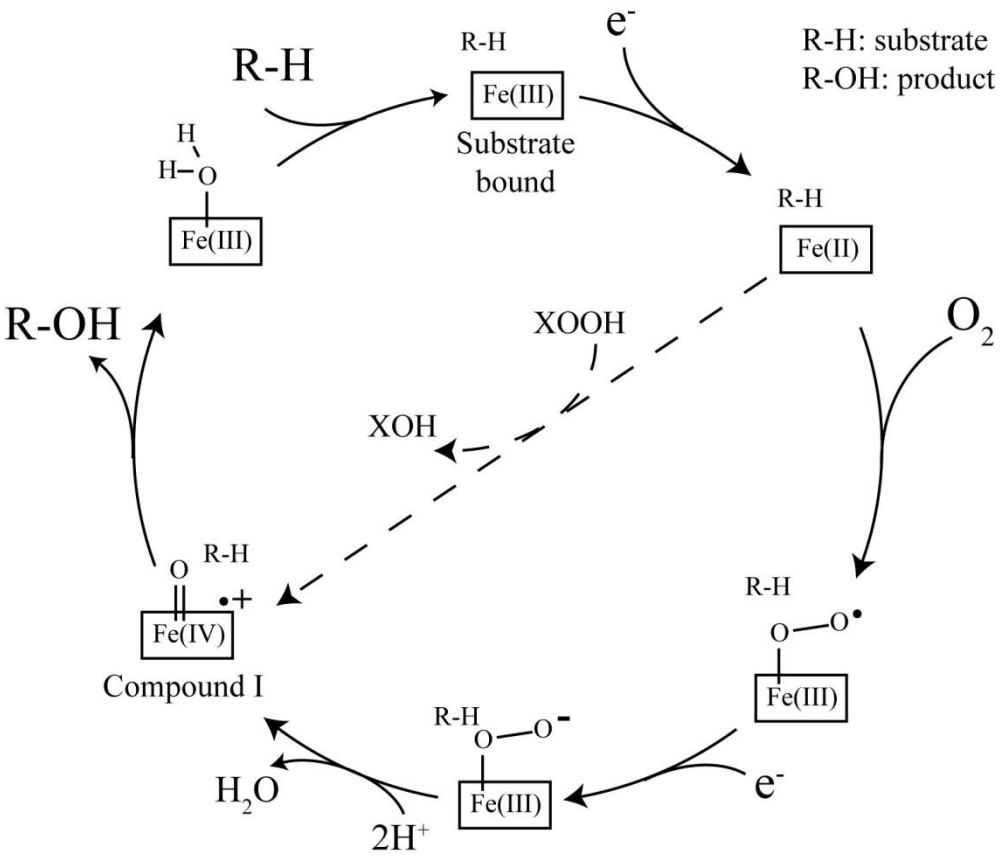

Figure 1.3: The catalytic cycle of cytochrome P450 monooxygenase.
This diagram shows the flow of electrons and protons in the P450 cycle. The initial binding of the reducing substrate to the enzyme initiates the first electron donation to the Fe(II) heme molecule to form Fe(III) heme. The dashed line depicts the peroxide shunt pathway, which uses peroxides as the oxidant to generate Compound I; thus, bypassing the need for the donation of electrons from accessory proteins. Adapted from Mansuy and Renaud [30].

However, P450s are also capable of using peroxides as the oxidant to form Compound I (peroxide shunt pathway); thus, bypassing the need for 2-electron reducing equivalents provided by the accessory proteins. The use this peroxide shunt pathway

allows researchers to study the activated Compound I species of P450 monooxygenases and their ability to catalyze oxidation reactions without the need for accessory proteins. This activated oxo-iron species contains an iron with a formal oxidation state of +5. However, an electron is donated from the porphyrin to form Fe(IV) with a radical cation delocalized on the porphyrin or in the case of cytochrome *c* peroxidase, an oxidized equivalent is located on an amino acid residue (tyrosine) of the apoprotein.

As previously stated, the natural substrates, or the known compounds that the enzymes encounter in their native systems, used as an oxidant to form Compound I for peroxidases and monooxygenases are chemically different. However, some P450 enzymes found in *Sphingomonas paucimobilis* and *Bacillus subtilis*, have been discovered that primarily use hydrogen peroxide as the oxidizing agent to form Compound I [31]. These P450 enzymes have thus been termed peroxygenases instead of monooxygenases. In addition to these natural peroxygenases, natural monooxygenases, such as cytochrome P450s, are capable of using peroxides as an oxygen donor to form Compound I. However, for monooxygenases the use of peroxides as the heme oxidant is a slower process than activation by dioxygen. Once Compound I is formed, monooxygenases catalyze oxygen transfer (2-electron oxidation) reactions, such as the hydroxylation of camphor, and monooxygenases are also capable of 1-electron oxidation reactions.

This array of oxidative activity is not limited to monooxygenases, as peroxidases that naturally catalyze 1-electron oxidation reactions are also capable of performing other oxidative catalysis. There are peroxidases that perform 2-electron oxidations as their primary function in nature, such as chloroperoxidases that oxidize chloride to

hypochlorous acid [28, 29]. However, the majority of peroxidases do not perform oxygen transfer reactions as their primary function. Instead, most peroxidases can be fed with specific non-natural, electron rich substrates to force oxygen transfer to take place. These non-natural substrates are compounds that the enzyme does not encounter in nature. These reactions require electron-rich substrates, and proceed slower than if they were catalyzed by the oxidatively more powerful monooxygenases, horseradish peroxidase oxidizes styrene 200 times slower than P450s [32].

Once activated by hydrogen peroxide to form Compound I, peroxidases are capable of inserting oxygen from hydrogen peroxide through the oxo-iron heme intermediate to the substrate. These substrates are electron rich, such as styrene, as compared to the substrates that monooxygenases are capable of oxidizing, such as camphor [28, 29]. Even though substrates for most 2-electron oxidation reactions are not the natural substrate for peroxidases, peroxidases still show a certain degree of specificity towards these non-natural substrates [28, 29]. The natural substrates/reactions are those that the enzyme catalyzes in nature. This means that not all peroxidases can perform the same oxygen transfer reactions to the same substrates, and that the peroxidases that catalyze the 2-electron oxidation of the same substrate may not produce the same products. The ability to differentiate between substrates is largely attributed to the active site of the peroxidase.

1.2.1 Key structural differences between peroxidases and monooxygenases that lead to different mechanisms of Compound I formation

Detailed analyses of crystal structures from peroxidases and P450s have shed light on some key structural differences that affect the catalysis performed by peroxidases

and monooxygenases. There are two sides in the active site of heme-enzymes, the proximal and distal sites, which is separated by the heme molecule. The distal site is where the reducing substrate and the oxidant come in contact with the heme molecule. The proximal site houses an axial ligand that coordinates the iron of the heme molecule.

The obvious difference between classical peroxidases and classical monooxygenases is the proximal ligand that coordinates the iron atom of the heme molecule. The proximal ligand or the fifth ligand of classical peroxidases is a histidine, whereas P450 enzymes contain a cysteine. The cysteine side chain contains a thiol functionality that is electron rich. As compared to the nitrogen in histidine, the thiol moiety is more capable of providing electron density to the iron atom in heme; therefore, the thiol has a stronger electron "push" effect.

The push effect is important in the cleavage of the bond between the oxygen atoms in the hydrogen peroxide molecule. The rate of hydrogen peroxide cleavage was reduced 5 orders of magnitude when the proximal histidine was mutated to leucine in cytochrome *c* peroxidase [33]. To further aid in the heterolytic cleavage of hydrogen peroxide, a proton is delivered to the terminal oxygen to "pull" apart the peroxide bond by creating a better leaving group. As depicted in Figure 1.4, the pull-push effect helps peroxidases to form the reactive oxo-iron species, Compound I [34].

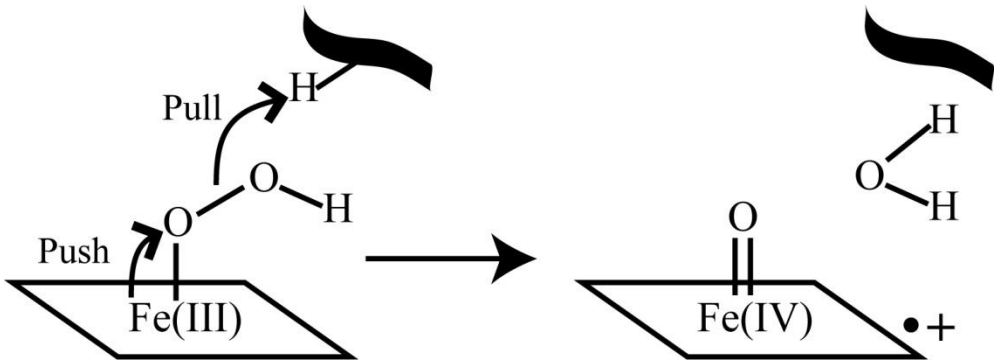

Figure 1.4: The pull-push effect in the heterolytic cleavage of the O-O bond.

The difference in electron density between the thiol sulfur and the imidazole nitrogen affects the electron distribution on the heme molecule; therefore, this would affect the formation and reactivity of Compound I [35]. Adachi and co-workers have performed mutagenesis of the proximal histidine residue in myoglobin to cysteine [36]. The resulting protein had a reduction potential of -200 mV, as compared to +50 mV for the histidine containing protein.

Even though there is a general difference between the fifth ligand in classical peroxidases compared to classical P450 monooxygenases, there is a peroxidase that contains a cysteine as the axial ligand, chloroperoxidase. As stated before, chloroperoxidase is a heme-enzyme that uses hydrogen peroxide as an oxygen donor and performs both 1- and 2-electron oxidations. The ability to perform 2-electron oxidations has been attributed to the thiolate ligand, possessed by both P450 monooxygenases and chloroperoxidases. However, it has been demonstrated that the axial ligand cysteine can be changed to histidine while still keeping most of the capabilities of chloroperoxidase intact [37].

The interchangeability of the axial ligand between histidine and cysteine suggests that the only requirement for the proximal ligand is an electron rich functionality and that the ligand's identity may not be as important. This further suggests that the proximal environment of the heme molecule in heme-enzymes may not be the ultimate determining factor for the degree of substrate oxidation and the type of substrates accepted by the enzyme. As a result, several groups propose that the distal pocket may contain residues that are responsible for the selectivity of the enzyme for both the reducing and oxidizing substrate.

The importance of several distal residues is evident as they are necessary for the heterolytic cleavage of hydrogen peroxide. As depicted in Figure 1.5, a histidine residue in the distal cavity of the active site acts as a general acid-base catalyst that protonates the terminal oxygen of the heme-peroxide species to promote heterolytic cleavage of the peroxide bond [29]. This residue is highly conserved in classical peroxidases [38]. In the case of chloroperoxidases, the histidine residue is replaced by a glutamate residue and plays a similar role as an acid-base catalyst [39].

Another key player in the distal pocket is an arginine side chain that is situated right above the plane of the heme cofactor. The arginine residue has been proposed to help assist in the formation of Compound I by stabilizing the negative charge build-up on the leaving oxygen group during heterolytic cleavage [40]. When the arginine residue was mutated to a leucine residue, the catalytic rate for the heterolytic cleavage of hydrogen peroxide was reduced by 55-fold. In contrast, P450 monooxygenases lack the distal machinery of classical peroxidases; as a result, P450s are much less efficient in catalyzing the heterolytic cleavage of hydrogen peroxide to form Compound I [41].

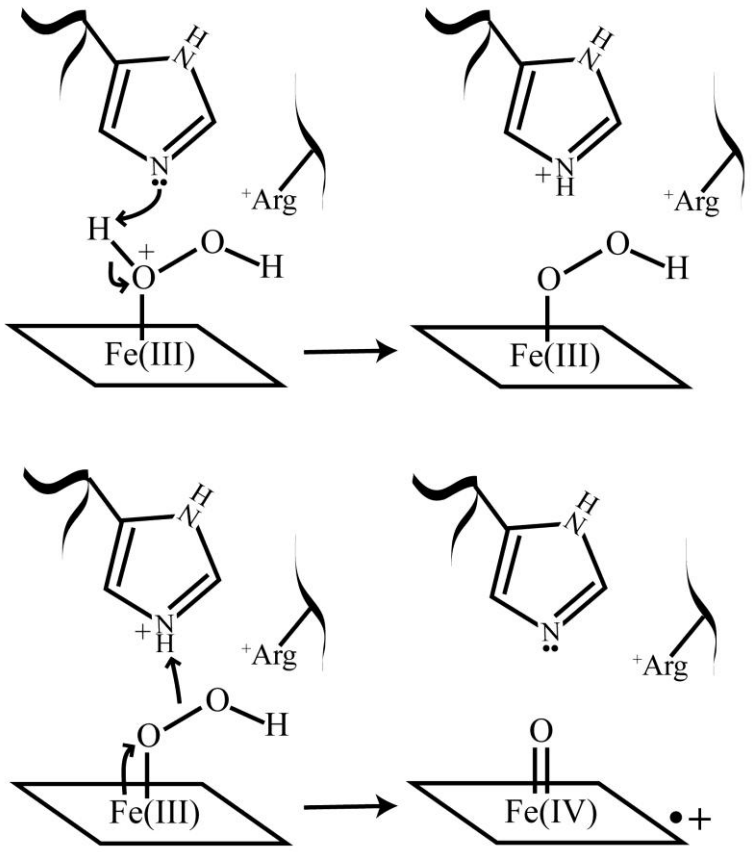

Figure 1.5: The classical peroxidase mechanism of Compound I formation by heterolytic cleavage of hydrogen peroxide inside the active site of peroxidases, such as horseradish peroxidase or cytochrome *c* peroxidase.

The distal cavity of P450 enzymes is more hydrophobic than the distal cavity of peroxidases. However, there is a need for hydrogen donors in the distal cavity of cytochrome P450 monooxygenases. Not unlike the heterolytic cleavage of hydrogen peroxide, the cleavage of dioxygen by cytochrome P450 monooxygenases to form Compound I involves protonating the oxygen leaving group. In monooxygenases, there is no obvious amino acid residue candidate in the distal cavity that would act as the general acid.

Two conserved residues in the active site are thought to play a crucial role in protonating the oxygen leaving group. Through mutation studies, a distal threonine has

been suggested to either directly protonate the leaving group or indirectly protonate the leaving group through a relay of ordered water molecules between a conserved threonine and a glutamic acid residue [42]. Furthermore, Gerber and Sligar proposed that an aspartic acid is important for leaving group protonation by shuttling a hydrogen in the ordered water molecule network [43]. The mutation of the aspartic acid residue to an asparagine residue decreases the rate of catalysis by an order of magnitude.

The data obtained from X-ray crystal structures shows only one hydrophilic residue, a threonine, in the distal cavity of P450 camphor monoxygenases ($P450_{cam}$) that is within 5 Å of the heme molecule. However, to complicate matters some P450s have an alanine in place of the threonine. Much of the problem stems from the static nature of the structures obtained from X-ray crystal structures. The active site of P450 monooxygenases and peroxygenases is more flexible than classical peroxidases; therefore, the binding of both oxidants and reductants causes slight changes in the structure of P450 enzymes.

For instance, when $P450_{cam}$ crystals are soaked in adamantane, a poor substrate, for an extended period of time, the helix that contains the threonine residue is shifted 1.1 Å away from the oxygen binding site. This movement is most likely a result of accommodating a water molecule in the position of the threonine. The mutation of the threonine residue to an alanine causes a similar distortion of the helix and a water molecule takes the place of threonine [44]. However, this change eliminates the control that the threonine residue imposed on the entry and positioning of the water molecule. The threonine to alanine mutant causes a slower Compound I formation and the reduction of the ferryl oxygen to form water and hydrogen peroxide.

Most of these observations are from studies of cytochrome $P450_{cam}$, but crystal structures of several other P450 enzymes show that few cytochromes P450 share exactly the same residues in the distal active site [45]. P450s are very numerous in nature and accept a wide range of substrates; therefore, the differences in distal site residues between P450s are required to accommodate the different preferred substrates. Even though the exact residues involved in Compound I formation may be different between P450s, it remains necessary that the different P450s need to protonate the distal oxygen of the dioxygen-heme complex to form a better leaving group.

1.2.2 Key structural differences between peroxidases and monoxygenases that lead to 1- or 2-electron oxidation

Despite the differences in active site residues between peroxidases and monooxygenases/peroxygenases, both sets of enzymes arrive at a common reactive intermediate called Compound I. Despite the formation of a similar reactive species, peroxidases and monooxygenases/peroxygenases perform two distinct oxidative reactions. Monoxygenases and peroxygenases perform 2-electron oxidation reactions by inserting an oxygen atom into a substrate, while classical peroxidases perform 1-electron oxidation reactions by abstracting a single electron from the substrate to create a radical species.

Despite the differences in the natural reactions that peroxidases and monooxygenases perform on their natural substrates, there is functional overlap between these two groups of enzymes. Peroxidases are capable of performing some 2-electron oxidation reactions, while monooxygenases and peroxygenases are capable of performing some 1-electron oxidation reactions [28, 29]. Even though these oxidative enzymes have

the capability to perform a spectrum of oxidation reactions, they are most efficient at catalyzing their respective "natural" reactions and perform other oxidative reactions much less efficiently [28, 29].

As previously stated, both the 1- and 2-electron oxidations of substrates require the formation of the reactive Compound I species. One of the major differences between these two sets of enzymes is the mechanism of Compound I formation: peroxidases and peroxygenases use hydrogen peroxide as the oxidant, while monooxygenases use molecular oxygen as the oxidant. However, once Compound I is formed, the oxidized heme species does not distinguish between substrates for 1- or 2-electron oxidation reactions. So why and how do peroxidases and monooxygenases perform two different oxidation reactions? This is a very intriguing question and the answer was at first not obvious to researchers.

Peroxidases have difficulty in performing 2-electron oxidations that result in direct oxygen insertion into the substrate because the active site of peroxidases poses a steric problem. Figure 1.6 illustrates the main difference between the active sites of peroxidases and cytochromes P450. For 2-electron oxidation reactions, P450 monooxygenases place the substrate directly above the ferryl oxygen of Compound I for oxygen atom insertion. In the case of 1-electron oxidations catalyzed by peroxidases, the substrate needs only to encounter the edge of the porphyrin ring system.

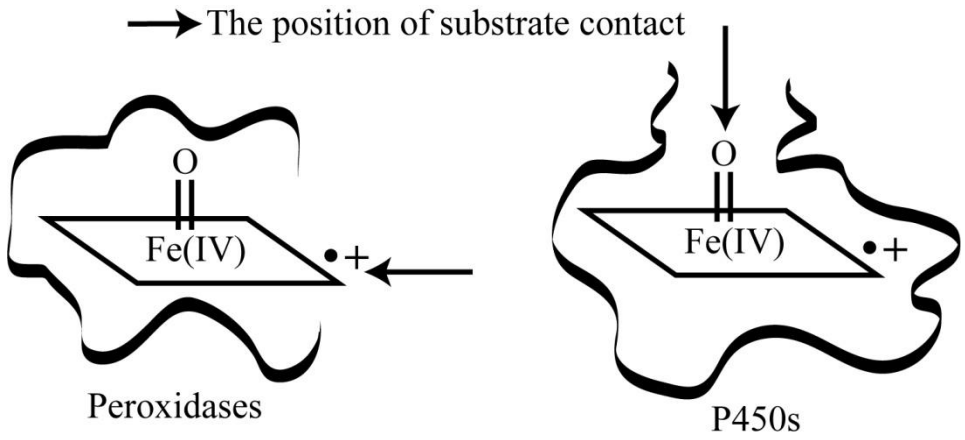

Figure 1.6: The different paths for substrate access to the heme cofactor in peroxidases and in P450s.
Adapted from Poulos' review [45]

The requirement for the substrate to come in contact with Compound I in a certain position is not obvious from the crystal structures of different peroxidases and monooxygenases. The structures determined by X-ray crystallography of $P450_{cam}$ do not show a clear channel between the exterior of the protein and the center of the heme cofactor [46]. When the substrate-bound and substrate-free crystal structures were compared to each other, there was almost no change in the overall structure of the enzyme [46]. As a result, it was thought to be unlikely that allosteric effects of the substrate binding controlled the channel for substrate entry.

As a result, researchers believe that the dynamic fluctuations of the active site residues of P450s are responsible for creating a substrate access tunnel. Evidence to support this claim stems from comparisons between the substrate-free and the substrate-bound crystal structures of $P450_{cam}$ that showed higher thermal motion in the residues that form the opening of the active site when the substrate is not bound [47]. A study using a large inhibitor to force the substrate access route to open demonstrated that

several phenylalanine and tyrosine residues change conformations to accommodate the long alkyl chain of the inhibitor [48].

The enzyme inhibitor structure does not provide direct evidence of a substrate access channel or the thermal motion of key residues that may form the substrate access channel. It has not been possible to obtain a crystal structure of cytochrome $P450_{cam}$ with an open substrate access channel. Fortunately for the research community, the crystal structure of cytochrome $P450_{BM-3}$, a fatty acid hydroxylase from *Bacillus megaterium*, does have a wide open substrate access channel [49]. As a result, $P450_{BM-3}$ presents the model monooxygenase for the substrate access channel between the solvent and the ferryl oxygen at the center of the heme molecule.

In contrast, classical peroxidases are believed to possess very restricted active sites that do not allow for direct substrate access to the ferryl oxygen. The heme cofactor is located near the surface of the protein and thus the edge of the heme is exposed to the solvent. These insights were induced from the crystal structures of peroxidases, such as the crystal structure of prostaglandin H (PGH) synthase [50]. In PGH synthase, the heme moiety is found near the surface of the protein and the edge of the heme is completely exposed to the solvent. It is actually very easy to dissociate the heme group from the enzyme during the purification process of PGH synthase [28, 29]. Even though the heme edge is exposed to the solvent, there are residues above the ferryl oxygen that restrict the direct access of reducing substrates.

Ortiz de Montellano's group has performed many chemical studies that provide further interesting insights into the solvent exposure of the heme cofactor [51]. Their results complement the crystal structures of peroxidases, such as the structure of PGH

synthase. Their studies demonstrated that in peroxidases, the substrate for 1-electron oxidations comes into contact with the heme edge; while in monooxygenases, the substrates come into contact with the center of the heme. Ortiz de Montellano's group cleverly employed suicide inhibitors to map the region where the substrate comes into contact with the heme cofactor [51]. The use of suicide inhibitors successfully accomplishes the mapping of the contact points between Compound I and the substrate by permanently attaching to the region of the heme molecule that is responsible for the oxidation of the suicide inhibitor. In classical peroxidases, the suicide inhibitor covalently attaches to the heme edge; while in monooxygenases, the suicide inhibitor covalently attaches to the nitrogen of the pyrrole rings at the center of the heme molecule [52, 53]. As depicted in Figure 1.7, the difference between the sites of modification for peroxidases and monooxygenases is assumed to be a reflection of the difference in the accessibility to the heme-oxo complex in these two classes of enzymes.

Additional reconstitution studies were performed to complement the suicide inhibitor studies. In these studies, peroxidases were reconstituted with modified heme cofactors [54]. The heme derivatives contained alkyl chains attached to the δ-*meso* edge of the porphyrin ring system. Another set of experiments involved reconstituting horseradish peroxidase with δ-*meso*-ethylheme. The researchers discovered that despite the heme-derivative reacting with hydrogen peroxide to form Compound I, the reactive heme intermediate did not oxidize substrates [54]. The additional ethyl group was thought to protrude from the side of the heme edge; thus, preventing the substrate from coming in close enough proximity to the heme ring system to allow for efficient charge transfer.

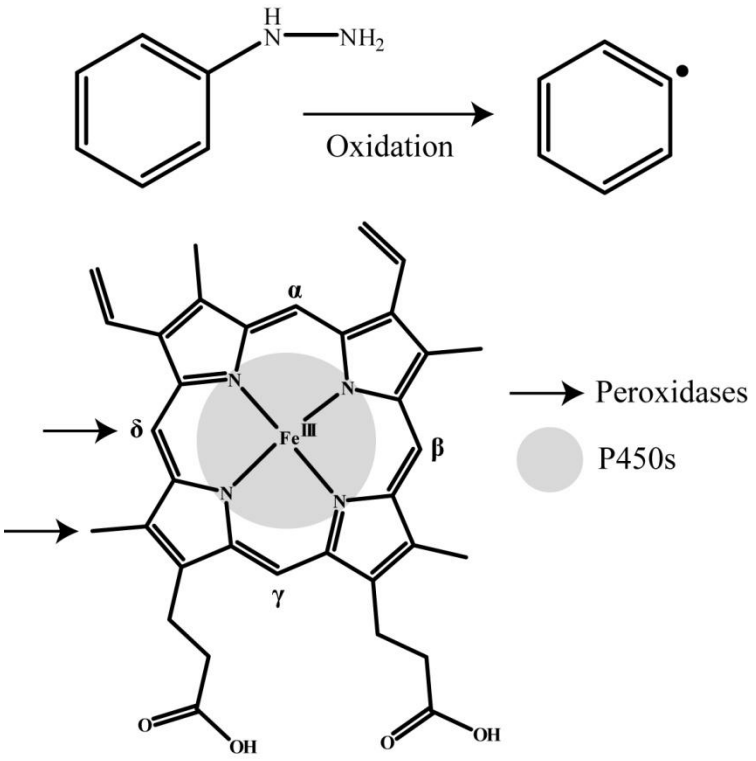

Figure 1.7: Probing the active site of peroxidases and P450s by using a suicide substrate to covalently attach to the heme molecule inside the enzyme.
The oxidation of phenylhydrazine by Compound I forms the highly reactive phenyl radical species. The areas in the heme molecule where the phenyl radical modifies are dependent on the accessibility of those positions to phenylhydrazine. The areas of phenyl addition are shown for peroxidases (arrows) and P450s (grey shaded area).

In addition, a complementary experiment was performed with horseradish peroxidase reconstituted with δ-*meso*-methylheme, which produced a catalytically active enzyme that oxidized substrates [54]. This study supported the idea that the hindrance of the oxidative capabilities of horseradish peroxidase was due to steric factors of the ethyl group and not its electronic properties. Therefore, from heme modification, heme-derivative reconstitution, and X-ray crystallography studies, researchers propose that oxidative substrates interact with monooxygenases at the iron-oxo heme center while these substrates interact with peroxidases at the edge of the heme cofactor.

The difficulty for peroxidases to transfer the ferryl oxygen to the substrate has been attributed to the restricted distal site above the oxygen atom of Compound I. Thus, substrates can only come into contact with the heme edge in classical peroxidases; as depicted in Figure 1.6. Mutational studies of peroxidases have demonstrated that the removal of amino acid residues with bulky side chains can enable or enhance the 2-electron oxidation capability of classical peroxidases. Miller *et al.* have demonstrated that by mutating the tryptophan residue in the distal cavity of the active site to an alanine residue, the mutant is capable of a larger array of 2-electron oxidation reactions [55]. The mutant cytochrome *c* peroxidase enzyme was shown to be even capable of catalyzing the epoxidation of styrene. More importantly, Miller *et al.* demonstrated that the epoxide oxygen atom was primarily derived from hydrogen peroxide, most likely *via* the Compound I species [55]. Similar results for horseradish peroxidase were obtained when the phenylalanine residue in the similar location as the tryptophan residue in cytochrome *c* peroxidase was mutated to a leucine residue [56].

Aside from the ability to perform 2-electron oxidations, the mutant peroxidases with enlarged distal cavities also catalyzed 1-electron oxidation reactions at a faster rate [55, 56]. This was also assumed to be the result of a less restricted access route to the heme cofactor. However, in the case of horseradish peroxidase, the mutation of the phenylalanine residue to a leucine residue also decreased the substrate specificity of the enzyme [56]. This example demonstrates the trade-off between the substrate specificity of the enzyme and the raw processing power of the enzyme.

1.2.3 Catalytic antibodies that perform peroxidase reactions

Aside from natural peroxidases and their derivatives, an intriguing class of non-natural protein enzymes can also perform peroxidase-like reactions. Catalytic antibodies or abzymes are antibodies that have catalytic properties. These enzymes were not naturally evolved to contain the same complex catalytic machinery as their natural enzyme counterparts. Instead, abzymes are produced from eliciting the humoral immune response to generate antibodies that specifically bind "transition state" analogue molecules [57]. Peter Schultz and colleagues pioneered the use of transition state mimics to generate numerous abzymes that catalyze a wide variety of chemistries [57]. One particular abzyme was found to be both a ferrochelatase-mimic and a peroxidase-mimic [58, 59].

Originally, the abzyme was specifically selected for its ability to bind a transition state analogue for the metallation of porphyrins. The transition state analogue, N-methyl mesoporphyrin, mimics the puckered geometry of the transition state of the porphryin molecule during the metallation process [58]. This ferrochelatase-mimic catalyzed the insertion of Zn(II) and Cu(II) into mesoporphyrin at comparable rates to the natural ferrochelatase [58]. Also, this group determined that Fe(III) mesoporphyrin was a potent inhibitor of the porphyrin metallation reaction [58].

The ability of this catalytic antibody to bind Fe(III) mesoporphyrin led to their subsequent studies of the peroxidase activity of the abzyme-Fe(III) mesoporphyrin complex [59]. This abzyme complex was capable of catalyzing several peroxidation reactions, including the oxidation of ABTS (2,2'-azinobis(3-ethylbenzothiozoline)-6-sulfonic acid) [59]. The studies of the peroxidative capabilities of abzymes demonstrated

that a protein, not naturally evolved to have the same machinery as a peroxidase, could catalyze peroxidase reactions and porphyrin metallation.

The work of Peter Schultz's group inspired our lab to pose similar questions about DNA/RNA. Specifically, if DNA/RNA molecules could be selected to bind a transition state analogue and if these DNA/RNA molecules could perform catalysis?

1.3 A guanine-rich aptamer with peroxidase activity when bound to heme

For several decades we have known that both RNA and DNA are capable of catalysis. Nature has provided several examples of enzymes composed primarily of RNA (ribozymes), while all DNA based enzymes (DNAzymes) have been artificially evolved in laboratories. The catalytic ability of both RNA and DNA is a topic of great interest because RNA is considered a key molecule in a hypothetical model used to explain the origin of life on Earth, known as the "RNA world" [60]. Walter Gilbert has described RNA as an ideal scaffold for the development of life, due to its powerful features of recombination and mutation [60].

Due to these theories, there has been a huge push to discover new ribozymes and DNAzymes either synthetically or naturally [61]. DNA is sometimes used as a surrogate for RNA because DNA is cheaper to synthesize and chemically more stable than RNA. Since DNA is also chemically similar to RNA, it is assumed that any catalysis performed by DNA is also possible for RNA. When comparing proteins to nucleic acids, it is evident that nucleic acids do not possess the same wealth of functional groups as proteins. Many see cofactors as a solution to this chemically complex problem; even in present day organisms, many protein enzymes use cofactors to boost their already vast chemical repertoire.

One such DNAzyme that performs catalysis when bound to a cofactor is PS2.M [62]. PS2.M is an artificial DNAzyme that was rationally designed from a parent sequence that was originally selected by using *SELEX* (Systematic Evolution of Ligands by Exponential Enrichment) [63]. This *in vitro* selection technique, *SELEX*, allows us to

condense Darwinian selection into a manageable amount of time, as depicted in Figure 1.8. Selection pressure is placed on a large initial pool of varying sequences of nucleic acids that form a variety of different shapes. It is assumed that there are molecules within this large pool that can perform the desired task. The sequences that survive the selection process are carried through to subsequent rounds and enriched. This iterative process is repeated until several dominant species of nucleic acids have taken over the initial pool. Using this approach the DNA molecules were selected for their ability to bind N-methyl mesoporphyrin (NMM), NMM is a transition state analogue for porphyrin metallation [63, 64]. Li *et al.* demonstrated that several sequences that they obtained from the *in vitro* selection process were indeed aptamers, a nucleic acid molecule that can specifically bind a ligand, for NMM [63]. Further studies by Li *et al.* demonstrated that clones PS2 and PS5 were capable of metallating porphyrins [64].

The parent oligonucleotides, PS2 and PS5, were truncated down to the minimal sequences that were needed for NMM binding as defined by foot printing and mapping studies [63]. These truncated species were also capable of metallating porphyrins, in the case of PS5.ST1, a truncated version of PS5, it enhanced the rate of porphyrin metallation over the uncatalyzed rate by 1400-fold [64]. Further modification of the shortened porphyrin metallating DNAzymes through rationale design produced two oligonucleotides, PS2.M, 18-nucleotides long and PS5.M, 24-nucleotides long [65]. These shortened DNAzymes were both superior porphyrin metallating catalysts than their parent sequences, PS5.M had a 37%-enhanced porphyrin metallating rate as compared to PS5.ST1 [62].

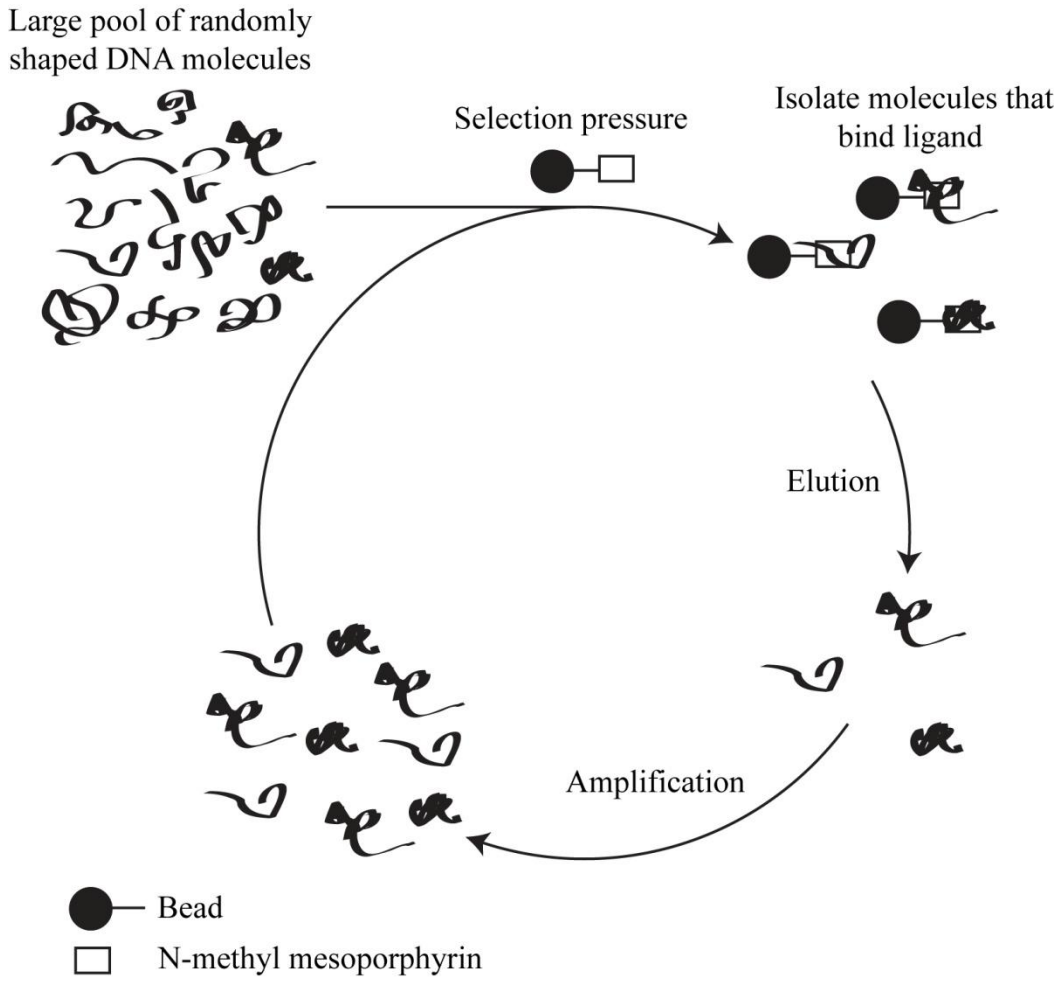

Figure 1.8: General *in vitro* selection scheme for an aptamer that binds N-methyl mesoporhyrin IX.

Even though PS5.M and PS2.M are *SELEX*-derived sequences that were originally selected to metallate porphyrins, PS5.M and PS2.M also displayed the ability to bind Fe(III) proporphyrin (heme) tightly with nanomolar affinity [62, 66]. Once bound to heme, both PS5.M and PS2.M displayed peroxidase activity [62]. This suggested that PS2.M and PS5.M may play a similar role to the apoenzyme of protein peroxidases to enhance the peroxidative ability of heme [62, 66]. PS2.M exhibited greater peroxidase activity than PS5.M; therefore, subsequent peroxidase-optimization and mechanistic studies were performed on PS2.M [62, 66-68]. The researchers rigorously optimized the

peroxidase activity of PS2.M-heme by modifying several conditions, such as potassium concentration, sodium concentration, pH, buffering agent, and detergent concentration [62, 66, 67].

At optimized conditions for peroxidase activity of PS2.M-hemin complex, Travascio *et al.* monitored the peroxidation of 2,2'-azino-bis(3-ethylbenzthiazoline-6-sulphonic acid) (ABTS) to $ABTS^{\bullet+}$ radical by PS2.M-hemin [66]. The oxidation of ABTS by H_2O_2 is readily monitored by UV-Vis spectroscopy, as the $ABTS^{\bullet+}$ radical cation exhibits an absorption maximum at 414 nm. In these studies ABTS was used in excess relative to the enzyme (10,000 times) and its oxidation is very fast; therefore, it was possible to measure the formation of Compound I by the reduction of H_2O_2 from the production of the $ABTS^{\bullet+}$ radical cation [66]. From such studies, the K_M value of H_2O_2-PS2.M binding was found to be 3 mM and the second-order rate constant was measured to be ~1 X 10^4 $M^{-1}\bullet s^{-1}$[66]. More surprisingly, Klibanov and collegues have reported that PS2.M-heme is capable of oxidizing certain substrates more efficiently than even protein peroxidases [69].

Structural investigation of PS2.M with DMS protection assays and cation assays have shown that this molecule forms a G-quadruplex [64, 70]. From the sequence of PS2.M, an 18-nucleotide long DNA with the following sequence, 5'-GTG GGT AGG GCG GGT TGG, one can notice that there are multiple tracts of guanines, which suggest the formation of G-quadruplexes. As a result of the highly stable nature of G-quadruplexes, these motifs form the core of the PS2.M structure. Furthermore, since both RNA and DNA can form G-quadruplexes, the ribonucleotide counterpart (rPS2.M) of PS2.M has similar heme binding properties as PS2.M despite the different structural

properties between DNA and RNA [66]. This particular G-quadruplex formed by PS2.M plays a large role in its heme binding ability and subsequent peroxidase activity.

Two methods of enhancing the peroxidase activity of heme have been proposed for PS2.M [66, 67]. The first method involves PS2.M or rPS2.M protecting the bound heme molecule from oxidative damage by the reactive Compound I species [66]. The second method is linked to the alkaline transition of the water molecule coordinated to heme iron at the sixth position [67]. Paola *et al.* demonstrated that when PS2.M is bound to heme, it favors the water molecule over the formation of a hydroxide molecule [67]. The water molecule, as compared to the hydroxide molecule, at the sixth position exchanges more readily with hydrogen peroxide to form Compound I [67].

After the initial discovery that PS2.M-heme was effectively a peroxidase, many groups have developed novel uses for PS2.M. These applications were primarily for detection purposes, such as, the detection of lead concentration, single nucleotide polymorphisms, telomerase activity and cancer markers [71-76]. Studies from Willner's laboratory primarily used a modified version of PS2.M, called CatG4 [71-75].

In recent years, multiple groups have demonstrated that many G-quadruplexes when bound to heme have peroxidase activity comparable to PS2.M-heme [77-80]. As a result, we would like to understand how PS2.M and other G-quadruplexes bind heme and how these nucleoheme complexes catalyze peroxidase reactions. Also, the research conducted by Klibanov and colleagues demonstrated that PS2.M-heme is very promiscuous and is capable of accepting a variety of substrates for 1-electron oxidation reactions. In this work, we investigated if this promiscuity of PS2.M-heme would allow it to catalyze 2-electron oxidation reactions of various electron rich substrates.

2: Folding studies of the active PS2.M species

2.1 Introduction

After discovering the versatility of PS2.M as a catalyst, it has become a more attractive enzyme for structural studies. As a result, several groups have probed the structure of PS2.M, and have produced contrasting results [68, 70, 79, 81, 82]. The most conflicting results stem from research from our group and a report by Majhi *et al.* [70, 81]. Previous research from our group had predicted a model for PS2.M as an anti-parallel intramolecular G-quadruplex [70]. In contrast, Majhi *et al.* have reported that PS2.M forms a parallel intermolecular G-quadruplex [81]. We attribute these dramatically different results to the different methodologies and conditions applied to the samples. In this work, we aim to determine the active G-quadruplex sturcture that binds heme and subsequently performs peroxidase activity from a potential mixture of different G-quadruplexes species.

2.2 Materials and methods

2.2.1 Materials

All DNA was purchased from Integrated DNA Technologies, Inc. The sequences of all DNAs and RNAs are given in Table 3.1. All nucleic acids were purified by preparative gel electrophoresis, eluted, ethanol precipitated, and then stored dissolved in TE buffer [10 mM Tris, pH 7.5, and 0.1 mM ethylenediaminetetraacetate (EDTA)] as decribed in section 2.2.2. All chemicals were purchased from Sigma-Aldrich, unless specified otherwise. Hemin was purchased from Porphyrin Products (Logan, Utah).

Table 2.1: DNA sequences.

Name	**Sequence**
SS18	5'-AAT ACG ACT CAC TAT ACT-3'
PS2.M	5'-GTG GGT AGG GCG GGT TGG-3'
CatG4	5'-TGG GTA GGG CGG GTT GGG AAA-3'
PS2.M_mut	5'-TGG GTA GGG CGG GTT GGG-3'

2.2.2 Purifying nucleic acids using polyacrylamide gel

We dissolved DNA and RNA pellets with tris(hydroxymethyl)aminomethane-ethylenediaminetetraacetic acid (Tris-EDTA or TE) buffer (10 mM Tris, pH 7.5; 0.1 mM EDTA) to make 1 mM stock solutions. We mixed 20 µL of 1 mM nucleic acids stock with 20 µL denaturing gel buffer solution with dye (99% formamide , 1 mM Tris-Cl, pH 7.5, 1 mM EDTA, 0.05% bromophenol blue, and 0.05% xylene cyanol). We heated the samples at 95ºC for 3 minutes and placed them on ice. We loaded the samples on a 10% denaturing polyacrylamide gel (45 mM Tris-borate; 1 mM EDTA, ~8 M urea) that was 20-25 cm in length. We placed a metal plate on the gel plate to evenly distribute the heat generated from electrophoresis. We ran the samples at 25-30 W or enough power so that

the gel reached 50ºC-55ºC on a Pharmacia ECPS 3000-150 electrophoresis power supply. We stopped the electrophoresis process when the bromophenol blue band migrated 10-15 cm from the bottom of the well at the top of the gel.

We visualized the nucleic acid band of interest using the UV shadowing technique. Briefly, we placed the gel on a plastic wrap over a UV-fluorescent thin-layer chromatography plate. We then exposed the gel to 254 nm UV light (UVGL-58 Mineralight® LAMP) to locate the nucleic acid band, which we marked and excised from the gel.

Subsequently, we crushed the gel piece and soaked it in 10 mL of TE buffer, and left it overnight at 4ºC to allow for the DNA/RNA to diffuse from the gel pieces. We filtered the gel pieces from the solution using a 0.2 µm filter (Acrodisc® Syringe Filters, PALL Corp.) attached to a 10 mL syringe (Luer-Lok™).

Then we concentrated the DNA/RNA by using the 2-butanol extraction procedure. Briefly, we added an equal volume of 2-butanol to the nucleic acid solution and then vigorously shook and vortexed the contents. We removed the organic layer (top) and performed several cycles of extraction to reduce the solution volume to ~1 mL. We separated the concentrated nucleic acid solution into three 300 µL aliquots before ethanol precipitation.

We further purified the 300 µL nucleic acid solution by ethanol precipitation. We added 30 µL of 3 M sodium acetate (NaOAc) and 2.5 volumes of cold ethanol to the nucleic acid solution and vortexed the mixture. Subsequently, we centrifuged the solution at 16,000 g for 30-60 minutes in an Eppendorf 5415D at a temperature of 4ºC. We removed the aqueous supernatant carefully, as not disturb the nucleic acid pellet.

Afterwards, we washed the pellet with 500 µL of cold 70% ethanol. Then we redissolved the pellet in TE buffer and we combined the contents from all of the aliquots to make up a 100 µL nucleic acid stock solution. We stored all nucleic acid stock solutions at -20ºC, unless otherwise specified.

2.2.3 Radiolabelling DNA by phosphorylation with γ-^{32}P-ATP

We purified oligonucleotides as previously described in section 2.2.2. We prepared 10 µM oligonucleotide solutions by diluting aliquots of stock oligonucleotide solutions with TE buffer. We combined 5 µL of 10 µM DNA solution with 2 µL T4 Kinase buffer from New England Biolabs Inc. (10X) and 10 µL of ddH_2O. After the γ-^{32}P-ATP stock was thawed, we added 2 µL of T4 Polynucleotide Kinase from New England Biolabs Inc. (10,000 units/mL) and 1 µL of γ-^{32}P-ATP from PerkinElmer (33 µL; 185 Mbq; 6000 Ci/mmol) to the mixture. The mixture was vortexed and incubated at 37ºC for 30-60 minutes. In order to stop the reaction we added 1 µL of 0.5 M EDTA to the reaction mixture and vortexed the contents.

We isolated the radiolabelled pellet by ethanol precipitation; briefly, we added 2 µL of 3 M NaOAc and 60 µL of cold ethanol to the arrested kinase reaction mixture. We placed the ethanol mixture in an ice bath for 10 minutes before we incubated it in dry ice until the aqueous solution was gel-like in viscosity. Then we centrifuged the ethanol mixture in 4ºC at 16,000 g for 45-60 minutes.

We carefully placed the centrifuged samples on ice to keep the pellet from dissolving into the ethanol/water mixture. We carefully removed the ethanol-aqueous layer and washed the radiolabelled pellet with 100 µL of 90% cold ethanol. After the

DNA pellet was dried, we dissolved it in 10 µL of denaturing gel buffer solution with dye and loaded it on a 10% denaturing gel.

We performed gel purification as previously described to separate the radiolabelled oligonucleotide from unincorporated γ-^{32}P-ATP. We used X-ray film (Blue XB X-OMAT, Kodak Film) to visualize the band of the radiolabelled DNA. Briefly, we wrapped the gel in Saran wrap and placed a piece of X-ray film on top of the area of the gel that contained the radiolabelled DNA band. We exposed the X-ray film to the radiolabelled DNA band for less than 10 seconds, meanwhile we placed marks at the interface between the X-ray film and the gel.

We developed The X-ray film with a Kodak X-OMAT 1000A Processor. We then lined-up the exposed film markings with the corresponding markings on the gel. We marked the radiolabelled DNA band and excised it from the gel. We crushed the gel piece and soaked it in 500 µL of TE buffer, unless otherwise specified, for over 16 hours at 4ºC.

We centrifuged the gel pieces at 16,000 g for 3 minutes and removed 400 µL of the supernatant. We lyophilized the solution by using a Labconco Centrivap console, which left a DNA and buffer salt pellet which we redissolved in 20 µL of ddH_2O.

Then we ethanol precipitated the radiolabelled DNA by adding 2 µL of 3 M NaOAc and ~2.5 volumes (60 µL) of cold ethanol. We treated the ethanol mixtures as described previously; briefly, and we then cooled and centrifuged the samples. We discarded the supernatant and washed the radiolabelled DNA pellet with 90% cold ethanol. Subsequently, we dissolved the DNA salt pellet in 20 µL of TE buffer and stored it at -20ºC.

2.2.4 Native gels of G-quadruplexes under varying conditions

2.2.4.1 Native gels that were composed of different salt conditions and ran in different temperature conditions

We prepared the samples under optimal folding potassium conditions prior to analysis on native gels with varying salt and temperature conditions. We prepared a 2X DNA solution and 2X folding buffer. We dissolved quantities of 0.04, 0.4 and 2 nmol of DNA with an adequate amount of radiolabelled DNA tracer in 18 µL of TE buffer to form the desired 2X DNA solutions (0.2, 20, and 100 µM DNA). We heated the samples at 95ºC for 3 minutes and placed them in an ice bath for 5 minutes.

We added 20 µL of 2X folding buffer (80 mM TrisOAc, pH 7.5; 50 mM KCl; 0.1% [w/v] Triton X-100) to the 2X DNA solution and incubated at room temperature (~21ºC) for 30 minutes. Afterwards, we split the sample into two 19 µL aliquots and 1 µL of either hemin (hemin was dissolved in dimethylsulfoxide (DMSO)) or DMSO was added to the sample to compare the structure of the DNA in the presence or absence of hemin. We added a hemin concentration to the mixture to give a 1:1 final molar ratio between DNA and hemin.

The final 20 µL samples contained 0.1-50 µM DNA, 0.1-50 µM hemin, 40 mM TrisOAc (pH 7.5), 25 mM KCl, 0.05% Triton X-100, 5% DMSO, ~0.5X TE buffer. After adding hemin or DMSO we incubated the mixture at 21ºC for 30 minutes. We added 20 µL of loading buffer for the non-denaturing gels with dye (0.05% bromophenol blue, 0.05% xylene cyanol, 15% Ficoll) to each mixture and vortexed the samples.

We prepared two gels for each salt concentration and DNA concentration condition; we placed one gel was placed in 4ºC and another in 21ºC. Briefly, we

prepared 60 mL of 20% polyacrylamide gel solution with 40 mM Tris-acetate (TrisOAc), 0, 5 or 25 mM KCl, and 5 mM EDTA. We polymerized the gel by the addition of 0.1 volume of 10% ammonium persulfate and 0.0004 volume of tetramethylethylenediamine (TEMED).

We separated each DMSO and hemin containing sample into two 15 µL aliquots and loaded into gels placed in both 4ºC and 21ºC; we also saved a 10 µL aliquot for future testing. We also loaded a 10 base pair ladder in each gel for size references (10 bp DNA ladder from Invitrogen). We ran the 25 mM KCl 4ºC gel at 3 W and the 21ºC gel at 1 W for 24 hours. While we ran the 5 mM KCl gels at the same wattage for both temperature conditions for 8 hours. The bromophenol blue marker for the above mentioned gels migrated 15 cm from the bottom of the well at the top of the gel.

Once adequate time had passed to allow for the migration of the bromophenol blue marker, we covered the gel with Saran wrap. We then exposed the gels to phosphorous screens (Amersham Biosciences) for various times (1-48 hours) to gain multiple exposures of the gels. The exposures were performed in 4ºC to limit the diffusion of the DNA bands in the gels. We scanned the phosphorous screens on a Molecular Dynamics Typhoon 9410 Variable Mode Imager to visualize the radiolabelled bands on the gel. We analyzed the gel images using either ImageQuant 5.2 or ImageJ.

2.2.4.2 Native gels of varying DNA concentrations in different temperature conditions

We treated all samples and gels with the same methods as the section above. Briefly, we combined a 2X DNA solution with a 2X buffer solution (80 mM TrisOAc (pH 7.5), 50 mM KCl, 0.1% Triton X-100, and 2% DMSO) and incubated over 30 minutes in 21ºC. The final volume of the solution was 20 µL with 40 mM TrisOAc (pH

7.5), 25 mM KCl, 0.05% Triton X-100, 1% DMSO, and ~0.5X TE buffer. The final concentrations of DNA covered a wide range: 0.1, 0.5, 2.5, 10 and 50 µM.

We added 20 µL of gel loading buffer for native gels to each sample, and subsequently the samples were split into two aliquots. We prepared two native gels, as previously described in section 2.2.4.1, with contents of 20% polyacrylamide, 40 mM TrisOAc, 25 mM KCl, and 5 mM EDTA. We placed one gel in 4ºC and the other in 21ºC.

For each DNA sequence, we loaded 20 µL of each sample containing a range of concentrations into both the gel in 4ºC and the gel in 21ºC. The 4ºC gel was run at 3 W and the 21ºC gel was run at 1 W for 24 hours; the bromophenol blue marker migrated 15 cm from the bottom of the well at the top of the gel. After sufficient time had passed to allow for the migration of the bromophenol blue marker, we covered the gel with Saran wrap. Then we exposed the gels to phosphorous screens for various times (1-48 hours) to gain multiple exposures of the gels. We performed the exposures at 4ºC to limit the diffusion of the DNA bands in the gels. We scanned the phosphorous screens on a Typhoon 9410 Imager to visualize the radiolabelled bands on the gel.

We quantified the different species, reflected by the different bands in a sample lane, using either ImageQuant 5.2 or ImageJ. Briefly, we drew a rectangle enclosing each band to designate an area on the gel to calculate the number of dark pixels in the band. We then compared the density of dark pixels within each designated band to the total number of dark pixels in each lane. We used this form of calculation to normalize the amount of radiolabelled DNA loaded in each well. We then plotted the percentage of

each band compared to the quantity of all DNA species over a range of DNA concentrations.

2.2.5 Verification of degradation of oligonucleotides

We aliquoted 10 µL from the samples mentioned in section 2.2.4.1 for further analysis. One such analysis was to check if the oligonucleotides had degraded over time. WE prepared a 60 mL denaturing gel solution with 20% polyacrylamide, 40 mM TrisOAc (pH 7.5), 5 mM EDTA and 50% [w/v] urea.

In addition, we added 10 µL of denaturing gel buffer solution with dye to the samples. Prior to loading the samples into the gel, we heated the samples at 95ºC for 3 minutes and placed them directly in an ice bath for 5 minutes. We ran the denaturing gel at >25 W, until the glass plate in contact with the gel reached 50-55ºC; we placed a metal plate behind the glass plates to allow for uniform heat distribution in the gel. The electrophoresis process took ~2 hours or the time it took the bromophenol blue marker to migrate 15 cm from the bottom of the well at the top of the gel.

After we waited a sufficient time to allow for the migration of the bromophenol blue marker, we covered the gel with Saran wrap. Then we exposed the gels to phosphor image screens for various times (1-48 hours) to gain multiple exposures of a gel. We performed the exposures in -20ºC to limit the diffusion of the DNA bands in the gels. We scanned The phosphor image screens on a Typhoon 9410 Imager to visualize the radiolabelled bands on the gel. We analyzed the gel images using either ImageQuant 5.2 or ImageJ.

2.2.6 Circular dichroism spectroscopy of PS2.M under varying conditions

2.2.6.1 Changing the concentration of DNA in fixed buffer solutions

We prepared a 2X DNA solution and various 2X folding buffers. We dissolved quantities of 0.2, 0.5, and 5 nmol of DNA in TE buffer to form the desired 2X DNA solutions (0.2, 10, and 100 µM DNA). For a final concentration of 50 µM and 10 µM of DNA, we prepared 2X DNA solutions of 100 µM and 10 µM of DNA, respectively by dissolving the above amount of DNA in 49 µL of TE buffer. We prepared the 2X DNA solution of 0.2 µM DNA by dissolving the above amount of DNA in 980 µL of TE buffer.

Note the volumes were different between the 0.2 µM sample from the other two larger DNA concentration samples (100 µM and 10 µM). In order to get sufficient absorption from all DNA samples, the cuvette pathlength needs to be longer for the sample with low DNA concentration than the two larger DNA concentration samples. Therefore, we placed the low DNA concentration sample in a larger quartz cuvette that required a minimum of 2000 µL.

We heated the DNA samples at ~100ºC with boiling water for 3 minutes and then cooled them in an ice bath for 5 minutes. We added 50 µL of 2X folding buffer (80 mM TrisOAc, pH 7.5; 50 mM KCl; 0.1% Triton X-100) for the two higher 2X DNA concentration samples (100 µM and 10 µM) and 1000 µL of the 2X folding buffer to the low 2X DNA concentration sample (0.1 µM). We incubated all DNA solutions combined with folding buffer solution at room temperature (~21ºC) for 30 minutes.

Afterwards, we added 1 µL or 20 µL of either hemin (hemin was dissolved in DMSO) or DMSO to the samples to compare the structures of the DNA in the presence

or absence of hemin. We added 1 µL of 50 mM or 5 mM hemin to the two larger DNA concentration samples to make up the solution to 100 µL. We prepared the hemin stock solutions by dissolving a specific amount of hemin in DMSO. We added 20 µL of 100 µM hemin to the smaller DNA concentration sample to make up the solution to 2000 µL. The hemin concentration that we added to the mixture resulted in a 1:10 final ratio DNA:hemin concentration. The 50 µM DNA samples had a final ratio of DNA to hemin of 1:3.

The 100 µL (50 and 5 µM DNA) and 2000 µL (0.1 µM) samples contained 0.1-50 µM DNA, 1-150 µM hemin, 40 mM TrisOAc (pH 7.5), 25 mM KCl, 0.05% Triton X-100, 5% DMSO, ~0.5X TE buffer. After adding hemin or DMSO, we incubated the mixture at 21ºC for 30 minutes.

Subsequently, we analyzed samples in a Jasco J-810 CD spectropolarimeter. We placed the 50 and 5 µM DNA samples in 0.05 cm path length cuvettes while the 0.1 µM sample was placed in a 1 cm path length cuvette. We programmed the scan settings for all samples to scan between 230 nm – 320 nm at a rate of 500 nm/min. We accumulated the spectrum for each sample from the average of 10 scans.

We analyzed the data for all samples using Spectra Manager from Jasco. We corrected all DNA samples for the absorbance of the buffer. We subtracted the spectra of the DNA samples that we incubated with hemin from the spectra of a hemin only reference sample. We subtracted the spectra of the DNA only samples from the spectra of a DMSO reference sample. The hemin only and DMSO only reference samples contained 0-150 µM hemin, 40 mM TrisOAc (pH 7.5), 25 mM KCl, 0.05% Triton X-100, 5% DMSO, ~0.5X TE buffer.

2.2.6.2 Observing the changes in PS2.M folding in various salt conditions

We prepared a 2X DNA solution and various 2X folding buffers as previously described in section 2.2.6.1. Briefly, we dissolved 1 nmol of DNA in 50 µL of TE buffer to form the desired 2X DNA solutions. We heated the samples at ~100ºC with boiling water for 3 minutes and then cooled them in an ice bath for 5 minutes. We added 50 µL of 2X folding buffers with different salts and varying salt concentrations (80 mM TrisOAc, pH 7.5; 0-100 mM KCl or 0-800 mM NaCl; 0.1% Triton X-100; 2% DMSO) to the 2X DNA solutions and incubated them in room temperature (~21ºC) for 30 minutes. The final 100 µL samples contained 10 µM DNA, 40 mM TrisOAc (pH 7.5), 0-50 mM KCl or 0-400 mM NaCl, 0.05% Triton X-100, 1% DMSO, 0.5X TE buffer.

Subsequently, we analyzed the samples with a Jasco J-810 CD spectropolarimeter. We placed the samples in 0.05 cm pathlength cuvettes. We programmed the scan settings for all samples to scan between 230 nm – 320 nm at a rate of 500 nm/min. We accumulated the spectrum for each sample from the average of 10 scans. We subtracted the spectra of the DNA samples from the spectra of reference samples that contained no DNA and only 40 mM TrisOAc (pH 7.5), 0-50 mM KCl or 0-400 mM NaCl, 0.05% Triton X-100, 1% DMSO, 0.5X TE buffer. The values obtained were given as deg, these values were converted to molar ellipticity. We converted deg to molar ellipticity by multiplying the deg value by the pathlength of the cuvette (in cm) and dividing by the concentration of DNA in the sample (in $dmol \bullet cm^{-3}$).

2.2.7 Dimethyl sulfate protection assay of G-quadruplex forming oligonucleotides

We prepared Samples as detailed in section 2.2.4.1. Briefly, we prepared samples with 0.1 µM and 50 µM of DNA in a buffer of 40 mM TrisOAc (pH 7.5), 25 mM KCl,

0.05% Triton X-100, 5% DMSO, ~0.5X TE buffer. The samples either contained no hemin or 1:1 molar ratio hemin and DNA. As described previously, we split the samples into 2 aliquots and placed one in 4ºC and another in 21ºC.

After we incubated the samples for an adequate amount of time, roughly for 30 minutes, were treated them with dimethyl sulphate (DMS). The DMS reaction scheme is depicted in Figure 2.7. We added 2 μL of 2% DMS (dissolved in distilled-deionized water) and 3 μL of 200 mM Li cacodylate (final Li cacodylate concentration was 25 mM) to each 20 μL sample. For the non-DMS treated samples, we added 2 μL of water instead of DMS. We incubated the samples for 30 mins at 21°C and 40 mins at 4°C. We added 2 μL of 25% [v/v] 2-mercaptoethanol to the DMS treated samples to stop the reaction. We loaded the samples in gels and ran them at the same temperatures as they were incubated in.

We prepared and ran the gels with the same method described in section 2.2.4. After we ran the gels for an adequate amount of time, we excised the species of interest from the gel. We employed the dip-and-dot method to visualize and mark the radiolabelled DNA band. Briefly, we wrapped the gel in Saran wrap. We marked dots on the gel and placed a trace amount of γ-^{32}P-ATP at every mark by puncturing the dots with a needle dipped in γ-^{32}P-ATP.

After we marked the gels with the dip-and-dot procedure, we wrapped the gel in another layer of Saran wrap before exposing it to phosphorous screens for 1-2 hours at 4ºC. We scanned the phosphorous screens on a Typhoon 9410 Imager to visualize both the radiolabelled bands and premade marks on the gel. We analyzed the gel images with either ImageQuant 5.2 or ImageJ. We used an image of the gel from the exposure to

mark the desired bands/species on the gel. Were excised the desired products from the gel and crushed the gel pieces and soaked them in 430 µL of TE buffer. We suspended the crushed gel pieces in TE buffer for 16-24 hours at 4ºC.

We centrifuged the gel pieces at 16,000 g for 3 minutes and removed 400 µL of the supernatant. We lyophilized the solution, leaving a DNA and buffer salt pellet which we redissolved in 20 µL of ddH_2O. Then we ethanol precipitated the DNA product by adding 2 µL of 3 M NaOAc and ~2.5 volumes (60 µL) of cold ethanol. We treated the ethanol mixtures as described in previous sections; briefly, we cooled and centrifuged the samples. We discarded the supernatant and washed the radiolabelled DNA pellet with 90% cold ethanol.

WE redissolved The pellet in 100 µL of 10% [v/v] piperidine and heated it at 90ºC for 30 minutes. After the piperidine treatment, we removed the piperidine by lyophilisation. In order to remove any residual piperidine after the first lyophilization, we redissolved the sample in 50 µL of ddH_2O and lyophilized again; we repeated this process once more.

We ran the samples, G-ladders, and 10 base pair ladders on a 15% denaturing gel (0.5X TBE and 50% [w/v] urea). We prepared the G-ladders a day prior to running the gel. Briefly, we prepared 20 µL of 2 µM DNA with trace amounts of radiolabelled DNA and heated this at 95ºC for 3 minutes and placed it in an ice bath for 5 minutes. We treated the G-ladder for each individual DNA sequence with DMS as described above. In order to stop the DMS reaction, we added 4 µL of stop solution (1.5 mM NaOAc and 7% [v/v] 2-mercaptoethanol) to each sample.

We ethanol precipitated the G-ladder samples by adding 60 µL of ethanol and treated them as previously described. Briefly, after we cooled the samples to a gel-like consistency we centrifuged them and removed the supernatant. We washed the DNA pellet with 90% ethanol before treating the pellets with piperidine.

We redissolved the pellets in 100 µL of 10% [v/v] piperidine and heated at 90ºC for 30 minutes. After the piperidine treatment, we removed the piperidine by lyophilisation. In order to remove any residual piperidine after the intial lyophilisation step, we redissolved the sample in 50 µL of ddH_2O and lyophilized again; we repeated this process once more.

Subsequently, we dissolved the dried pellets in denaturing gel buffer with dyes. We ran the samples on a 15% denaturing gel at 40-60 W or at a power that sufficiently heated the gel to 55ºC until the bromophenol blue marker had migrated 15 cm from the bottom of the well. Then we covered the gel with Saran wrap and exposed it to a phosphorous screen for various times (2-4 days) to gain multiple exposures of the gels. We performed the exposures at -20ºC to limit the diffusion of the DNA bands in the gels. We scanned the phosphorous screens on a Typhoon 9410 Imager and analyzed the images using either ImageQuant 5.2 or ImageJ software.

2.2.8 Kinetics of 2,2'-azino-bis(3-ethylbenzthiazoline-6-sulphonic acid) (ABTS) oxidation at 4ºC and 21ºC

The final volume of all samples was 1 mL. Initially, we dissolved 2 nmol DNA in 760 µL of TE buffer to make a 2X DNA solution. We heated the 2X DNA solution in boiling water at 100ºC for 3 minutes before cooling in an ice bath for 5 minutes.

We separated the 2X DNA solution into two 380 µL aliquots and added 500 µL of 2X ABTS oxidation buffer to each aliquot. We incubated one aliquot at 4ºC and the other at 21ºC for 30 minutes. The 2X ABTS oxidation buffer contained 100 mM 4-(2-hydroxyethyl)-1-piperazineethanesulfonic acid pH adjusted with ammonium hydroxide (HEPES-NH_4OH), pH 8.0, 40 mM KCl, 0.1% Triton X-100, and 2% DMSO.

Then we added 10 µL of 10 µM hemin to all aliquots and incubated for an additional 30 minutes in their respective temperatures (4ºC or 21ºC) for a final hemin concentration of 0.1 µM. Note, when we added the 10 µM hemin to the sample in the cold room (4ºC), the we placed hemin in a warm water bath to prevent the DMSO from freezing. We added 100 µL of 50 mM ABTS to all samples before initiating the reaction with H_2O_2. We allowed all samples to mix for 5 minutes after the addition of ABTS and then transferred them into a 1 mL cuvette.

We used a Varian Cary Bio 300 UV-Vis Spectrophotometer to measure the oxidation of ABTS to $ABTS^{\bullet+}$ radical. We used the Kinetics program from Cary UV Win software package to follow the formation of the radical, which has an increased absorbance at 414 nm ($\varepsilon_{414\ nm}$ = 31,100 M^{-1} cm^{-1}) compared to the unoxidized ABTS. We placed the cuvettes in the sample holder, which we held at the temperature that the samples were incubated at, during the initial processes. After 5 minutes in the sample holder to make sure the solution obtained the desired temperature, we used the sample as the reference point or the absorbance at time 0 prior to the addition of H_2O_2.

After we corrected the samples for the background absorbance at 414 nm, we used 10 µL of H_2O_2 (varying concentrations) to initiate the reaction. We performed the initiation process very quickly (within 10 seconds) to maintain constant temperature. We

measured the absorption of the final reaction mixture (1 µM DNA, 0.1 µM hemin, 0-12 mM H_2O_2, 5 mM ABTS, 50 mM HEPES-NH_4OH (pH 8.0), 20 mM KCl, 0.05% Triton X-100, and 2% DMSO) at 414 nm over 30 minutes or until a plateau of the absorbance at 414 nm was reached. We obtained the initial rate of ABTS oxidation from the initial slopes of absorbance over time graphs. We plotted the initial rate values against the concentration of H_2O_2 used in each reaction.

2.2.9 Measuring binding constants between hemin and G-quadruplex forming oligonucleotides at 4ºC and 21ºC.

We prepared a 2X DNA solution and a 2X folding buffer. We dissolved a sufficient amount of non-radiolabelled DNA and radiolabelled DNA tracer in 490 µL of TE buffer to form the desired 2X DNA solutions. We heated the samples at 100ºC for 3 minutes and then cooled them in an ice bath for 5 minutes.

We prepared a 2X folding buffer with 100 mM TrisOAc (pH 7.5), 50 mM KCl, 2% DMSO, and 0.1% Triton X-100. We added 500 µL of 2X buffer solution to each 2X DNA solution and the mixture was incubated at 4 º C or 21 º C for 30 minutes. Afterwards, we added 10 µL of 50 µM hemin dissolved in DMSO to the mixture for final concentrations of 0.5 µM hemin, 0 – 5 µM DNA, 50 mM TrisOAc (pH 7.5), 25 mM KCl, 0.05% Triton X-100, and ~2 % DMSO. We incubated the samples for an additional 30 minutes at 4ºC or 21ºC.

We placed the samples in 1 mL cuvettes and loaded in a Cary 300 Bio UV-Visible Spectrophotomer. We obtained the spectra for each sample (200 nm – 800 nm) using the Spectrum program from the Cary UV Win software package. We compared each sample to a reference sample which contained the same buffer as the sample with

TE buffer and DMSO added in place of DNA and hemin. We subtracted the spectrum of each sample against their relative reference samples. We plotted the peak absorbance values over a range of DNA concentrations.

$$[\mathrm{DNA_0}] = \mathrm{K}_d \left(\frac{A - A_0}{A_{max} - A}\right) + [\mathrm{H_0}] \left(\frac{A - A_0}{A_{max} - A_0}\right)$$

We obtained the K_d value from fitting the data to the above equation, obtained from Wang *et al*. [84]. Where *A* represents the absorbance of the soret peak; A_{max} represents the maximum absorbance when heme is completely bound by DNA; A_0 represents the minimum absorbance when heme is free in solution; H_0 represents the total concentration of hemin. The above equation was derived from the equilibrium equation for hemin-DNA dissociation.

2.2.10 Measuring the pK_a values of various water-hemin complexes

We prepared various buffering components at 1 M concentrations to span a pH range of 3-10: glycine-HCl (2.5, 3, 3.5, 4), sodium acetate (4, 4.5, 5, 5.5), sodium phosphate (5.5, 6, 6.5, 7, 7.5, 8.0), Tris-HCl (8, 8.5, 9.0), and glycine-NaOH (8.5, 9.0, 9.5, 10). We prepared a 2X buffer for each pH with 100 mM buffer solution, 50 mM KCl, 2% DMSO, and 0.1% Triton X-100.

We dissolved 3 nmol of DNA in 10 µL of TE buffer, and then heated at 95ºC for 3 minutes and then cooled in an ice bath for 5 minutes. The solution was made up to 490 µL with the addition of ddH_2O. We added the 2X buffer solution to the DNA solution and the mixture was incubated at 21ºC for 30 minutes.

Afterward, we added 10 µL of 50 µM hemin dissolved in DMSO to the mixture for final concentrations of 0.5 µM hemin, 3 µM DNA, 50 mM buffer, 25 mM KCl, 0.05% Triton X-100, and ~2 % DMSO. We incubated the samples for an additional 30 minutes at 21ºC.

We placed the samples in a 1 mL cuvette and loaded in a Cary 300 Bio UV-Visible Spectrophotomer. Wre obtained the spectra for each sample (200 nm – 800 nm) using the Spectrum program from the Cary UV Win software package. We compared each sample to a reference sample, which contained the same buffer as the sample with TE buffer, and DMSO added in place of DNA and hemin. We subtracted the spectrum of each sample against their relative reference samples. We compared the absorbance at 355 nm to the absorbance at 404 nm. We plotted the ratio between 355 nm and 404 nm over the corresponding pH values.

We obtained the pK_a value from fitting the data to the equation below; where *A* represents the ratio between the absorbance at 355 nm and 404 nm; A_{max} represents the maximum ratio value where heme is completely bound by hydroxide molecules; A_{min} represents the minimum ratio value where heme is completely bound to water molecules. The above equation was derived from the Henderson-Hasselbalch equation.

$$\mathrm{A} = A_{min} + \frac{A_{max} - A_{min}}{1 + 10^{pK_a - pH}}$$

2.3 Results and discussion

2.3.1 Structural analysis of G-quadruplexes with native gels under various conditions

The controversy of the folded species of PS2.M was the initial motivator for our structural studies of PS2.M [70, 81]. Lee *et al.* proposed that PS2.M would fold into an anti-parallel G-quadruplex and Majhi *et al.* proposed that PS2.M would fold into a parallel intermolecular G-quadruplex [70, 81]. As a result, we wanted to determine the folded structure of PS2.M under optimal heme-binding and peroxidase conditions.

We began by verifying the results of the two conditions that provided the two conflicting proposed-models of PS2.M [70, 81]. Since non-denaturing gels provided the primary evidence for both structures, we continued using this method of analysis. The conditions that varied between the two sets of experiments, such as temperature, salt conditions, and DNA concentration were rigorously tested for the folding of PS2.M.

In addition, numerous studies employed the peroxidase activity of PS2.M-heme complex in various detection strategies; however, these studies used a modified version of PS2.M, called CatG4 [71-76]. Since both PS2.M and CatG4 are capable of binding heme and catalyzing peroxidase reactions, we wanted to compare the folding of CatG4 to PS2.M as well.

All the native gels shown in Figure 2.1 demonstrate that the G-quadruplexes formed by all the oligonucleotides examined are polymorphic in nature. In addition to presence of multiple bands in the PS2.M lanes, PS2.M also seems to form intramolecular and intermolecular species, denoted by an asterisk (*). As a result, the anti-parallel

intramolecular G-quadruplex structure proposed in Lee *et al.* and the parallel intermolecular G-quadruplex structure proposed Majhi *et al.* may both exist [70, 81].

In the case of the intramolecular species, the faster mobility bands compared to the SS18 control, were verified to be compact structures of the parent sequences and not degradation products. The results from the denaturing gel in panel D*i* demonstrates that after heat and urea denaturation of the various oligonucleotides, there is only one species in each lane. The addition of heme during the incubation process does not appear to cause any visible DNA degradation products.

The hemin-containing and no-hemin lanes for each oligonucleotide differ in band patterning in all conditions except for the low DNA concentration gels. In the low DNA concentration gels (panel A), the hemin-containing lanes for PS2.M, PS2.M_mut and CatG4 at 0.1 μM DNA concentration (panel A) look exactly the same as the no-hemin lanes. In panel B and C, there is a visible difference between the no-hemin and hemin-containing lanes. The reason no difference is observed for the low DNA concentration gels can be attributed to the small concentration of hemin in those samples (0.1 μM hemin).

Figure 2.1: Analysis of the folding pattern of G-quadruplex forming sequences in various conditions by polyacrylamide gel electrophoresis.

All samples were composed of 40 mM TrisOAc (pH 7.5), 25 mM KCl, 0.05%, Triton X-100, 5% DMSO, ~0.5X TE buffer, and 1:1 ratio of DNA to heme. All gels contain 40 mM TrisOAc, 0, 5 or 25 mM KCl, and 5 mM EDTA and 20% polyacrylamide. The amount of DNA in each set of samples was 0.1 µM (A), 10 µM (B), and 50 µM (C and D). The gel in panel Di contained an additional ~ 8 M urea.

The KCl concentration in each set of gels was 0 mM (D), 25 mM (A and C), and 5 mM (B). For all panels (A-C) except for panel D, one image represents the gel experiment at 4ºC (i) and other image represents the gel experiment at 21ºC (ii).

In the case of panel D, all electrophoresis experiments were performed at 21ºC. Also for panel D, one gel image represents denaturing conditions (i) and the other represents non-denaturing conditions (ii).

Each gel experiment contains a specific set of oligonucleotides, as denoted in the figure: SS18, PS2.M, PS2.M_mut, and CatG4. SS18 is a 18-nucleotide non-G-quadruplex forming single stranded oligonucleotide. PS2.M is an 18-nucleotide DNA-aptamer for heme that was selected using *SELEX* [63, 64]. PS2.M_mut has the same general sequence as PS2.M, but a single G has been moved from the 5'-end to the 3'-end. CatG4 is a DNA-aptamer for heme that was rationally designed from PS2.M. The – and + signs denote samples that either contained DMSO (no hemin) or hemin.

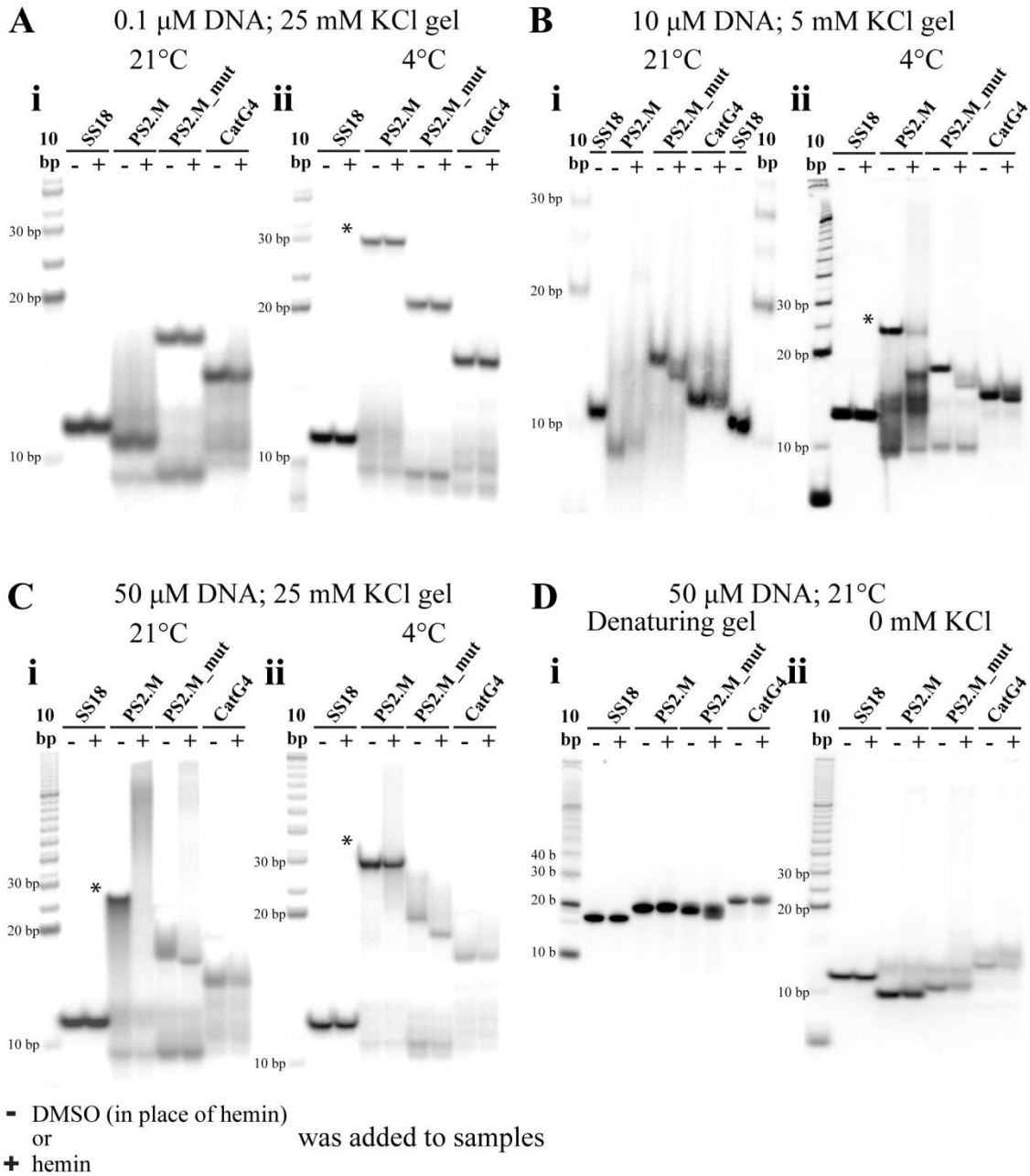

- DMSO (in place of hemin) or
+ hemin

was added to samples

All hemin-containing samples contained 1:1 ratio of DNA to hemin. The binding constant of PS2.M has been previously reported by Travascio *et al*. to be sub-0.5 μM. In order to bind > 90% of the PS2.M, it was not adequate to use a 1:1 ratio of hemin to DNA for 0.1 μM PS2.M samples [62]. The binding constants for both PS2.M_mut and CatG4 also have been determined to be around the same magnitude as PS2.M; therefore, a 1:1 ratio of hemin to DNA for 0.1 μM PS2.M_mut and CatG4 samples is not sufficient to form complexes with hemin. As a result, the low DNA concentration gels do not show a difference between the non-hemin and hemin-containing samples.

From the gel images in panels A-C, the structures of PS2.M_mut and CatG4 do not seem to change much at different salt concentrations or at different DNA concentrations. This can be seen in the similar mobility products for PS2.M_mut and CatG4 in the different conditions.

In contrast, the structures formed by PS2.M seem to be more sensitive to changes in DNA concentration, KCl concentration, and temperature than PS2.M_mut and CatG4 samples. The distribution of different folding species of PS2.M varies significantly from one condition to another; where one condition only contains bands formed by intramolecular species and another condition where a slow mobility product (marked with *) appears.

Intramolecular folded species are present in all gel conditions; this can be observed from the bands that have migrated faster than the 18-nucleotide long single stranded non-G-quadruplex-forming control, SS18. The formation of intermolecular species by PS2.M is evident in the high DNA concentration and 4ºC samples denoted by an asterisks (*) in Figure 2.1 and by ‘2’ in Figure 2.2. This slow mobility product

migrates roughly the same distance as the 30 base pair band in the 10 base pair ladder. These gel experiments demonstrate that at lower concentrations of DNA, PS2.M favours intramolecular-folded structures. At high DNA concentrations, low temperature conditions, and high KCl concentrations, the formation of intermolecular folded structures by PS2.M becomes apparent.

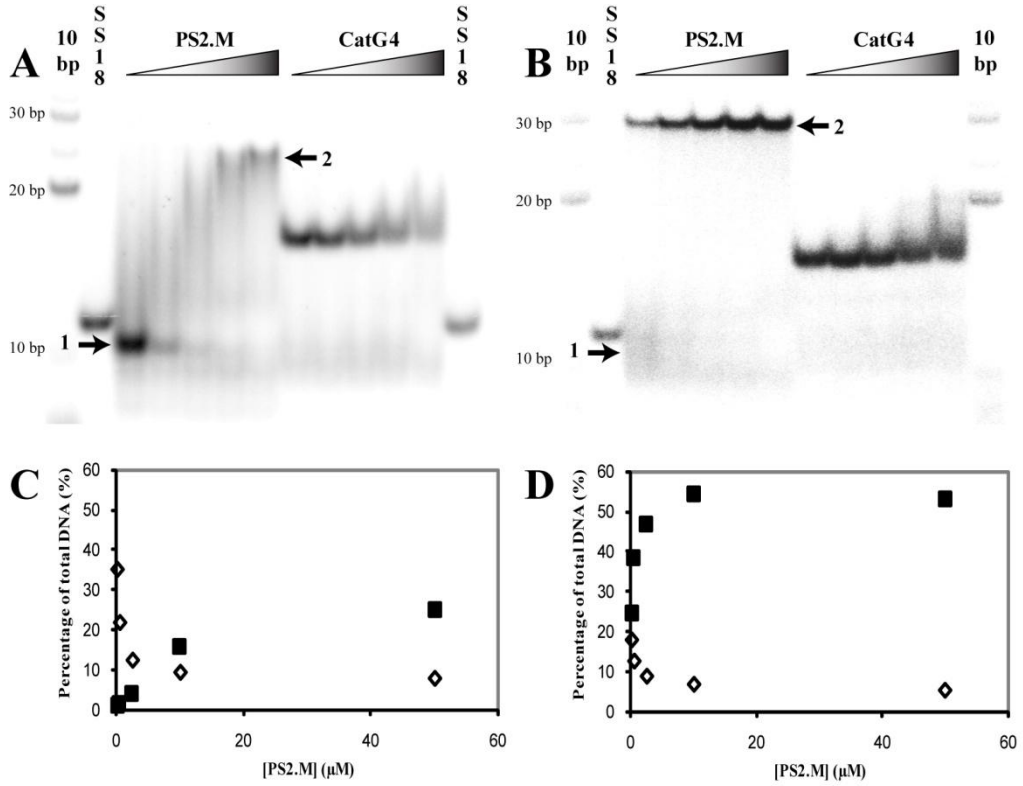

Figure 2.2: The effects of increasing DNA concentration on the structure of G-quadruplex forming oligonucleotides.
All gels contain 40 mM Tris-acetate (TrisOAc), 25 mM KCl, and 5 mM EDTA, and 20% polyacrylamide. All samples were composed of 40 mM TrisOAc (pH 7.5), 25 mM KCl, 0.05% Triton X-100, 5% DMSO, ~0.5X TE buffer. Concentrations of DNA in each gel included 0.1 μM, 0.5 μM, 2.5 μM, 10 μM, and 50 μM. A) Ran gel in 21ºC. B) Ran gel in 4 ºC. C) Graph of results from gel A. D) Graph of results from gel B. The graphs depict the changes of bands 1 and 2 as a result of increasing DNA concentration. The amount of each band was plotted as a percentage of the total amount of DNA. ◊ represents band 1 and ■ represents band 2.

The effect of increasing DNA concentration on the relative proportions of intermolecular and intramolecular species can be seen in Figure 2.2. As the amount of DNA is increased, there is an increase in the amount of the intermolecular species. The increase in intermolecular structures is attributed to shifts in equilibrium concentrations of the various conformers in response to the addition of single-stranded DNA. This can be seen in both the 4ºC and the 21ºC conditions; however, in 4ºC, the amount of intermolecular species starts as a greater proportion of the total DNA for the low DNA concentrations.

In both Figure 2.1 and Figure 2.2, the 4ºC conditions promote the formation of intermolecular species. Intermolecular species form under low temperature conditions because the unfavorable entropic contribution when multiple strands of DNA come together is diminshed [85, 86]. Conversely, the formation of an intermolecular species is enthalpically favored because of the increase in the amount of bonds formed. Therefore, at low temperature conditions, the unfavorable entropic contribution is minimized and offset by the favorable enthalpic contributions of multiple strands of DNA coming together to form a G-quadruplex.

The other crucial factor in determining the folding of PS2.M is the salt condition. It was previously determined that PS2.M can form a G-quadruplex [64]. The abundance and type of metal cations in solution have significant effects on G-quadruplex formation [25]. In Figure 2.1, gel D*ii* is a 21ºC non-denaturing gel that contains no KCl and 50 µM DNA samples. In the absence of KCl in the gel, the slow mobility band, equivalent to 30 base pairs, does not form because intermolecular/multimeric G-quadruplexes have a

greater need for cations to neutralize the very high negative charge density at the core of the G-quadruplex.

A diagram of the relationship between the folded structure of PS2.M and the solution conditions is depicted in Figure 2.3.

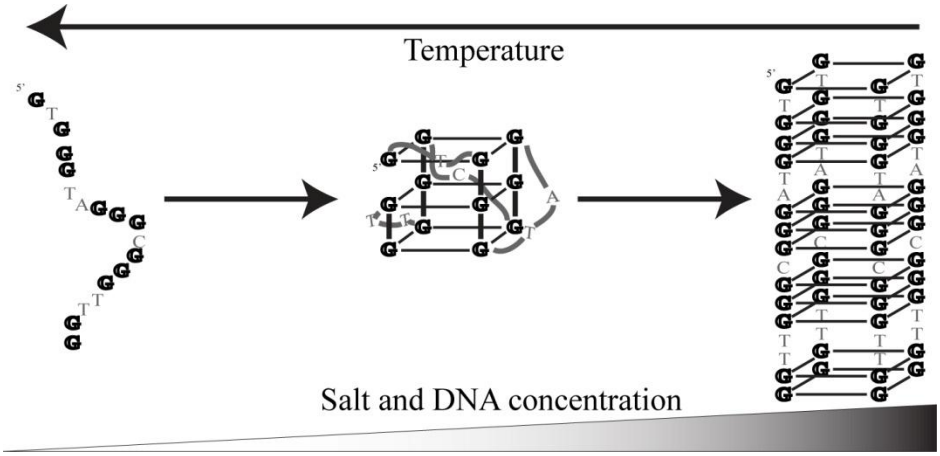

Figure 2.3: The relationship between the structure of PS2.M and various conditions.

2.3.2 Investigation of the structure of PS2.M in various conditions using circular dichroism spectroscopy

Circular dichroism spectroscopy has been a useful investigative tool for the study of G-quadruplexes. By using both CD spectroscopy and gel electrophoresis, a number of structural features of G-quadruplexes can be observed, including the number of strands and the strand polarity.

In Figure 2.4, samples with 0.1 μM, 5 μM and 50 μM PS2.M in 25 mM KCl were analyzed by CD spectroscopy. Panel D contains all the spectra of SS18 non-G-quadruplex-forming oligonucleotides for all the different conditions analyzed in experiments presented in panels A through C. All SS18 samples give similar spectra after normalizing the ellipticity value for the concentration of DNA in each sample. The traces for the SS18 samples with hemin show no difference when compared to the

samples without hemin. These observations suggest that the different DNA and salt conditions do not affect the folding of SS18, nor does SS18 bind heme.

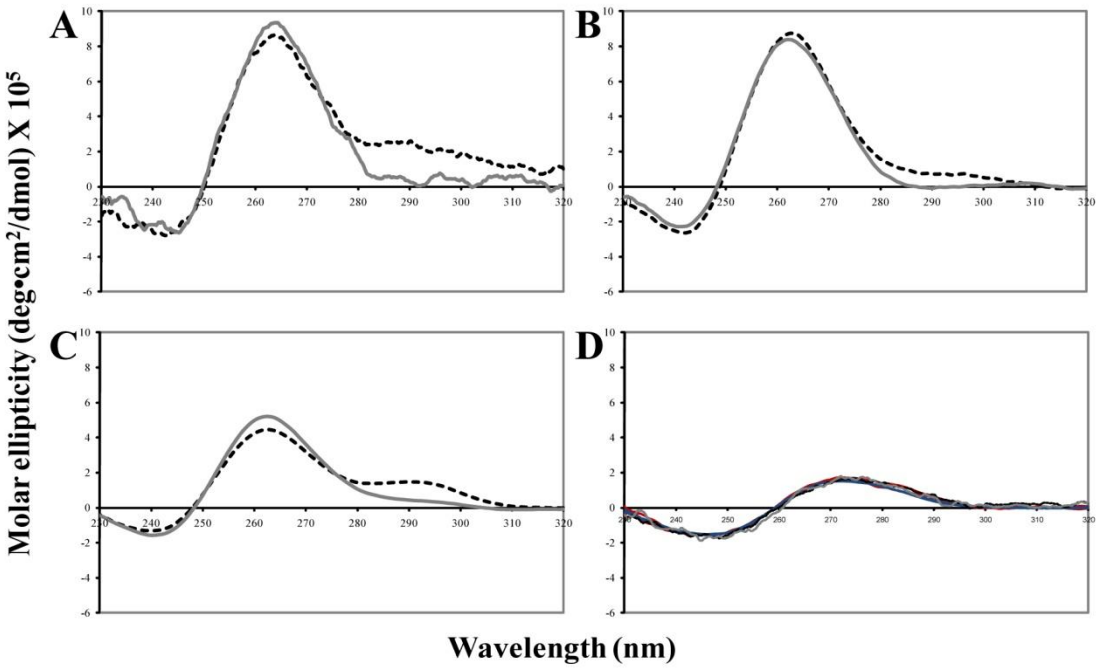

Figure 2.4: CD spectra of PS2.M, a G-quadruplex-forming oligonucleotide that has peroxidase activity when bound to heme.
All samples were prepared in 40 mM TrisOAc (pH 7.5), 25 mM KCl, 0.05% Triton X-100, 5% DMSO, ~0.5X TE buffer system. A) 0.1 µM PS2.M samples with or without added 1 µM hemin. B) 5 µM PS2.M samples with or without added 50 µM hemin. C) 50 µM PS2.M samples with or without added 150 µM hemin. D) Traces of all SS18 samples that reflect the conditions of the PS2.M samples. The dashed trace (- - -) shows DNA without added hemin and the solid gray line (—) shows DNA with added hemin.

The CD spectra of various concentrations of PS2.M demonstrate that PS2.M primarily forms a parallel G-quadruplex. A positive maximum at 260-265 nm and a negative maximum at 240-245 nm are indicative of a parallel G-quadruplex; a positive maximum at ~295 nm and a negative maximum at 260-265 nm are indicative of an anti-parallel G-quadruplex [87]. These characteristics are based on comparisons of data from

known G-quadruplexes and their strand orientations with their corresponding CD spectra [87]. However, all the samples without added hemin show a small shoulder around the 295 nm region which is indicative of an anti-parallel G-quadruplex.

This shoulder at 295 nm is most likely the result of a heterogeneous mixture of G-quadruplexes, where the dominant species is parallel, but some anti-parallel species exist in smaller quantities. It is unlikely that the 295 nm shoulder would exist due to the formation of a hybrid G-quadruplex structure with strands that are both parallel and anti-parallel to each other because the shoulder would lie closer to 270 nm [88]. When excess hemin was added to all PS2.M samples, the small shoulder at 295 nm decreased, which we attribute to hemin promoting PS2.M to fold into parallel G-quadruplexes from anti-parallel G-quadruplexes [78].

The CD spectra from panels A and B are very similar, which suggests that the mixture of species in 0.1 μM and 5 μM PS2.M samples may be similar as well. However, the 50 μM PS2.M sample shows a difference in the intensity of the positive 265 nm peak and negative 245 nm peak than the 0.1 μM and 5 μM PS2.M samples.

From the gels in Figure 2.2, one can notice that there is a change in the amount of intermolecular species as a function of PS2.M concentration. As a result, the lower intensity of the peaks in the CD spectrum of the 50 μM PS2.M samples may be the result of PS2.M folding into intermolecular G-quadruplexes. However, Lin *et al.* reported that an increase in intermolecular parallel G-quadruplexes causes an increase in the intensity of the peaks at 265 nm and 245 nm [89].

The discrepancy in results above may have several explanations. The intensity was normalized for the concentration of single stranded PS2.M and not the concentration

of tetrameric G-quadruplexes. Each tetrameric G-quadruplex requires four strands of DNA. The formation of tetrameric G-quadruplexes as compared to monomeric G-quadruplexes would reduce the effective amount of G-quadruplexes in the solution. The concentration of the tetrameric G-quadruplex is a quarter of the concentration of total single-stranded DNA. As a result, the molar ellipticity values for the high DNA concentration samples would be 4-fold larger as well. Another explanation stems from the empirical nature of CD spectroscopy for G-quadruplex investigation. The interpretation of the optical properties from CD spectra is quite controversial; therefore, hyperchromicity of a peak in one case may not be the same in another case [90, 91].

In addition to observing the changes in G-quadruplex strand polarity over several DNA concentrations, we also observed the impact of different monovalent cations on G-quadruplex formation by PS2.M. The use of either KCl or NaCl to stabilize the G-quadruplexes formed by PS2.M caused ethier parallel-stranded or anti-parallel-stranded G-quadruplexes to form. Figure 2.5 demonstrates that KCl concentrations of >10 mM lead to PS2.M forming a parallel G-quadruplex whereas NaCl promotes an anti-parallel G-quadruplex formation by PS2.M.

A similar cation specific effect was observed when an oligonucleotide derived from tandem repeats of the human telomeric sequence was exposed to either Na^+ or K^+ [92, 93]. However, despite the similarity in response of PS2.M and an oligonucleotide from the human telomeric sequence to the same cationic species, there is no definitive rule that dictates the specific strand orientation of a given G-quadruplex in response to different cations [25].

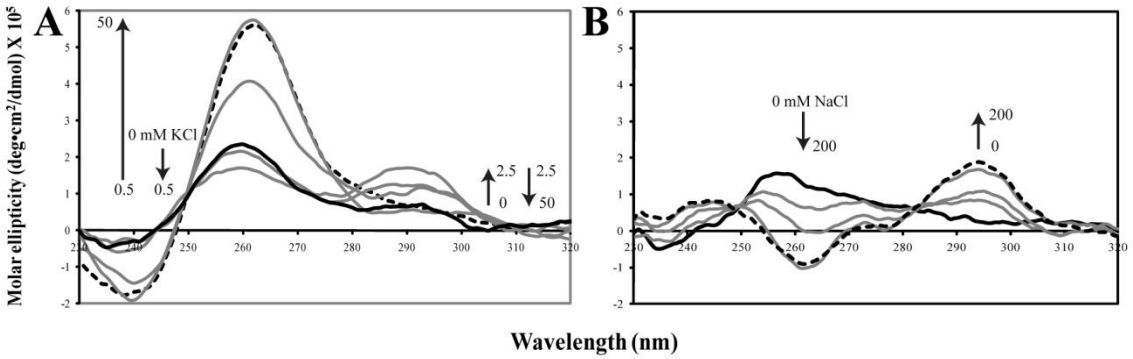

Figure 2.5: CD spectra of PS2.M in the presence of several salt conditions. All samples contained 10 µM PS2.M, 40 mM TrisOAc (pH 7.5), 0.05% Triton X-100, 5% DMSO, ~0.5X TE buffer system. A) CD spectra of PS2.M in the presence of various KCl concentrations. B) CD spectra of PS2.M in the presence of various NaCl concentrations. The heavy black line (—) is from the 0 mM salt condition and the dashed line (- - -) is the trace of the most concentrated salt sample.

In the case of NaCl, shown in panel B, PS2.M folds into a G-quadruplex structure with increasing anti-parallel characteristics as the NaCl concentration was increased to 200 mM. This observation stems from the appearance of the positive 295 nm peak and the negative 260 nm peak.

The addition of KCl creates a more complicated outcome. From the original 0 mM KCl sample to the final 50 mM KCl sample, PS2.M folds into a parallel G-quadruplex as defined by the positive 265 nm peak and the negative 245 nm peak. However, between 0 to 2.5 mM KCl incubation conditions, a positive peak at 295 nm grows in intensity which is indicative of the formation of anti-parallel G-quadruplexes. An anti-parallel G-quadruplex was proposed by our group with two G-quartet stacks [70].

If the parallel G-quadruplex structure contained three G-quartet stacks instead of two, the formation of the parallel G-quadruplex would require an increased KCl concentration. The mechanism of PS2.M folding, as depicted in Figure 2.6, demonstrates

that the anti-parallel-stranded structure on the left folds quicker because there is only a single potassium ion that is needed to stabilize the formation of two G-quartets. The parallel-stranded structure on the right requires two potassium ions to form a G-quadruplex with three G-quartet stacks; therefore, it is a slower folding pathway.

Even though PS2.M can fold into an anti-parallel G-quadruplex, Travascio *et al.* have demonstrated that PS2.M is not an active peroxidase in anti-parallel G-quadruplex folding conditions, KCl concentrations lower than 5 mM or in NaCl conditions [62]. Along with evidence from other groups, the anti-parallel G-quadruplexes are thought to be poor peroxidase enzymes, most likely due to their poor heme binding ability [78-80].

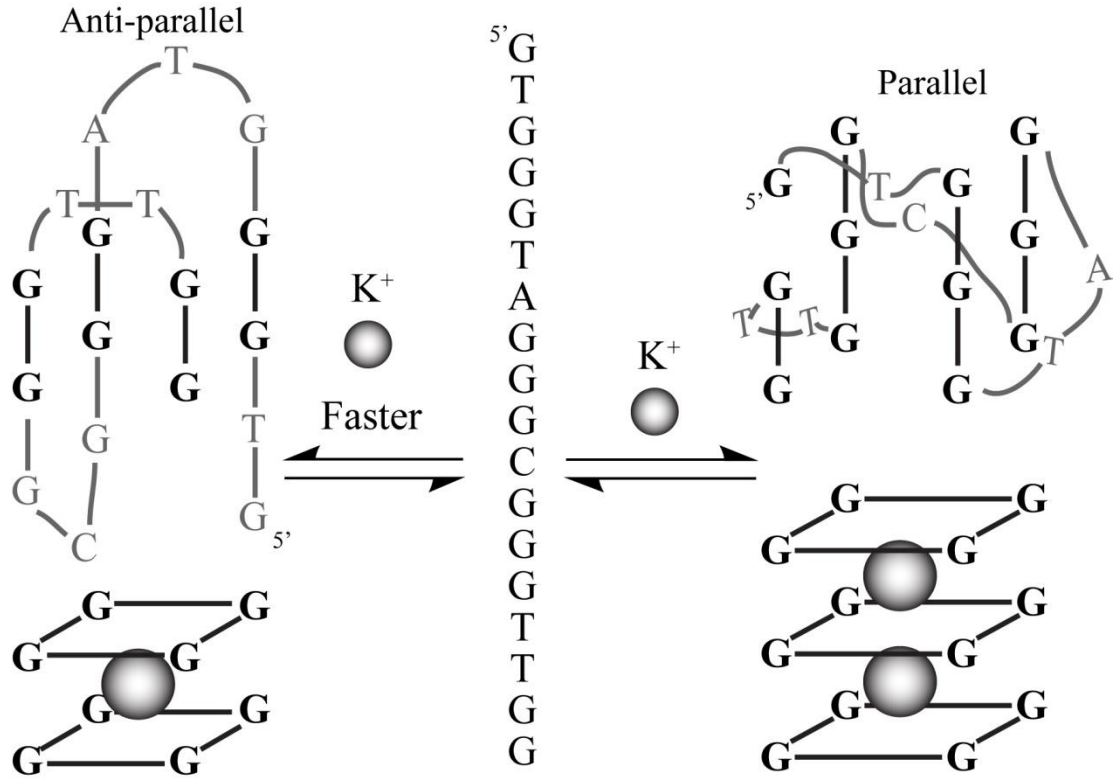

Figure 2.6: Scheme of PS2.M folding in the presence of potassium ions.

2.3.3 Using a methylation protection assay to probe the folding of PS2.M

Methylation protection experiments continue to be a hallmark in identifying and analyzing G-quadruplexes. It is a technique that probes the reactivity of the nitrogen at the seventh position on guanines, as illustrated in Figure 2.7. When the Hoogsteen face of guanines are involved in hydrogen bonding in a G-quartet, as shown in Figure 1.1, the reactivity of N7 is lower than non-H-bonded N7 guanines. Once methylated, the guanine becomes base labile which allows us to identify the guanines that are not participating in the formation of a G-quartet.

After methylation, the different species in the samples were separated on non-denaturing gels, which allows us to observe the susceptibility of each species to DMS treatment. Each band, as seen in panel B and C of Figure 2.8, was cut out and the contents within the bands was eluted in TE buffer. Subsequently, these samples were treated with piperidine to cleave the phosphodiester backbone of DNA where a guanine has been methylated. The piperidine treated samples were run in a denaturing gel along with a ladder that marks the mobility of the products for every guanine methylation. The products of DMS treatment, as seen in panel A of Figure 2.8, are representative of the guanines that were reactive to DMS treatment; therefore, these guanines are not participating in G-quartet formation.

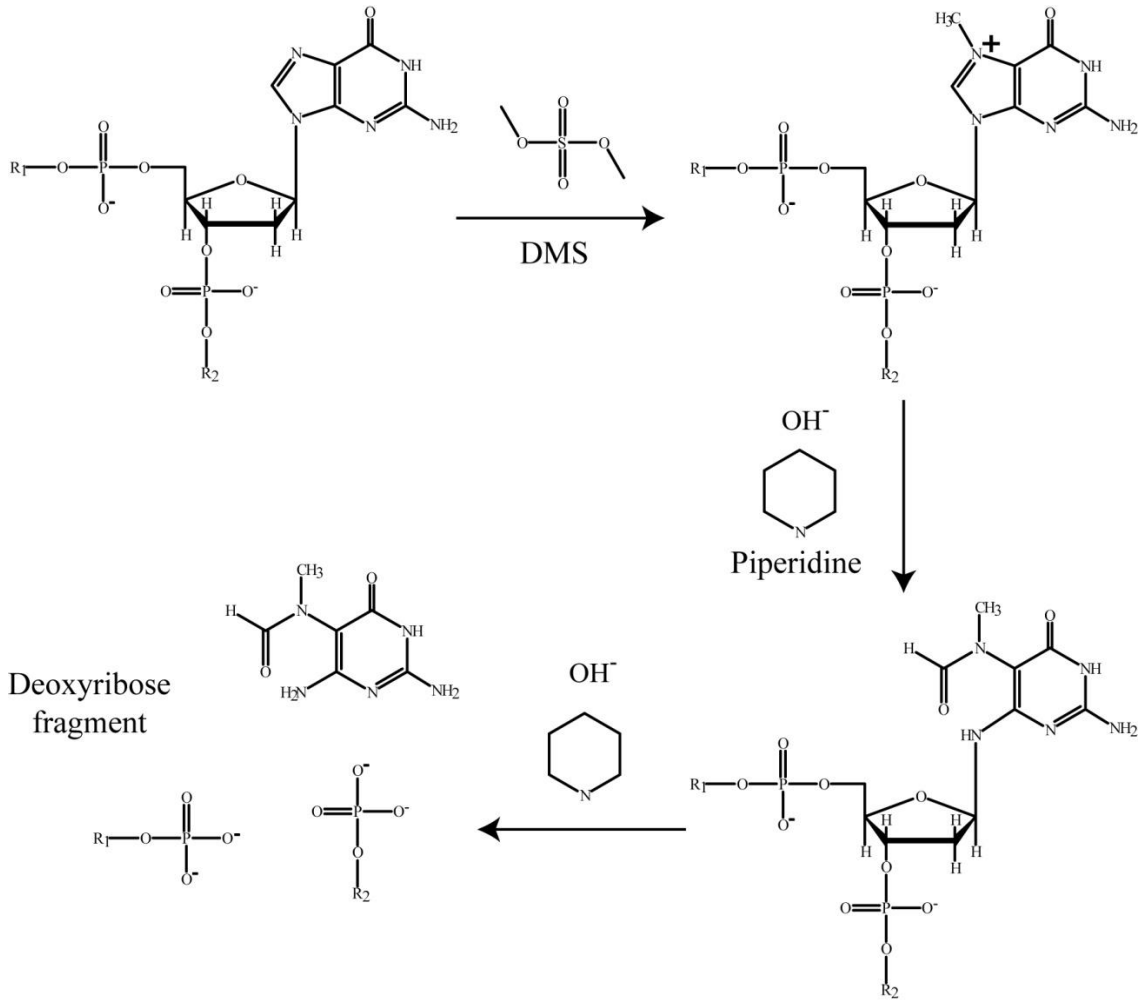

Figure 2.7: Guanine specific reaction with dimethylsulfate.
Adapted from Bloomfield et al. [83].

In Figure 2.8, the methylation protection of different bands from panels B and C are sequenced in panel A. Band P0.1-21-1 is the most prominent band in the samples that contain 0.1 μM PS2.M in 25 mM KCl incubated in 21ºC. This particular band reflects an intramolecular species that has all of its guanines protected from DMS methylation. In Figure 2.4, the CD spectroscopy studies demonstrated that parallel G-quadruplex structures dominate the mixture during all examined conditions. This may suggest that P0.1-21-1 is a unimolecular parallel G-quadruplex depicted in panel D. Studies on other guanine-rich sequences have demonstrated that a short linker length of two or less

nucleotides between G-tracts favor the formation of a parallel unimolecular G-quadruplex [94, 95]. In PS2.M's case, the linker lengths are either 1 or 2 nucleotides; therefore, it is highly probable that PS2.M folds into an intramolecular parallel G-quadruplex.

Band P0.1-21-2 on the other hand does not show complete protection from DMS methylation. Guanines 1, 5, 10 and 12, all demonstrate increased reactivity towards DMS which suggests that these guanines are located on the loops in the G-quadruplex structure. This reactivity pattern is the same as previous results from our lab and two possible models were described to explain those results [70]. Both models were anti-parallel unimolecular G-quadruplex structures, and the difference between the two models involves a diagonal loop in place of a lateral loop.

Band P0.1-21-2 is less than 10% of the total DNA in the solution which may explain the presence of a small shoulder at 295 nm in the CD spectra of PS2.M samples. However, another model that fits the methylation protection patterning is a parallel unimolecular G-quadruplex that contains loops with 3 and 2 nucleotides seen in Figure 2.8. Since the results from CD spectroscopy show that the majority of the G-quadruplexes in the PS2.M samples are parallel-stranded, it is reasonable to suggest that the species in band P0.1-21-2 is parallel-stranded as well.

In the case of the intermolecular species that reside in the slow migrating bands, P0.1-4-1, P50-21-1 and P50-4-1, these may all represent the same species. All species from the slow migrating bands were not reactive to DMS. The mobility of the band suggests that the species within it are intermolecular G-quadruplexes. Since all guanines are non-reactive to DMS, this suggests that all guanines participate in G-quartet formation.

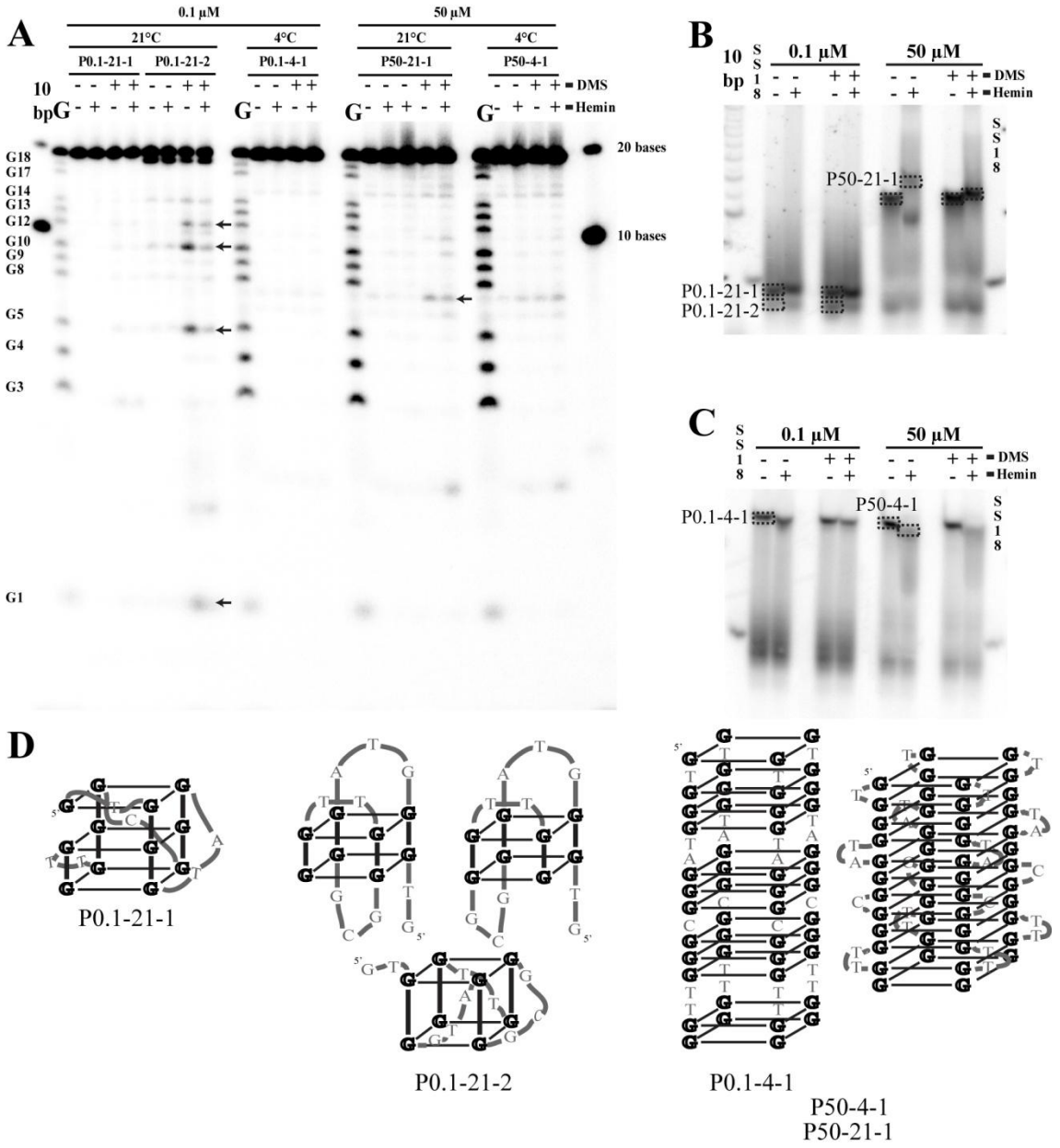

Figure 2.8: Methylation protection assay to probe the structure of PS2.M.
A) A 15% denaturing gel with PS2.M samples treated with DMS. Samples were obtained after separation on 20% native gels shown in B and C. The numerical codes correspond to bands in B and C; the G lane is a ladder that marks the guanines in the sequence; the 10 bp lane contains the 10 base-pair ladder. The plus sign (+) denotes lanes that contained DNA samples incubated with hemin prior to DMS treatment. The minus sign (–) denotes lanes that contained DNA samples not incubated with hemin prior to DMS treatment. B) Native gel in 21ºC. C) Native gel in 4ºC. The SS18 lane contains a non-G-quadruplex-forming single stranded control. D) Possible structures of each band obtained from gels B and C after analysis of methylation protection data.

Two possible tetrameric models are depicted in panel D of Figure 2.8. One structure involves continuous stacking of all the G-quartets that results in the linker nucleotides between guanine tracts to protrude outwards to form a loop. The other structure involves non-continuous G-quartet stacking where the linker nucleotides are not forced away from the core of the G-quadruplex structure. P50-21-1 and P50-4-1 are most likely the former, while P0.1-4-1 is most likely the latter structure.

The guanines of P50-21-1 and P50-4-1 are not reactive to DMS; however, the linker nucleotides are more reactive to base treatment than the same linker regions in P0.1-4-1. The continuous G-quartet stacking model would force the linker nucleotides away from the core of the G-quadruplex, exposing the linker nucleotides to the solvent. The increased solvent exposure of the linker nucleotides can increase their sensitivity to base treatment and become more labile. However, when the samples were treated with piperidine, the samples were ethanol precipitated (desalted) and they were heated at 90ºC. This treatment should denature the G-quadrulex into linear single strands, but the sheer number of G-quartets stacked together may have allowed some of this tetrameric species to persist during the base treatment. As a result, it is difficult to make a distinction between the continuous and non-continuous G-quartet stacking intermolecular/ multimeric species.

The addition of hemin also has different effects on the different G-quadruplex species. Band P0.1-21-2 shows a decrease in the reactivity of the guanines when hemin was added to the samples. The three proposed structures for band P0.1-21-2 have guanines in the loops, which are exposed to the solvent. The addition of the hemin molecule may compact the folded G-quadruplex structure; the loops may be sequestered

within the grooves of the backbone of the G-quadruplex, which reduces the reactivity of the guanines to DMS. In contrast, for band P50-21-1, the intermolecular species at 21°C has the opposite effect when hemin was added to the samples. The reactivity of the linker regions increased with the addition of hemin. When hemin was added to the samples, the linkers became more exposed to solvent because the hemin molecule may have compacted the structure of the non-continuous tetrameric G-quadruplex to the continuous tetrameric G-quadruplex. These results demonstrate that hemin may play a role in the overall folding of PS2.M, perhaps *via* an induced fit model as opposed to a lock and key model.

2.3.4 Investigating the peroxidase active species of PS2.M by observing the kinetics of ABTS oxidation at 4ºC and 21ºC

In order to investigate the structure formed by PS2.M that catalyzes peroxidase reactions when bound to heme, we compared the ability of PS2.M-heme complex to oxidize ABTS at 4ºC and 21ºC. For all G-quadruplex-forming oligonucleotides presented in Figure 2.9, the initial rates for ABTS oxidation were greater for samples in 21ºC than in 4ºC. The inset in panel C shows the initial rates of ABTS oxidation by SS18, a non-G-quadruplex-forming oligonucleotide control, which oxidizes ABTS at a much slower rate than the G-quadruplex-forming oligonucleotide samples.

From the gel experiments presented in Figure 2.1, the band patterning for PS2.M_mut and CatG4 changes less over a range of DNA concentrations, KCl concentrations and temperature conditions than PS2.M. The PS2.M folding pattern changes drastically from a predominantly intramolecular/unimolecular structure to a

predominantly intermolecular/multimeric structure when it is incubated at low DNA concentrations at 21ºC and 4ºC with added hemin.

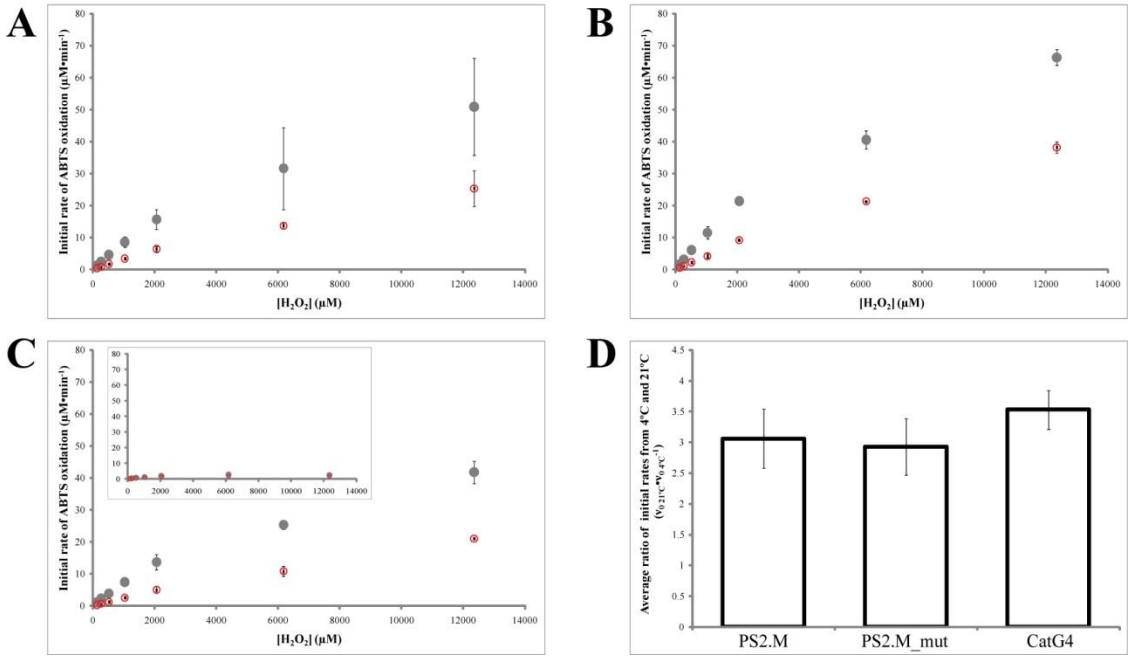

Figure 2.9: Kinetics of ABTS oxidation by G-quadruplex-forming oligonucleotides in the presence of hemin at 4ºC and 21ºC.
The initial rate of ABTS oxidation (μM•min^{-1}) by G-quadruplexes bound to hemin is plotted over a range of hydrogen peroxide concentrations (μM) for A) PS2.M. B) PS2.M_mut. C) CatG4. C also contains an inset of SS18, a non-G-quadruplex single stranded DNA. D) The average ratio of initial rates at 21ºC and 4ºC for 125 μM and 250 μM H_2O_2. The solid grey circles (●) are the initial rates at 21ºC. The hollow circles with red outline (○) are the initial rates at 4ºC. The final solution contained 1 μM DNA (excess DNA was used to completely bind all the hemin), 0.1 μM hemin, 0-12 mM H_2O_2, 5 mM ABTS, 50 mM HEPES-NH_4OH (pH 8.0), 20 mM KCl, 0.05% Triton X-100, and 2% DMSO.

By comparing ABTS oxidation at low H_2O_2 concentrations, 125 μM and 250 μM, we can compare the catalytic efficiency of the enzyme at 21ºC and 4ºC because the initial rates at low H_2O_2 concentrations increase linearly as a function of H_2O_2 concentration. Briefly, the ratio of the initial rates for PS2.M at 21ºC over 4ºC was averaged between both 125 μM and 250 μM H_2O_2 concentrations. We expected the ratio of catalytic

efficiencies between reactions at 21ºC and 4ºC for PS2.M and the other two DNAzymes (PS2.M_mut and CatG4) to be different because there is a larger change in the mixture of structures that is formed by PS2.M than the other two DNAzymes.

Panel D of Figure 2.9, shows the initial rate ratio of ABTS oxidation at 21ºC and 4ºC between PS2.M, PS2.M_mut and CatG4 to be statistically similar. The ratios were 3.1±0.5, 2.9±0.5, and 3.5±0.3 for PS2.M, PS2.M_mut and CatG4 respectively. Generally, a 10ºC decrease in temperature causes a 2-fold decrease in the reaction rate; therefore, a roughly 3-fold decrease in the reaction rate is reasonable for a drop in temperature from 21ºC and 4ºC. Since there is no statistical difference between the temperature-dependent-ratio of reaction rates between PS2.M and the other two DNAzymes, this suggests that the amount of catalytically active species in PS2.M samples is the same at 21ºC and 4ºC.

In Figure 2.1, the gels clearly show a substantial difference in PS2.M band patterning between the PS2.M lanes in 21ºC and 4ºC, which would suggest a difference in the distribution of structures formed by PS2.M at the two temperature conditions. However, it is possible that both tetrameric G-quadruplexes and monomeric G-quadruplexes formed by PS2.M are capable of binding heme. Other studies have demonstrated that multimeric and unimolecular parallel G-quadruplexes have peroxidase-like activity when bound to heme [79, 80, 82]. Therefore, as long as there is the same number of heme-bound complexes at 21ºC and 4ºC, there would be the same number of catalytically active species as well.

The amount of DNA in the different solutions is 10-fold greater than the amount of heme molecules; however, when PS2.M folds into a tetrameric species there would

only be a 2.5-fold excess of tetrameric species to hemin. Several factors may help explain how a decrease in the effective molecules that can bind hemin would allow for a similar amount of catalytically active molecules. At low temperature conditions, it is energetically more favourable for heme to form a complex with G-quadruplex species; therefore, a smaller amount of aptamer is needed to bind heme. This is reflected by the lower binding constants for hemin binding for PS2.M, PS2.M_mut and CatG4 at 4°C than at 21°C, as shown in Table 2.2. The binding constants were calculated from changes in the soret band (maximum absorbance at 404 nm) of the heme spectra during titration of the oligomer of choice with a fixed amount of hemin, 0.5 μM. As a result, this 2.5-fold excess of aptamer molecules to heme may be sufficient to give the same proportion of catalytically active PS2.M species at 4ºC and at 21ºC as PS2.M_mut and CatG4.

Table 2.2: Binding constants of various G-quadruplex-forming oligonucleotides

Sequences	**K_d (nM)**	
	21ºC	**4ºC**
PS2.M	312	144
PS2.M_mut	258	143
CatG4	115	41

2.3.5 Studies to determine the pK_a values of water-hemin complexes in the presence of various DNA oligonucleotides.

In previous research by our group, Travascio *et al.* demonstrated that PS2.M reduced the acidity of the iron-bound water molecule [67]. This has been suggested as one of the possible mechanisms that enhance the peroxidative capabilities of heme.

When heme is in solution, water molecules coordinate with the ferric iron atom. The rate of water dissociating from the water-heme interaction in myoglobin has been measured to be roughly 10,000 s^{-1} [96, 97]. In comparison, the dissociation rate of hydroxide from the hydroxide-heme complex for horseradish peroxidase was measured to be less than 100 s^{-1} [98]. As depicted in Figure 2.10, the dissociation of water from heme is much quicker than the dissociation of hydroxide from heme. Therefore, when there is a hydroxide molecule coordinated to the iron in heme, the hydroxide molecule obstructs the entry of hydrogen peroxide molecule for a longer period of time than if water was coordinated to the heme molecule. If hydrogen peroxide was unable to interact with the iron atom of heme, there would be no Compound I formation.

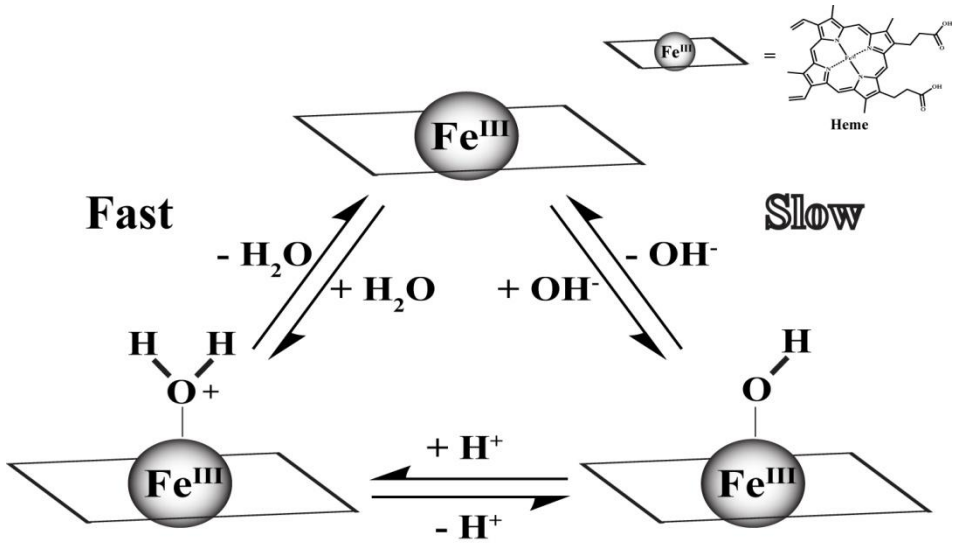

Figure 2.10:Acid-alkaline transition of water molecules bound to the ferric iron of heme

Heme enzymes, like horseradish peroxidases, provide an environment for heme that raises the pK_a of the water molecule that coordinates with the iron atom of heme. As a result, at physiological pH, more water molecules coordinate with heme than hydroxide molecules. Therefore, increasing the pK_a of the alkaline transition of peroxidases is

important. For instance, the pK_a of horseradish peroxidase is 10.8-11.0 compared to 3.0-4.0 for free heme in detergent [28, 67].

Previously, the reported pK_a of the hydrogen on the water-heme complex when bound to PS2.M was 8.7; the present study, depicted in Figure 2.11, measured the pK_a of the water-heme complex when bound to PS2.M to be 9.1. The pKa values for both PS2.M_mut and CatG4 were 9.3 and 9.7 respectively. In comparison, heme in solution with detergent and non-G-quadruplex forming oligonucleotide, SS18, the pK_a for the alkaline transition is 3.5. These results further support the idea that one of the mechanisms that enhances the peroxidative ability of heme is by increasing the pK_a of the alkaline transition. G-quadruplexes formed by PS2.M, PS2.M_mut and CatG4 perform this task to a similar extent when compared to metmyoglobin and methemoglobin, but not to the same extent as horseradish peroxidase [67].

Even though the alkaline transition of heme was the only mechanism that was tested in these studies, there may be numerous other features that G-quadruplexes may provide heme to enhance the peroxidase capabilities of heme. For instance, Travascio *et al.* suggested that PS2.M may protect heme from self-oxidation by Compound I [68]. Other peroxidative enhancing strategies include, but are not limited to distal residues that facilitate peroxide binding, distal residues that facilitate reducing substrate binding and distal residues that process the peroxide to form Compound I.

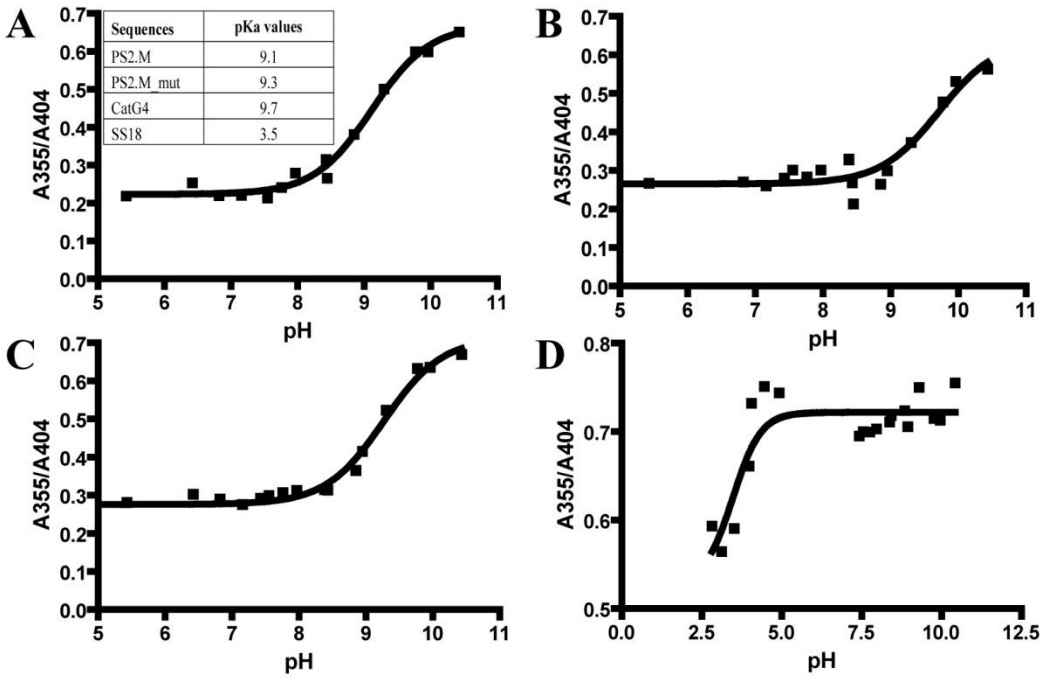

Figure 2.11:Plots of ratios of absorbance at 355 nm and 404 nm over a range of pH values to determine the pK_a values of water-hemin complexes.
Graphs to determine the pK_a values of water-hemin complexes in the presence of A) PS2.M, B) PS2.M_mut, C) CatG4 and D) SS18. SS18 is a non-G-quadruplex-forming oligonucleotide control. The inset in panel A contains a table of experimentally obtained pK_a values. The final solution contained 0.5 µM hemin, 3 µM DNA, 50 mM buffer, 25 mM KCl, 0.05% Triton X-100, and ~2 % DMSO.

2.4 Chapter conclusion

In our structural studies, we have attempted to elucidate the structure of the active species of PS2.M that is capable of binding heme and providing enhanced peroxidative catalysis. Different groups have provided evidence for possible structures formed by PS2.M, we brought clarity to these results by thoroughly investigating the folding of PS2.M under various conditions [70, 81].

PS2.M folds in a highly polymorphic manner and forms multiple types of G-quadruplexes. In order to form G-quadruplexes, monovalent cations are required to

neutralize the concentrated negative dipoles of oxygen atoms. PS2.M varies in its G-quadruplex strand orientation in the presence of specific monovalent cations.

In sodium, PS2.M folds into antiparallel G-quadruplexes; while in potassium, PS2.M begins by folding into anti-parallel G-quadruplex structures, but parallel G-quarduplexes are favoured when the concentration of KCl is >2.5 mM KCl. The anti-parallel G-quadruplex structure formed by PS2.M folds in lower amounts of KCl because it has only two G-quartets to stabilize as compared to the proposed parallel G-quadruplex structure that contains three G-quartets.

These structural features were supported by methylation protection studies that demonstrated the existence of complete DMS-protected species and partially DMS-protected species. In addition to the intramolecular G-quadruplex species, multimeric G-quadruplexes also exist in the mixture. All guanines in the multimeric species participate in forming G-quartets, which increases the amount of bonds formed as compared to intramolecular G-quadruplexes. The proposed tetrameric G-quadruplexes are enthalpically favoured; however, the assembly of a multiple component structure is entropically unfavourable. As a result, decreasing the temperature of the environment minimizes the entropic component and favours the formation of the tetrameric G-quadruplex. In addition to the change in temperature, the increase in monomer concentration also increases the amount of tetramer formation by shifting the equilibrium towards the formation of the tetrameric G-quadruplex.

In the midst of elucidating the complex folding pattern of PS2.M, we also attempted to identify the structure that binds heme and enhances the peroxidative ability of heme. The comparison of ABTS oxidation at both 4ºC and 21ºC for PS2.M and the

other G-quadruplex and non-G-quadruplex forming oligonucleotides showed that the proportion of catalytic species was the same for all G-quadruplex-forming oligonucleotides at 4ºC and 21ºC. Since non-denaturing gels show that the folded structures of PS2.M are more temperature sensitive than the other G-quadruplex-forming sequences, the above results demonstrate that there is the same amount of catalytically active species in the PS2.M samples at 4ºC and 21ºC. This suggests that the peroxidative activity may be generated by either a common structure of similar concentration that exist in both temperature conditions or that the structures that form in different proportions in the two temperature conditions can bind heme equally in solution. The latter reasoning is more likely, as many G-quadruplexes of different shapes and sizes have been demonstrated to have peroxidative ability when bound to heme [78-80].

The reason for the enhanced peroxidative ability afforded by G-quadruplexes to heme may be explained by the alkaline transition of the water-heme complex. All three G-quadruplex-forming oligonucleotides, PS2.M, PS2.M_mut, and CatG4 reduce the acidity of the complex. The increased pK_a of the water-heme complex when bound to G-quadruplexes means that the hydroxide-heme complex is small in quantity at physiological pH. The water-heme complex dissociates faster than the hydroxide-heme complex; therefore, Compound I formation is less impeded under conditions favouring the water-heme complex than the hydroxide-heme complex.

3: Exploration of a new catalytic property of nucleoheme complexes

3.1 Introduction

Peroxidases catalyze 1-electron oxidation reactions, but numerous peroxidases can also perform some 2-electron oxidation reactions as well [99, 100]. However, peroxidases require hydrogen peroxide (peroxygenation) to form the iron-oxo species, whereas, monooxygenases such as cytochrome P450 can activate molecular oxygen (monooxygenation) to form the same higher energy species called Compound I [99, 100].

Once Compound I is formed, two distinct mechanisms for 2-electron oxidation can proceed. These two mechanisms are depicted in Figure 3.1, one route follows the direct transfer of oxygen to the substrate; thus, using both oxidizing equivalents of oxygen simultaneously to perform a 2-electron oxidation [99]. In this mechanism Compound I, Fe(IV) with one oxidizing equivalent delocalized on the porphyrin ring is directly reduced to its resting state, Fe(III) [99]. The second mechanism involves two successive 1-electron oxidations taking place to return Compound I back to Fe(III) [99]. In this mechanism the oxygen is transferred *via* Compound II, Fe(IV), to return to its resting state [99]. There is evidence for both mechanisms, but the latter oxygen rebound mechanism is favored in the cytochrome P450 community [99].

Since protein peroxidises are capable of 2-electron oxidations, we wanted to examine if PS2.M-hemin was capable of a similar function. Peroxygenase activity was investigated using three classic 2-electron oxidation substrates: thioanisole, indole, and

styrene. Furthermore, it has been demonstrated that many DNA G-quadruplexes are capable of catalyzing the 1-electron oxidation of ABTS [77]. We would like to determine if other DNA and RNA oligonucleotides that fold into G-quadruplexes can catalyze 2-electron oxidation reactions as well. The particular 2-electron oxidation reaction of interest is characterized by transfer of an oxygen atom from hydrogen peroxide, *via* Compound I, to the substrate. The following chapter contains published results from our various studies [101].

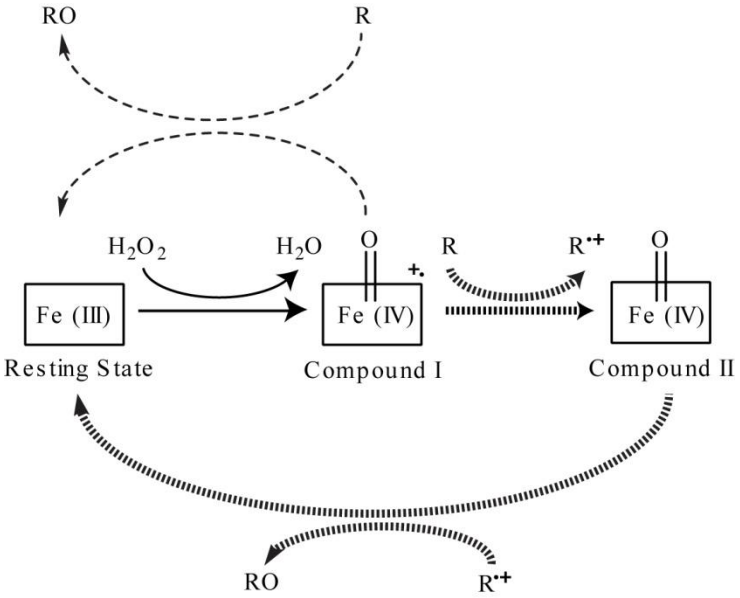

Figure 3.1: Scheme of the two possible oxygen transfer mechanisms.
Once Fe (III) heme is activated by hydrogen peroxide to form Compound I, there are two routes that can lead to oxygen transfer to the substrate (R). The direct oxygen insertion mechanism is depicted by the dashed lines (- - -) and the oxygen rebound mechanism is depicted by the scaled lines (|||||).

3.2 Materials and methods

3.2.1 Materials

All DNA was purchased from Integrated DNA Technologies, Inc. All RNA was purchased from University Core DNA Services (University of Calgary). The sequences of all DNAs and RNAs are given in Table 3.1. All nucleic acids were purified by preparative gel electrophoresis, eluted, ethanol precipitated, and then stored dissolved in TE buffer [10 mM Tris, pH 7.5, and 0.1 mM ethylenediaminetetraacetate (EDTA)], as described in section 2.2.2. All chemicals were purchased from Sigma-Aldrich, unless specified otherwise. Hemin was purchased from Porphyrin Products (Logan, Utah). Hydrogen peroxide-$^{18}O_2$ was purchased from Icon Isotopes (Summit, New Jersey).

Table 3.1: DNA and RNA sequences[a,b]

Name	Sequence
dsDNA	5'-TTT AGT CGA CCT CGC CCC CGC TGC CAT AGT GAC ACA-3' 3'-AAA TCA GCT GGA GCG GGG GCG ACG GTA TCA CTG TGT-5'
SS18	5'-AAT ACG ACT CAC TAT ACT-3'
rSS18	5'-AAU ACG ACU CAC UAU ACU-3'
PS2.M	5'-GTG GGT AGG GCG GGT TGG-3'
rPS2.M	5'-GUG GGU AGG GCG GGU UGG-3'
CatG4	5'-TGG GTA GGG CGG GTT GGG AAA-3'
Hum4	5'-TTA GGG TTA GGG TTA GGG TTA GGG-3'
rHum4	5'-UUA GGG UUA GGG UUA GGG UUA GGG-3'
c-Myc	5'-TGA GGG TGG GGA GGG TGG GGA A-3'
Bcl-2	5'-GGG CGC GGG AGG AAG GGG GCG GG-3'

[a] *RNA has a "r" prefix*
[b] *Double stranded DNA has a "ds" prefix*

3.2.2 Time course of thioanisole sulfoxidation

We added 32 µL of 100 µM DNA and 10 µL of 100 µM hemin in DMF to 500 µL of 2X buffer containing 80 mM HEPES-NH_4OH (pH 8.0), 40 mM KCl, 0.1% Triton

X-100, 2% DMF in a 1.5 mL glass vial. We added ddH_2O to make up the volume to 980 µL. We incubated the solution for 5 minutes in room temperature to allow for aptamer-hemin binding if binding is possible. We added 10 µL of 20 mM thioanisole dissolved in DMF to the mixture and vortexed the reaction mixture.

Prior to the start of the reaction we removed a 99 µL aliquot for time 0 and treated it as described later. We initiated the reaction by the addition of 9 µL 100 mM H_2O_2. We incubated The 900 µL volume containing 0.2 mM thioanisole, 1 µM hemin in DMF, 3 µM DNA, 1 mM H_2O_2, and buffer (40 mM HEPES-NH_4OH (pH 8.0), 20 mM KCl, 0.05% Triton X-100, 3% DMF) at room temperature.

We removed 95 µL aliquots of the reaction mixture at 0, 15 s, 30 s, 1 min, 2 min, 5 min, and 30 min after initiation of the reaction. We added 5 µL of 1 mM benzophenone as an internal standard to each aliquot prior to addition of CH_2Cl_2. We added 200 µL CH_2Cl_2 to quench the reaction and to extract the contents of the reaction mixture.

We analyzed the organic layer by gas chromatography on a Hewlett Packard Model 5890 system equipped with a flame ionization detector. We employed a DB-5MS column (0.32 mm i.d. x 50 m) for the analysis. We programmed the column temperature to rise 20°C/min from 80°C to 300°C and to hold at 300°C for 4 min. We quantified the sulfide and the sulfoxide using standard curves with benzophenone as the internal standard.

The retention times of the components were as follows: thioanisole, 4.8 min; thioanisole sulfoxide, 6.8 min; benzophenone, 9.0 min. We established the identity of the thioanisole sulfoxide peak by elution with commercially available thioanisole sulfoxide (methyl phenyl sulfoxide) by gas-chromatography.

3.2.3 Source of the oxygen in thioanisole sulfoxide

We prepared reaction mixture as described above, in section 3.2.2. However, we initiated reaction mixtures with PS2.M with either $H_2{}^{16}O_2$ or $H_2{}^{18}O_2$. The SS18 negative control reaction contained $H_2{}^{16}O_2$.

We took 95 µL aliquots after 2 and 4 hours; we added 5 µL 1 mM benzophenone as an internal standard. We quenched the reactions with 200 µL CH_2Cl_2 and analyzed the organic layer with a Varian 3800 gas chromatograph equipped with a Varian Saturn 2000 ion trap. We determined the percentage of ^{18}O incorporation by the integration of the contents in the $H_2{}^{18}O_2$ reaction with a m/z of 142 compared to the m/z of both 140 and 142.

3.2.4 Stereochemistry of thioanisole sulfoxidation

We prepared the reaction mixture as described above, in section 3.2.2 with the exception that we scaled the reaction mixture up to 2 mL. We quenched the reaction at 4 hours with 4 mL CH_2Cl_2 and removed the organic layer. We determined the ratio of the sulfoxide enantiomers by chiral-phase high-pressure liquid chromatography. We dried down and redissolved the samples in 500 µL hexanes.

We analyzed the samples on an Agilent 1200 series HPLC system with a Chiracel OD column (0.46 cm i.d. x 25 cm, Daicel Chemical Industries, Ltd.). We monitored the eluents at 254 nm with a variable wavelength detector. We eluted the column isocratically at a flow rate of 1 mL/min with 95:5 hexanes:isopropanol for 35 min. Fruetel *et al*. previously identified the *S*- and *R*- sulfoxide enantiomers [102]. The retention times of the *S* and *R* sulfoxide enatiomer were 21.9 min and 28.8 min respectively.

3.2.5 Para substituted thioanisole sulfoxidation

We used the procedure described above in section 3.2.2. The para-substituted substrates include 4-chlorothioanisole, 4-nitrothioanisole, 4-methoxythioanisole, and 4-methylthioanisole. We analyzed Samples extracted with CH_2Cl_2 by GC/FID as described above. We used a different column temperature program for the analysis of some para-substituted thioanisole reactions.

For 4-chlorothioanisole: we programmed the column temperature to rise 20°C/min from 120°C to 300°C and to hold at 300°C for 4 min. For 4-nitrothioanisole and 4-methylthioanisole: we programmed the column temperature to rise 20°C/min from 100°C to 300°C and to hold at 300°C for 4 min. For 4-methoxythioanisole: we programmed the column temperature to rise 10°C/min from 100°C to 230°C, then we ramped up the temperature to 300°C at 70°C/min and held it at 300°C for 4 min.

The retention times of the components for the 4-chlorothioanisole reactions were as follows: 4-chlorothioanisole, 4.7 min; 4-chlorothioanisole sulfoxide, 6.3 min; benzophenone, 7.1 min. The retention times of the components for the 4-nitrothioanisole and 4-methylthioanisole reactions were as follows: 4-methylthioanisole, 4.8 min; 4-methylthioanisole sulfoxide, 6.8 min; 4-nitrothioanisole, 7.6 min; benzophenone, 8.0 min; 4-nitrothioanisole sulfoxide, 8.8 min. The retention times of the components for the 4-methoxythioanisole reactions were as follows: 4-methoxythioanisole, 7.8 min; 4-methoxythioanisole sulfoxide, 11.5 min; benzophenone, 11.8 min.

We established the identity of the sulfoxide peaks by the analysis of 15 second samples with a Varian 3800 gas chromatograph equipped with a Varian Saturn 2000 ion

trap. We determined the initial rates of each reaction by the conversion of the sulfide over the initial 15 seconds.

3.2.6 Hammett analysis of thioanisole sulfoxidation

We obtained the substituent coefficient (σ and σ^+) values for para-substituted thioanisole from Issac's *Physical Organic Chemistry* [103]. The plot of log (V) versus σ or σ^+ is a linear relationship where the slope of the graph provides the reaction constant ρ. The V value is the ratio between the initial rate of the production of the *p*-thioanisole sulfoxide and the initial rate of the production of the thioanisole sulfoxide under the same conditions discussed in section 3.2.5. We obtained the values for the different parameters from fitting the data to the Hammett equation.

$$\log V = \sigma\rho \text{ or } \log V = \sigma^+\rho$$

3.2.7 Thioanisole sulfoxidation by various DNA and RNA sequences

We followed the procedure described above, in section 3.2.2. Most reactions contained the same nucleic acid concentration as described above (3 µM). Exceptions included the Hum4 and rHum4 reaction mixtures, which contained 120 µM DNA or RNA by the addition of 24 µL of 5 mM DNA or RNA to make up the 1 mL reaction mixture. We performed The dsDNA and SS18 control reactions with both 3 µM and 120 µM single or double stranded DNA. We took Aliquots of the reaction mixture at 0 min, 2 min and 30 min and treated them as described above.

3.2.8 Indole oxidation reactions

Final concentrations of all components in the reaction mixture were: hydrogen peroxide (1 mM), indole (1 mM), DNA (25 μM) and hemin (10 μM) in the reaction buffer (40 mM HEPES-NH4OH (pH 8.1), 20 mM KCl, 0.05% Triton X-100, 1% DMF). At specified times, we added 95 μL of reaction mixture to 5 μL of 1 mM benzophenone standard and then immediately froze this on dry ice to stop the reaction.

We then thawed samples and ran them on HPLC for analysis. We performed the analysis with a Zorbax Eclipse 3.0 X 50 mm, 1.8 micron, octadecylsilane column, using gradients of ddH_2O (A) and CH_3CN (B). 0-1 min: 85% A; 1-5.33 min: program from 85% to 10% A; 5.33-7 min: program from 10% to 0% A; 7-10 min: hold at 0% A. We made Traces at 255 nm for peak detection, and recorded online spectra (200 to 800 nm) using the G1315B DAD (Agilent 1100 series). Characterization of products was done by HPLC/MS analysis and comparing the A255 traces detected with a G2315C DAD SL (Agilent 1200 series) with mass peaks detected on a 6210 Time-of-flight LC/MS (Agilent 1200 series).

3.2.9 Indigo cuvette image protocol

We carried out each reaction out on a 500 μL scale. Reactions consisted of indole (2 mM), DNA (25 μM), and Fe(III) heme (10 μM) in I-oxidation buffer. A we added 5 μL volume of hydrogen peroxide (100 mM) to specific cuvettes for a final hydrogen peroxide concentration of 1 mM, and not to other cuvettes, and mixed the contents. After approximately 5 min, the blue color reached saturation; we then set up the cuvettes on a white light box for photography. We adjusted the brightness and contrast for the images with Adobe Photoshop CS5.

3.2.10 Time course of styrene oxidation

We added 25 µL of 1 mM DNA and 10 µL of 1 mM hemin in DMF to 500 µL of 2X buffer containing 80 mM HEPES-NH_4OH (pH 8.0), 40 mM KCl, 0.1% Triton X-100, 2% DMF in a 1.5 mL glass vial. We added ddH_2O to make up the volume to 980 µL. We incubated the solution for 5 minutes at room temperature to allow for aptamer-hemin binding if binding is possible. We added 10 µL of 1 M styrene in DMF to the mixture and the reaction mixture was vortexed.

Prior to the start of the reaction we removed a 99 µL aliquot for time 0 and treated it as described later. We initiated the reaction by the addition of 9 µL 100 mM H_2O_2. We incubated the 900 µL volume containing 10 mM styrene, 10 µM hemin in DMF, 25 µM DNA, 1 mM H_2O_2, and buffer (40 mM HEPES-NH_4OH (pH 8.0), 20 mM KCl, 0.05% Triton X-100, 2% DMF) at room temperature.

We removed 95 µL Aliquots of the reaction mixture at 0, 15 s, 1 min, 5 min, and 30 min after initiation of reaction. We added 5 µL of 0.33 mM benzophenone as an internal standard to each aliquot prior to addition of CH_2Cl_2. We added 200 µL CH_2Cl_2 to quench the reaction and to extract the contents of the reaction mixture.

We analyzed the organic layer by gas chromatography on a Hewlett Packard Model 5890 system equipped with a flame ionization detector. We employed a DB-5MS column (0.25 mm i.d. x 50 m) for the analysis. We programmed the column temperature to rise 5°C/min from 80°C to 120°C, increase from 120°C to 300°C at 30°C/min and hold at 300°C for 4 min. We quantified the epoxide and the aldehyde using standard curves with benzophenone as the internal standard.

The retention times of the components were as follows: styrene, 4.3 min; phenylacetaldehyde, 6.8 min; styrene oxide, 7.2 min; benzophenone, 13.7 min. We established the identities of the epoxide and aldehyde peaks by elution with commercially available phenylacetaldehyde and styrene oxide by gas-chromatography.

3.2.11 Source of the oxygen atom in styrene oxide

We prepared reaction mixture as described above, in section 3.2.10. However, we initiated the reaction mixtures with PS2.M with either $H_2{}^{16}O_2$ or $H_2{}^{18}O_2$. The SS18 negative control reaction contained $H_2{}^{16}O_2$. We took 95 µL aliquots after 15 and 30 minutes.

We quenched the reactions with 200 µL CH_2Cl_2 and analyzed the organic layer with a Varian 3800 gas chromatograph equipped with a Varian Saturn 2000 ion trap. We employed a DB-5MS column (0.25 mm i.d. x 50 m) for the analysis.

We programmed the column temperature to hold at 50°C for 2 minutes, increase from 50°C to 130°C at 5°C/min, then increase from 130°C to 280°C at 30°C/min. The retention times of the components were as follows: styrene, 12.1 min; benzaldehyde, 14.5 min; phenylacetaldehyde, 17.3 min; styrene oxide, 18.1 min.

We established the identities of all peaks by elution with commercially available styrene, benzaldehyde, phenylacetaldehyde and styrene oxide by gas-chromatography. We determined the percentage of ^{18}O incorporation in styrene oxide by the integration of the contents in the $H_2{}^{18}O_2$ reaction with a m/z of 121 compared to the m/z of 121 and 119.

3.3 Results and discussion

3.3.1 Catalyzing the oxidation of thioanisole to thioanisole sulfoxide

Having shown that PS2.M was capable of catalyzing a single electron transfer, we were interested in investigating if PS2.M-heme was capable of any of the other known activities of heme proteins, such as catalyzing the mechanistically more complex 2-electron oxidations. First, we chose to test if PS2.M-heme could oxidize thioanisole, a widely used test substrate for oxygen transfer reactions [55, 102, 104-109].

PS2.M-heme was activated with 1 mM H_2O_2, under solution conditions for PS2.M-heme's peroxidase activity [62]. Analysis over a 30 minute period, at 21ºC, showed the production of the thioanisole sulfoxide product in the PS2.M-heme solutions but not in the control solutions containing Fe(III) heme and the non-G-quadruplex-forming oligonucleotide, SS18. Figure 3.2 plots the time courses for two sets of experiments.

The SS18/Fe(III) heme solution does not generate any detectable amount of the product. Whereas the calculated turnover rate of 3.5 s^{-1} for PS2.M-heme complex (initial rate of 3.5 $\mu M \cdot s^{-1}$ catalyzed by 1.0 μM PS2.M-heme) compares favourably with those of classical peroxidases: myeloperoxidase, 4 s^{-1}; lactoperoxidase, 0.1 s^{-1}; HRP, 0.05 s^{-1} [107, 109, 110]. As a result, we have demonstrated that PS2.M-heme is capable of catalyzing the 2-electron oxidation of thioanisole to thioanisole sulfoxide.

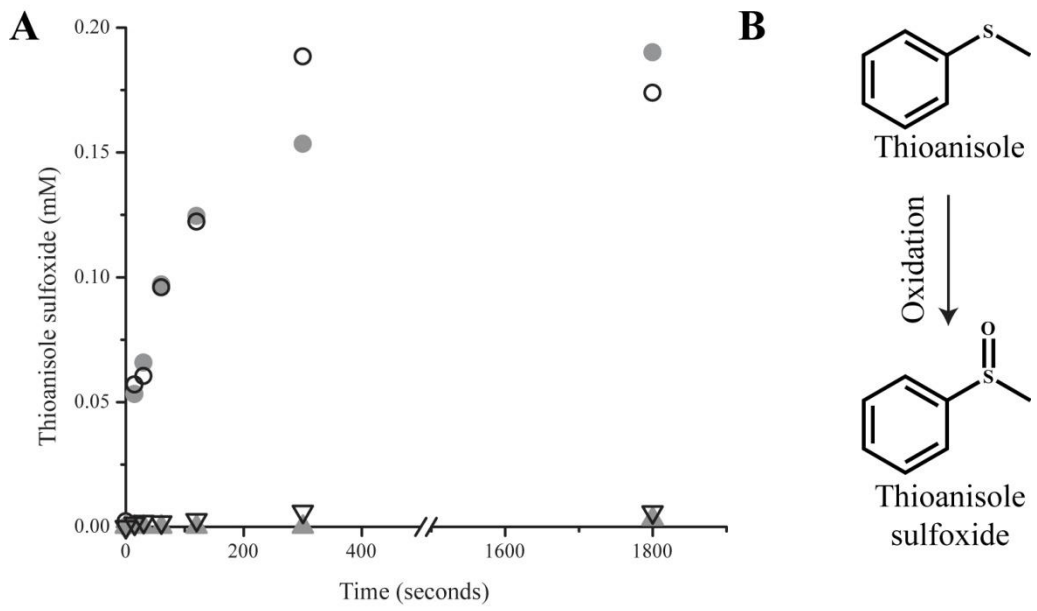

Figure 3.2: Time course study of thioanisole oxidation by PS2.M-heme complex. A) Time courses for the generation of thioanisole sulfoxide from incubations of 0.2 mM thioanisole, at 21ºC, in 40mM HEPES-NH_4OH, pH 8.0, 20 mM KCl, 0.05% Triton X-100, 3% DMF in the presence of 1 μM Fe(III) heme, 1mM H_2O_2, and 3 μM DNA. Two sets of independent measurements are shown. The open symbols (○, Δ) depict one set of experiments and the closed symbols (●,▲) depict another set of experiments. The circles (○,●) represent thioanisole sulfoxide production in the presence of PS2.M and the triangles (Δ,▲) represent thioanisole sulfoxide production in the presence of SS18, a non-G-quadruplex-forming oligonucleotide control. B) Chemical structures of thioanisole and thioanisole sulfoxide.

3.3.2 Determining the source of the oxygen atom in thioanisole sulfoxide, the oxidation product of thioanisole

Once it was established that PS2.M-hemin was capable of catalyzing the sulfoxidation reaction of thioanisole, we wanted to determine the origin of the oxygen atom. In order to investigate if the oxygen atom was directly transferred from Compound I to thioanisole to form the product, thioanisole sulfoxide, we performed experiments using ^{18}O labelled H_2O_2, shown in Figure 3.3.

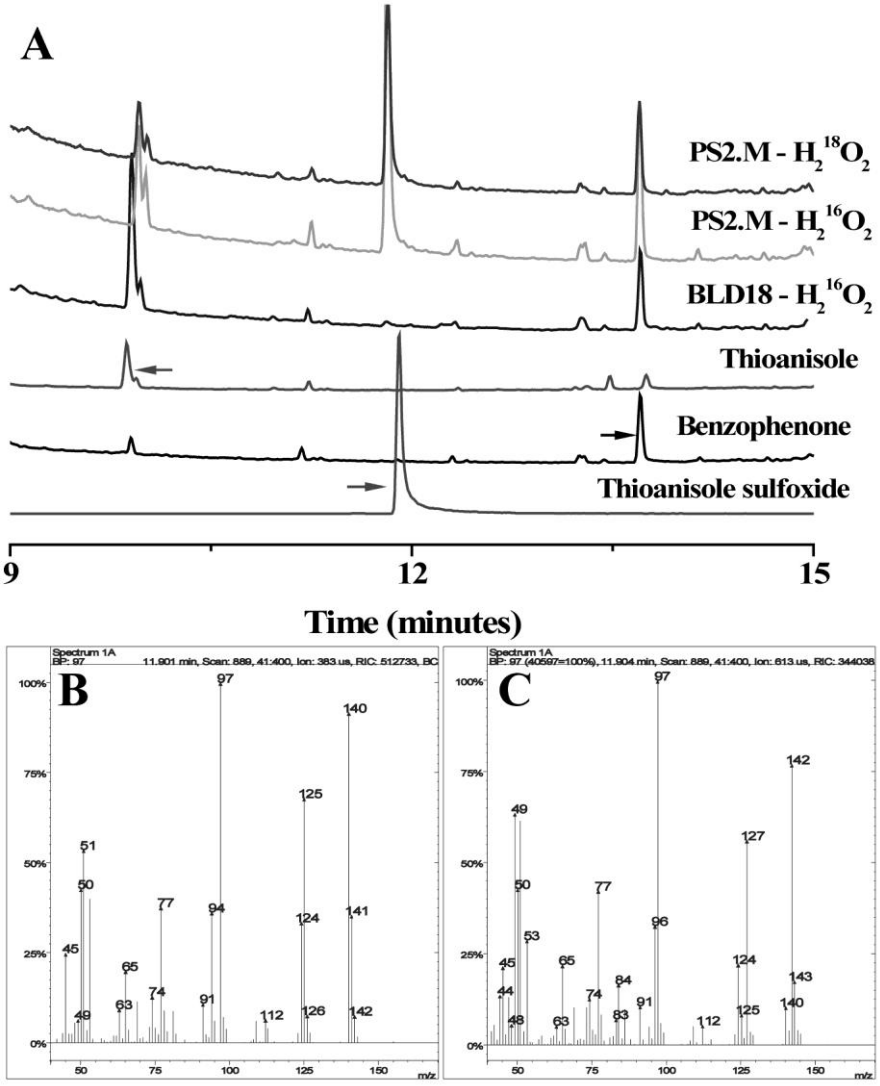

Figure 3.3: Determining the source of the oxygen atom in the final oxidation product, thioanisole sulfoxide by GC-MS.

Thioanisole oxidation reactions were carried out in the presence of Fe(III) heme and either PS2.M-heme or SS18. The PS2.M-heme solutions were treated with either $H_2{}^{18}O_2$ or $H_2{}^{16}O_2$. All samples contained 1 mM thioanisole, 1 μM Fe(III) heme and 3 μM DNA, dissolved in oxidation buffer (40 mM HEPES·NH4OH, pH 8.0, 20 mM KCl, 0.05% Triton X-100, 3% DMF). A) GC-MS chromatograms of both reaction mixtures and standards, as labelled. The arrows mark the elution peak of each standard as labelled. B) The mass spectrum of the thioanisole sulfoxide peak in the PS2.M/ $H_2{}^{16}O_2$ chromatogram. C) The mass spectrum of the thioanisole sulfoxide peak in the PS2.M/ $H_2{}^{18}O_2$ chromatogram.

Reactions were initiated with either $H_2{}^{18}O_2$ or $H_2{}^{16}O_2$ and the product was analyzed by gas chromatography (GC) coupled with a mass spectrometer (MS). The identity of the mass fragments are presented in Table 3.2. If the oxygen of the sulfoxide originated from H_2O_2, the mass of the sulfoxide would be 2 mass units greater for the reaction using $H_2{}^{18}O_2$ than $H_2{}^{16}O_2$. The mass spectrometry data in Figure 3.3 shows that 89% of the product was labelled with ^{18}O. Since the $H_2{}^{18}O_2$ was 90% pure, as indicated by the manufacturer, the oxygen from Compound I is quantitatively transferred to the sulfide. The origin of the oxygen atom is depicted in Figure 3.4.

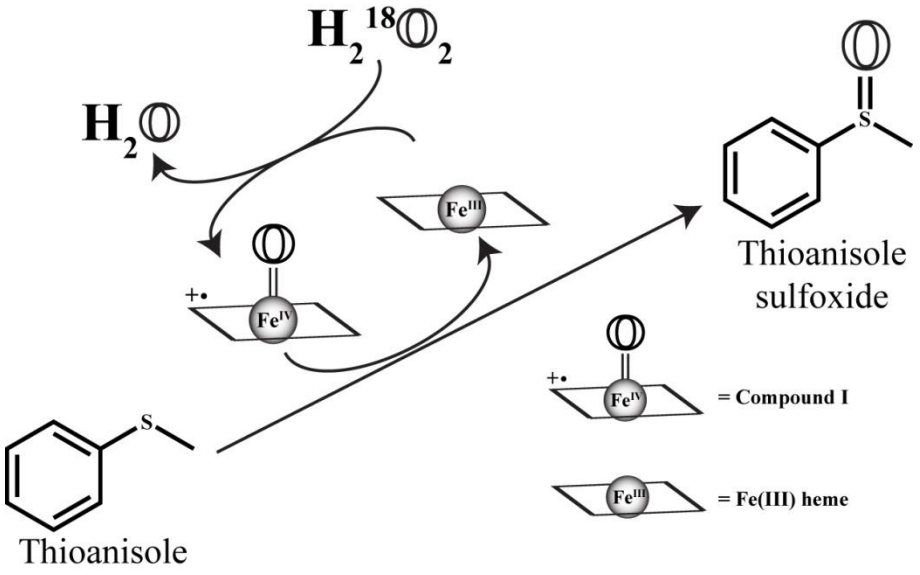

Figure 3.4: A scheme of the possible origin of the oxygen atom in the PS2.M-heme catalyzed oxidation of thioanisole to thioanisole sulfoxide.

This amount of oxygen incorporation from H_2O_2 has been reported for cytrochrome c peroxidase, but is higher than the amount reported for horseradish peroxidase [54, 55]. The 2-electron oxidation products of peroxidases when proceeding through the oxygen rebound mechanism generally show <100% incorporation of oxygen from H_2O_2, since a proportion of the radical intermediate diffuses away from the active

heme center and receives oxygen from sources other than H_2O_2 [54]. However, it has been shown that quantitative oxygen insertion from the ferryl-oxygen is possible even when 2-electron oxidation proceeds through an oxygen rebound mechanism [55]. This may be the result of a tightly bound substrate; therefore, the sulfur radical from the first 1-electron oxidation lingers in the active site to allow for a quick second 1-electron oxidation by the ferryl-oxygen [55].

Table 3.2: The identities of masses from the ionization of thioanisole.

Identity	**^{16}O**	**^{18}O**
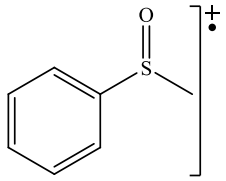	140	142
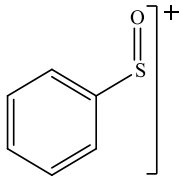	125	127
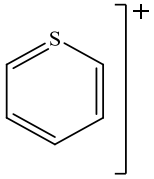	97	97
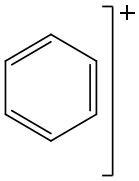	77	77

Even though these labelled hydrogen peroxide experiments are not capable of discerning between the oxygen rebound and the direct oxygen insertion mechanism, they provide some insight on the interaction of PS2.M-heme and the substrate. These studies suggest that thioanisole does not transiently come in contact with the catalytic core of

PS2.M-heme, but must be positioned near the ferryl-oxygen for enough time for quantitative oxygen atom transfer to take place.

3.3.3 Probing the active site of the PS2.M-heme complex by investigating the enantioselectivity of the enzyme

In order to investigate the possible structure of the PS2.M-hemin active site, we examined the enantioselectivity of PS2.M-hemin complex. Most native peroxidases when tasked with the 2-electron oxidation of thioanisole demonstrate a preference for the production of a particular enantiomer. Lactoperoxidase, chloroperoxidase and myeloperoxidase favour the formation of the *(R)*-sulfoxide, while horseradish peroxidase and *Coprinus cinereus* peroxidase favour the *(S)*-sulfoxide [111].

The absolute configuration of the sulfoxide product of the PS2.M-heme catalyzed thioanisole sulfoxidation reaction was determined by high performance liquid chromatography (HPLC) using a chiral column following a protocol from Ortiz de Montellano's research [102]. From the HPLC data in Figure 3.5, we compared the proportion of thioanisole sulfoxide enantiomers produced from two separate PS2.M-heme reaction mixtures with commercially obtained thioanisole sulfoxide. Both reaction mixtures produced a 50:50 mixture of thioanisole sulfoxide enantiomers, matching the distribution in the commercially obtained thioanisole sulfoxide.

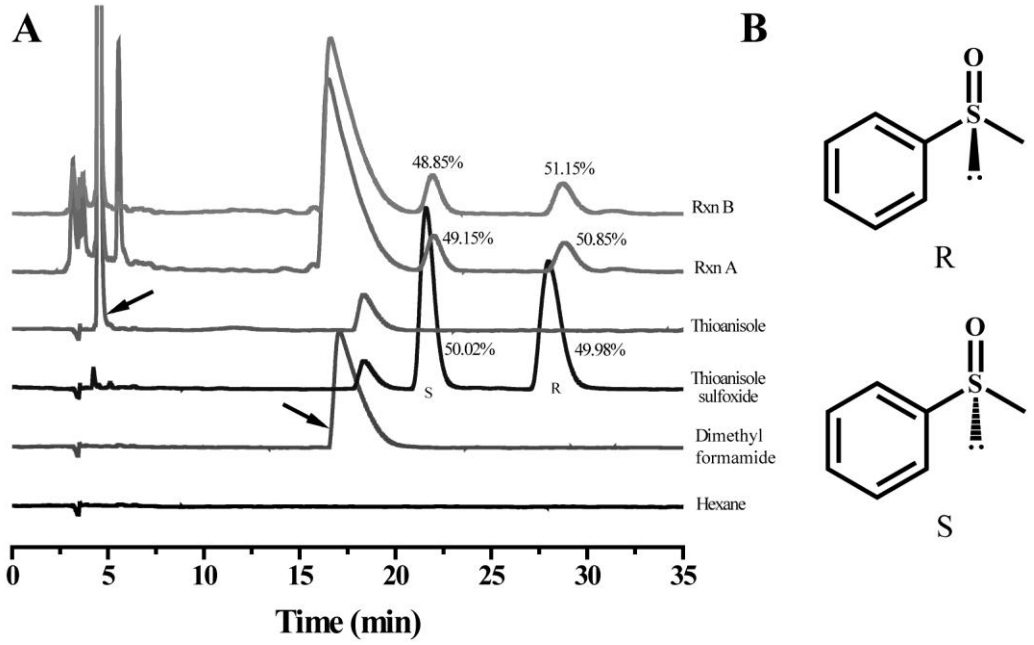

Figure 3.5: Enantioselectivity of the PS2.M-heme complex was determined by chiral HPLC of the thioanisole oxidation product.
A) HPLC chromatograms of thioanisole oxidation reactions and standards. All reaction mixtures contained 1 mM H_2O_2, 1 mM thioanisole, 1 μM Fe(III) heme and 3 μM DNA (PS2.M) dissolved in oxidation buffer (40 mM HEPES-NH_4OH, pH 8.0, 20 mM KCl, 0.05% Triton X-100, 3% DMF). The standards were diluted in DMF and dissolved in hexane. The arrows mark the elution peaks of thioanisole and DMF. The trace of the thioanisole sulfoxide standard are marked for the elution peaks of both the *(S)*- and *(R)*-enantiomers. B) Chemical structures of the enantiomers of thioanisole sulfoxide.

Since PS2.M-hemin catalyzed the formation of a racemic mixture of thioanisole sulfoxide, the active site of PS2.M-hemin is most likely in an "open" conformation or the binding site for thianosole above the heme is large enough to accommodate both binding modes of thianosole. This is possible if the heme cofactor stacks on the ends of parallel G-quadruplexes; therefore, the active site does not contain residues that restrict the entry of thioanisole. Klibanov and colleagues have reported that PS2.M-heme lacks stereospecificity in its peroxidase activity; it is interesting to note that a lack of stereoselectivity is also a feature of its catalysis of the more complex oxygen transfer

reaction [69]. In the case of protein peroxidases, cytochrome c peroxidase gave similar results to PS2.M-heme in the amount of ^{18}O incorporation in the product from $H_2{}^{18}O_2$ and the ratio of enantiomers of the final products [55].

3.3.4 Hammett analysis of thioanisole sulfoxidation as catalyzed by PS2.M-heme

A Hammett analysis was conducted to further elucidate the mechanism of thioanisole sulfoxidation as catalyzed by PS2.M-heme. In a Hammett analysis, one investigates the degree of negative or positive charge build-up during the formation of the rate limiting transition state or intermediate species. This is accomplished by measuring the initial rates for the sulfoxidation of para-substituted thioanisole with electron donating or electron withdrawing groups relative to the sulfoxidation of thioansiole.

Subsequently, these figures are plotted against the substituent constants for the para-substituents, which are values from empirical measurements of the degree of electron donating or withdrawing ability of each functional group. The slope (ρ) of the correlation between log[(initial rate of *p*-thioanisole)/(initial rate of thioanisole)] values and the respective substituent constants (σ or σ^+) gives insight into the charge build-up during the transition state [103]. If ρ is a negative value, it means that the electron-donating substituents increase the rate of the reaction by stabilizing a positively charged transition state. Whereas a positive ρ value indicates that electron-withdrawing substituents increase the rate of the reaction by stabilizing a negatively charged transition state.

In addition, the comparison between σ and σ^+ values also gives considerable insight into the mechanism of the reaction. The electron donating or withdrawing nature

of a substituent is due to a combination of effects, the inductive and resonance effects as seen in panel C of Figure 3.7. The σ value correlates more favourably to reactions where the charge build-up is at a location where the substituent does not directly withdraw or donate electrons through resonance. The σ^+ value puts greater weight to the resonance effect and correlates more favourably to reactions where a substituent directly withdraws or donates electrons to the reaction center through the resonance effect.

In the case of thioanisole, there are two main mechanisms that have been proposed by the peroxidase community, the oxygen rebound mechanism and direct oxygen insertion mechanism [28]. In Figure 3.6, one of the differences between the oxygen rebound mechanism and the direct oxygen insertion mechanism can be seen by comparing the transition state and the intermediate species of the two mechanisms. The direct oxygen insertion mechanism involves a transition state where there is a positive charge build-up at the sulfur atom. In comparison, if thioanisole sulfoxidation proceeds through the oxygen rebound mechanism, the sulfur goes through a sulfenium radical cation intermediate with a permanent positive charge on the sulfur atom. This permanent charge can be directly affected by a para-substituent on thioanisole through the resonance effect; therefore, the oxygen rebound mechanism should correlate more favourably with σ^+ values than σ values.

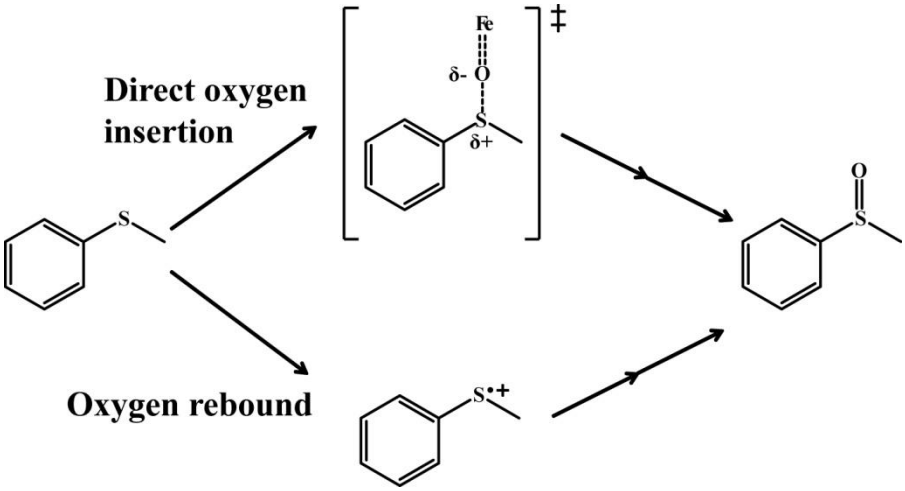

Figure 3.6: The transition state and intermediate of two possible thioanisole sulfoxidation routes.

The ρ value using σ is -0.96±0.12 and gives a good correlation (R^2 = 0.96), while σ^+ plot gives an equally good correlation (R^2 = 0.97) with a ρ value of -0.7±0.07 as seen in panel A and B of Figure 3.7. These values are consistent with a build-up of positive charge in the transition state or in the intermediate species. Also shown in panel B of Figure 3.7 is a fit that excludes the most electron-donating substituent for the σ^+ plot (ρ = -0.81±0.05; R^2 = 0.99). The correlations between both the σ^+ and σ substituent constants with the initial rates of the para-substituted substrates are not significantly different. The omission of the most electron-donating substituent improves the fit for the σ^+ plot. However, there is no significant difference between the correlations of all the fits; therefore, the Hammett studies that were performed were not sufficient to discern between the oxygen rebound and the direct oxygen insertion mechanism.

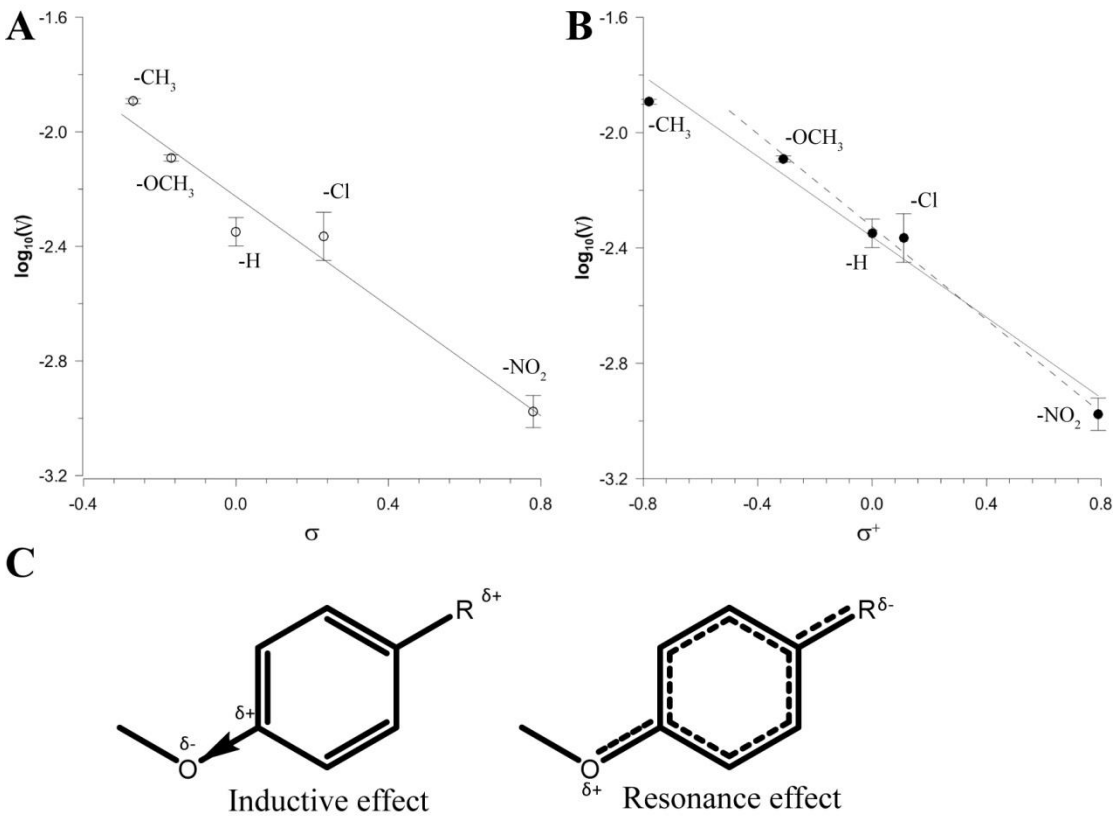

Figure 3.7: Hammett analysis of the PS2.M-heme catalyzed oxygen transfer reaction of thioanisole substrates.
Hammett plots for oxidation rates of various para-substituted thioanisoles. Log V (where V = the ratio obtained from the initial rate of para-substituted thioanisole oxidation over the initial rate of thioanisole oxidation) is plotted against the substituent constants σ (A) and σ^+ (B). The data shown are the average of duplicate determinations, and the errors shown are the N - 1 standard deviations rather than the differences from the average. The uninterrupted line in either plot shows the best fit to all five data points. The dashed line in the σ^+ plot (B) shows the best fit for four data points, excluding that for *p*-methoxythioanisole. C) Illustrations of *p*-methyl anisole and the two effects that affect the stabilization of transition states and intermediates.

The lack of additional points that correspond to highly electron-donating and highly electron-withdrawing substituents may have made distinguishing between the two above mechanisms difficult. This is particularly true for substitutents that contain a lone pair of electrons that can directly contribute to the stabilization of the sulfenium cation through resonance.

In panel A of Figure 3.7, the methyl substituent point is above the fit and other stronger electron-donating substituents may continue this trend. When points for strong electron-donating groups are above the fit for σ values, this is indicative of a possible better fit with σ^+ values. However, we were unable to test the effects of stronger electron-donating substituents because they tend to contain heteroatoms that can be oxidized by PS2.M-heme. Another pitfall of substituents that increase the rate of sulfoxidation, is the difficulty in measuring the initial rates of the reaction because the reaction takes place too quickly to be measured by our current extraction method. Hence, our use of Hammett analysis to discern between the oxygen rebound mechanism and the direct oxygen insertion mechanism was a worthy venture that could have used some refinement.

3.3.5 Investigating the general ability of G-quadruplex-heme complexes in catalyzing the sulfoxidation of thioanisole

Finally, the ability to catalyze the sulfoxidation of thioanisole was examined for a variety of G-quadruplex and non-G-quadruplex-forming oligonucleotides. Several G-quadruplexes are derived from biological sequences that represent parts of promoter regions and telomeric ends [112]. It has been previously reported that many proposed biologically relevant G-quadruplexes are capable of performing peroxidase function when bound to heme [77, 79].

The ability of G-quadruplexes to perform the function of heme protein apoenzymes, led us to evaluate if the G-quadruplexes formed by telomeric ends and oncogene promoters could catalyze the 2-electron oxidation of thioanisole. All G-quadruplexes tested were capable of oxidizing the sulfur substrate to the sulfoxide product, as seen in Figure 3.8. The comparable peroxygenation activity of many G-quadruplexes from biologically relevant sequences to PS2.M and CatG4 demonstrates an underlying function of G-quadruplexes to catalyze oxidation reactions. These results suggest that when bound to heme, G-quadruplexes *in vivo* may cause oxidative damage to surrounding DNA by 1- or 2-electron oxidations. Furthermore, the RNA version of PS2.M, rPS2.M, also demonstrated peroxygenase activity. This is not surprising since rPS2.M is also able to catalyze the 1-electron oxidation of ABTS [66]. Nonetheless, the ability to catalyze 2-electron oxidation reactions adds to the growing list of catalysis performed by RNA.

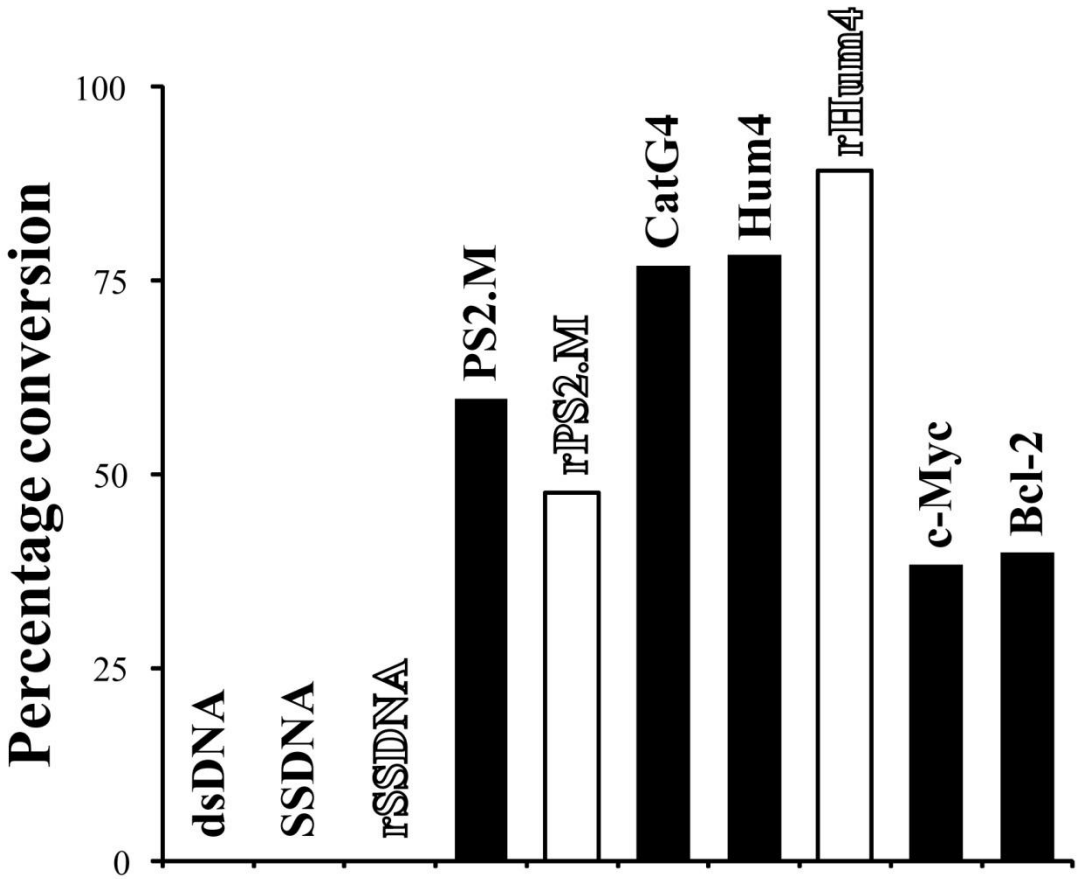

Figure 3.8: The sulfoxidation of thioanisole catalyzed by G-quadruplex-heme complexes. The histogram shows the conversion (in %) of thioanisole to thioanisole sulfoxide after 2 min of incubation in the presence of different DNAand RNA oligonucleotides, as well as a double-stranded DNA control (all sequences shown in Table 3.1). CatG4 has a slightly modified sequence but the same heme-binding properties as PS2.M [71]. Hum4 represents a four-repeat human telomeric DNA sequence, rHum4 represents an RNA version of Hum4, and c-Myc and Bcl-2 represent single-stranded G-rich DNAs from the respective oncogene promoters [112]. The reactions contain 0.2 mM thioanisole, at 21ºC, in 40mM HEPES-NH_4OH, pH 8.0, 20 mM KCl, 0.05% Triton X-100, 3% DMF in the presence of 1 μM Fe(III) heme, 1mM H_2O_2, and 3 μM DNA (with the exception that the Hum4 and rHum4 solutions contained 120 μM DNA/RNA to ensure >90% binding of the heme to the DNA/RNA). The SS18 and dsDNA controls were tried with both 3 and 120 μM DNA, and no difference was found in the outcome.

3.3.6 Catalyzing the 2-electron oxidation of indole

In order to demonstrate that the peroxygenation activity of PS2.M-hemin is not substrate specific, indole was chosen as a second substrate. Previously, others have reported the ability of cytochrome P450 to oxygenate indole to numerous products [113]. This mixture of indole products includes dimerization of oxidized indole subunits, such as indigo and indirubin [113]. In contrast, the oxidation of indole by chloroperoxidase primarily produces one dominant product, 2-oxindole [114]. Corbett and Chipko further demonstrated that horseradish peroxidase catalyzed minimal indole oxidation in contrast to a previous report [114].

Once again, PS2.M-hemin was activated by H_2O_2 to form Compound I. In Figure 3.9, analysis by HPLC coupled with a UV-Vis dectector showed a mixture of products similar to the trace from indole oxygenation by cytochrome P450 [113]. Reaction mixtures were also analyzed by HPLC/MS to further help identify the products of the mixture. Peaks from HPLC chromatograms were assigned possible identities by comparing PS2.M-hemin traces with cytochrome P450 traces from Gillam *et al.* and identifying the mass of each peak through high resolution mass spectrometry [113].

From Figure 3.9 and Table 3.3, the PS2.M-heme catalyzed oxidation of indole produced a mixture of products that is reminiscent of the mixture produced by cytochrome P450 monooxygenase. In 5 minutes, a rich mixture of products is produced by the PS2.M-heme catalyzed reaction; by comparison, the SS18, non-G-quadruplex-forming oligonucleotide and heme sample produced only traces of the same mixture of products.

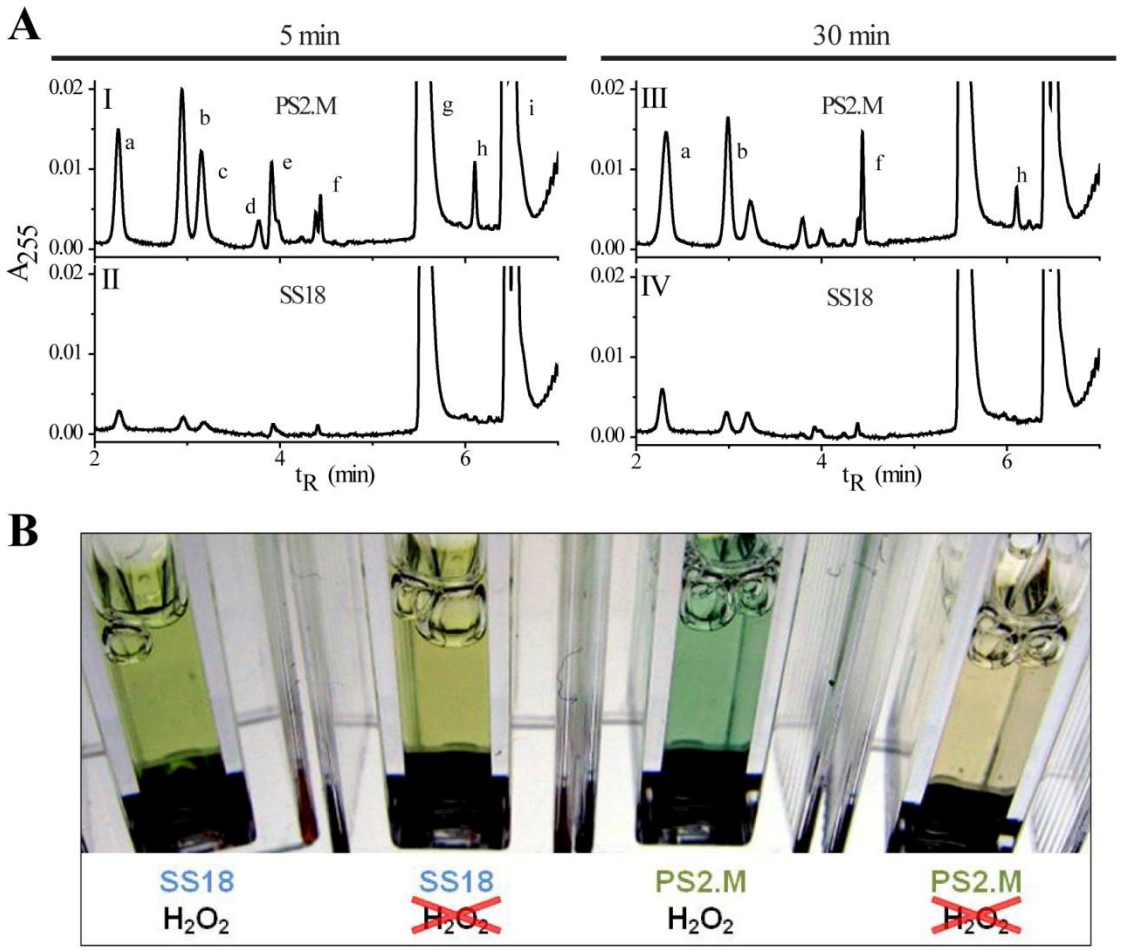

Figure 3.9: PS2.M-heme catalyzed oxygen transfer to indole.
A) HPLC traces of indole oxidation products formed in incubations of 1 mM indole in 40 mM HEPES-NH4OH, pH 8.0, 20 mM KCl, 0.05% Triton X-100, 1% DMF, at 21ºC, in the presence of 10 μM Fe(III) heme, 1 mM H_2O_2, and 25 μM DNA (PS2.M or SS18). Incubation traces of 5 min (left) and 30 min (right) are shown. The major peaks, labeled a-i, were identified using LC-MS and by comparison with pure standards, as follows: *a*, isatin; *b*, 2-oxindole; *c* and *f* had the same molecular mass as indigo and indirubin (262 Da), but had absorption spectra that were distinct from those of indirubin and indigo; *d*, unidentified product with the same molecular mass as isatin (147 Da); *e*, unidentified product; *g*, unreacted indole; *h*, indigo; *i*, benzophenone (added internal standard). B) Appearance of an indigo blue color after a 1 min incubation of 2 mM indole in the presence of PS2.M-heme and the same conditions as in *A* (third cuvette from left). Controls containing SS18 instead of PS2.M, and those with no added H_2O_2, are shown as indicated. It is notable also that the PS2.M incubation without added H_2O_2 (far right) has the red color characteristic of the PS2.M-heme complex, relative to the yellow color of unbound Fe(III) heme (second from the left).

The major products identified (Table 3.3) include isatin (a in Figure 3.9), 2-oxindole (b), indigo (g), and indigoid products (c and f, each with the mass of indigo and indirubin, 262Da), whose absorption spectra differ from those of indirubin and indigo.

Table 3.3: Table of the identities and the masses of peaks labelled in Figure 3.9.

Peak	**Retention time (mins)**	**Mass (g/mol)**	**Known identity**
a	2.298	147.04	Isatin
b	2.987	133.06	Oxindole
c	3.220	262.08	Isomer of indigo
d	3.805	147.04	Isomer of isatin
e	4.010	unknown	
f	4.460	262.08	Isomer of indigo
g	5.560	117.06	Indole
h	6.152	262.08	Indigo
i	6.512	182.08	Benzophenone (internal standard)

These results demonstrate that PS2.M-hemin is capable of catalyzing the peroxygenation of indole to give rise to similar products as the monooxygenation of indole by cytochrome P450. This may be attributed to the "open" nature of the PS2.M-hemin active site, which also caused the formation of racemic products for the sulfoxidation of thioansiole.

In addition to the formation of a mixture of products, it is also interesting that the relative yield of products changes over time. After 30 minutes of incubation, the relative yield of the products at 30 minutes differs from the relative yield at 5 minutes, this may be due to the air oxidation of the initial products.

Another notable result, in earlier time points, oxindole and isatin peaks are roughly 10 times greater for PS2.M-heme catalyzed mixtures than reaction mixtures

containing heme and SS18. However, this ratio decreases over time, which may indicate that the amount of H_2O_2 in the PS2.M mixture may have depleted. Since PS2.M binds heme to allow for Compound I formation, the DNA apoenzyme is also exposed to the possibility of oxidative damage which results in a decrease of PS2.M-hemin complex. The heme (with SS18 in the solution) catalyzed oxidation or the direct H_2O_2 oxidation of indole are slower reactions than the PS2.M-heme catalyzed reaction. As the H_2O_2 concentration decreases and while the PS2.M-heme enzyme is destroyed by oxidative damage, the accelerated rate of indole oxidation by PS2.M-heme is greatly reduced or eliminated altogether. A combination of these factors and others may be responsible for the decrease in the rate of products produced overtime by PS2.M-heme catalyzed reaction.

Despite the smaller difference for indole oxidation between SS18 and PS2.M containing samples when compared to the sulfoxidation of thioanisole, the visual difference of the reaction mixtures between the catalyzed and uncatalyzed reactions are quite striking. Figure 3.9B shows that within 1 min of the incubation of indole with PS2.M-heme and H_2O_2, the reaction mixture develops a blue color that we attribute to the production of indigo. Both SS18 samples, containing H_2O_2 or not containing H_2O_2, do not generate the same intense blue colour as the PS2.M-heme sample with H_2O_2. The known products of indole oxidation are illustrated in Figure 3.10. In addition the PS2.M-heme sample without H_2O_2 is red, as compared to the yellowish hue of the SS18 samples, presumably because the redish hue is indicative of PS2.M binding to heme and forming a complex.

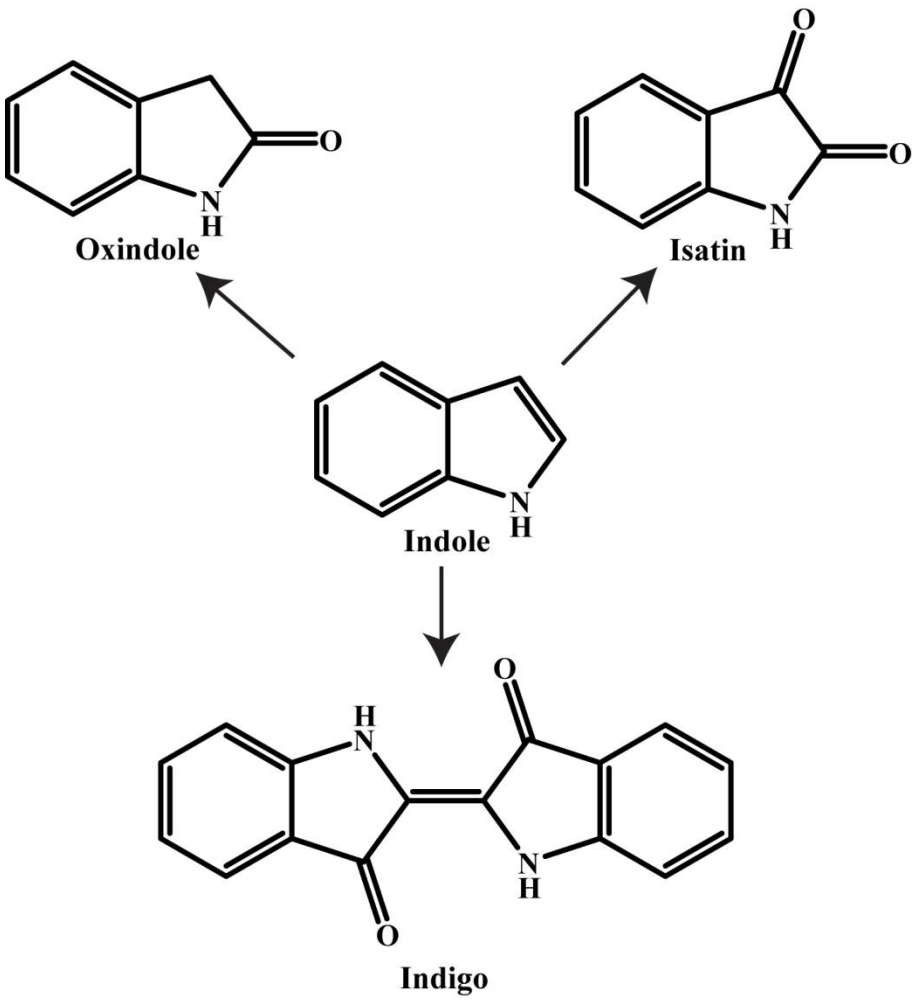

Figure 3.10:The products identified from the oxidation of indole by PS2.M-heme.

3.3.7 Investigating the general ability of G-quadruplex-heme complexes in catalyzing the oxidation of indole

As with the sulfoxidation of thioanisole, the ability to catalyze the oxidation of indole was examined for a variety of G-quadruplex and non-G-quadruplex-forming sequences. Several G-quadruplexes are derived from biological sequences that are part of promoter regions and telomeric ends [112]. Many of these proposed biologically relevant G-quadruplexes have been shown to be capable of catalyzing the 1-electron oxidation of ABTS and we have reported their ability to catalyze the 2-electron oxidation of thioanisole [77, 79]. The ability of G-quadruplexes to perform the function of heme protein apoenzymes, led us to evaluate if the G-quadruplexes formed by telomeric ends and oncogene promoters could catalyze the 2-electron oxidation of indole.

All G-quadruplexes tested were capable of oxidizing indole to a mixture of products. The primary products produced were 2-oxindole and isatin, their production is displayed graphically in Figure 3.11. The comparable peroxygenation activity of many G-quadruplexes from biologically relevant sequences to PS2.M and CatG4 further cements the underlying ability of G-quadruplexes to bind heme and catalyze 2-electron oxidations. Since many of these telomeric and promoter sequences form G-quadruplexes *in vitro*, these results further suggest that there may be a possible oxidative role for G-quadruplexes *in vivo.* Furthermore, the RNA version of PS2.M and Hum4, rPS2.M and rHum4, also demonstrated the ability to oxidize indole, as they did with thioanisole.

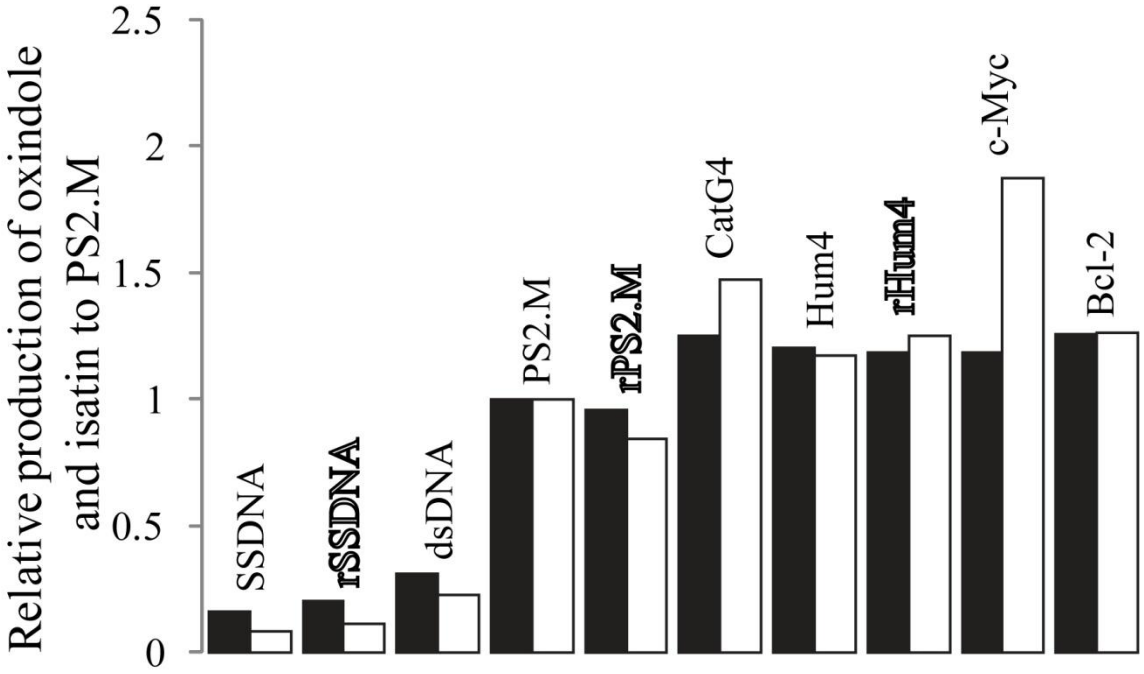

Figure 3.11:The oxidation of indole catalyzed by G-quadruplex-heme complexes.
A histogram showing yields of the two major indole oxidation products (2-oxindole and isatin) in the presence of 1 mM H_2O_2, 1 mM indole, 10 μM Fe(III) heme and 25 μM DNA (black) /RNA (red), dissolved in I-oxidation buffer (40 mM HEPES·NH_4OH, pH 8.0, 20 mM KCl, 0.05% Triton X-100, and 1% DMF) at 21°C. The data represent 5-minute reactions in all cases; the yields of isatin and 2-oxindole are both normalized relative to the yields from PS2.M-heme. The isatin data is depicted by the black bars and the 2-oxindole data is depicted by the white bars with black outline. The *r* prefix denotes RNA, while the other names are of DNA oligonucleotides. The sequences of all oligonucleotides are in Table 3.1.

3.3.8 Catalyzing the 2-electron oxidation of styrene

An epoxidation reaction is a relatively challenging oxidation reaction due to the relatively higher redox potential of alkenes compared to heteroatoms [115]. A classical peroxidase, such as horseradish peroxidase, poorly catalyzes the epoxidation of styrene [55, 56]. P450 monooxygenases and nonclassical peroxidases (such as chloroperoxidase) show more efficient catalysis of styrene epoxidation than classical peroxidases (chloroperoxidase has k_{cat} values of 0.1-4.0 s^{-1} and the P450 enzymes show comparable values) [32]. The oxidation of styrene produces the expected styrene oxide product, phenylacetaldehyde (formed by a hydrogen rearrangement); furthermore, some enzymes generate benzaldehyde using an unknown mechanism [105].

Figure 3.12A shows that PS2.M-heme catalyzes the formation of two main products which, upon mass identification by mass spectrometry and comparison with standards, can be identified as styrene oxide and phenylacetaldehyde. A very small amount of benzaldehyde (relative to yields of styrene oxide and phenylacetaldehyde) could also be detected by GC-MS in the 30 minute PS2.M-heme incubation.

The measured initial rate for phenylacetaldehyde production was ~1.7 $\mu M \cdot s^{-1}$ and for styrene oxide production was ~0.4 $\mu M \cdot s^{-1}$ (per 10 μM of enzyme). As with thioanisole sulfoxidation, PS2.M-heme appears to be a superior catalyst for styrene oxidation relative to the classical peroxidases [55, 56]. In addition, the reaction of PS2.M-heme with styrene in this system proceeds only for a short time (~1 min), owing to the likely destruction of the heme cofactor. Similar observations have also been made with a number of heme enzymes [116]. The radical intermediate that is generated for epoxide and aldehyde formation is attached to the ferryl oxygen of Compound I and will

form a covalent bond with the nitrogens in the pyrrole rings, resulting in the inactivation of the enzyme.

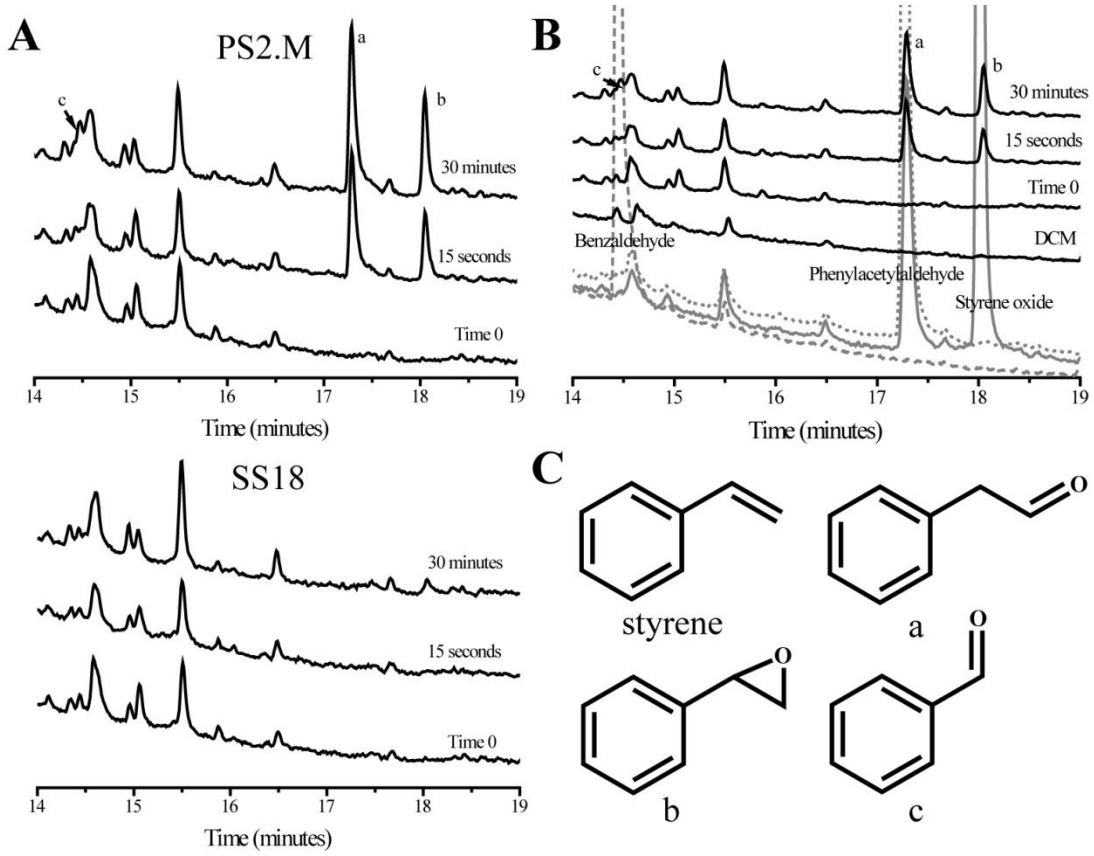

Figure 3.12:PS2.M-heme catalyzed 2-electron oxidation of styrene.

A) Chromatographs from GC-MS show the production of phenylacetaldehyde (*a*) and styrene oxide (*b*) from incubations of PS2.M-heme with styrene and hydrogen peroxide. There is an absence of formation of the same products, under the same conditions, from a solution in which the DNA oligomer SS18 substitutes for PS2.M. A trace of benzaldehyde (*c*) can be detected in the 30 min incubation of PS2.M-heme with styrene and hydrogen peroxide. B) Chromatographs of the pure compounds phenylacetaldehyde (solid grey line), styrene oxide (dotted grey line), benzaldehyde (dashed grey line), and dicholoromethane are shown below the products from the PS2.M-heme incubations. It should be noted that the styrene oxide standard contains a small amount of phenylacetaldehyde as a contaminant. C) Chemical structures of styrene, phenylacetaldehyde (*a*), styrene oxide (*b*), and benzaldehyde (*c*).

3.3.9 Determining the source of the oxygen atom in styrene oxide, a product of styrene oxidation

When styrene is oxidized to styrene oxide by a PS2.M-heme catalyzed reaction, does the oxygen atom within styrene oxide originate from the ferryl oxygen, which is generated by H_2O_2? In order to investigate this question we performed reactions using ^{18}O labelled $H_2{}^{18}O_2$. If the oxygen atom in styrene oxide originated from hydrogen peroxide, the mass of the molecule would be 2 mass units greater than a reaction using $H_2{}^{16}O_2$.

Among heme enzymes, chloroperoxidase incorporates ^{18}O from $H_2{}^{18}O_2$ quantitatively into styrene oxide [116]. Only 79% of the styrene oxide generated by modified horseradish peroxidase originates from H_2O_2; the rest has been proposed to originate from dioxygen [56]. In contrast, wild-type horseradish peroxidase is able to use H_2O_2 and dioxygen together to co-oxidize phenols and styrene (here, the oxygen of styrene oxide is derived purely from the dioxygen) [117].

The data shown in Figure 3.13 indicate that 73% of the oxygen of styrene oxide (corrected for the ^{18}O purity of the $H_2{}^{18}O_2$, as described by the manufacturer) catalyzed by PS2.M-heme is derived from $H_2{}^{18}O_2$. The identity of the major mass peaks are shown in Table 3.4. Thus, as observed with the thioanisole substrate, oxygen transfer to styrene substrate proceeds primarily from the activated ferryl species within PS2.M·heme. In addition to the thioanisole ^{18}O data, the high incorporation of the ferryl oxygen into 2-electron oxidation products suggests that that the interaction between the enzyme and the substrate is not simply collisional, but the substrate is held in position close to the ferryl oxygen for oxygen transfer to take place.

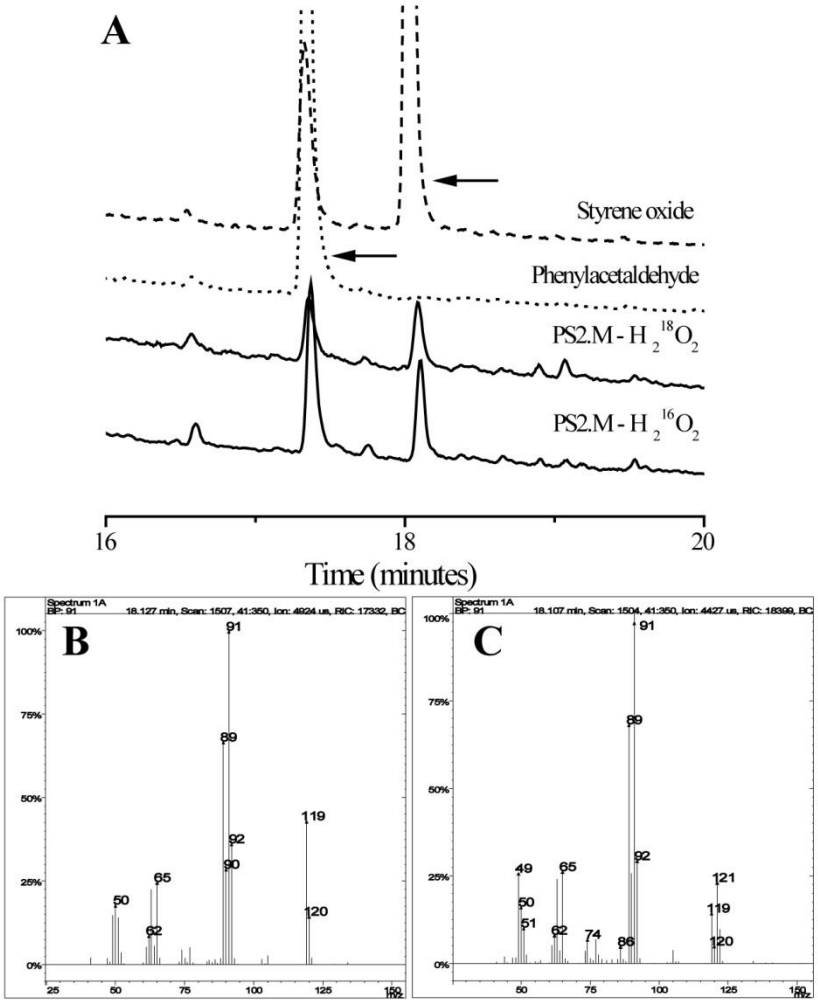

Figure 3.13:GC-MS data of $H_2{}^{18}O_2$ experiments for styrene oxidation.

Reactions were carried out in the presence of PS2.M-heme. The samples were treated with either $H_2{}^{18}O_2$ or $H_2{}^{16}O_2$. All samples contained 10 mM styrene, 10 μM Fe(III) heme and 25 μM DNA in the presence of 40 mM HEPES·NH_4OH, 20 mM KCl, 0.05% Triton X-100, 1% DMF. Reactions were quenched and extracted after 15 minutes with DCM. Products in DCM were analyzed by gas chromatography coupled to a mass spectrometer. A) Chromatograms of both reaction mixtures and standards. Black solid traces are reaction mixture chromatograms. Dotted and dashed traces are chromatograms of standards. B) The mass spectrum of the styrene oxide peak in the PS2.M/ $H_2{}^{16}O_2$ chromatogram. C) The mass spectrum of the styrene oxide peak in the PS2.M/ $H_2{}^{18}O_2$ chromatogram.

Table 3.4: The identities of masses from the ionization of styrene oxide.

Identity	16O	18O
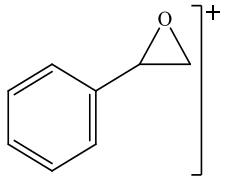	119	121
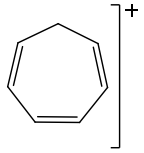	91	91
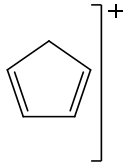	65	65

3.4 Chapter conclusion

The exploration of the catalytic repertoire of DNA and RNA has led to the discovery of a new catalytic property of DNA and RNA. Previously, it has been demonstrated that DNA and RNA molecules that form G-quadruplexes are capable of binding heme. Subsequently, G-quadruplex-heme complexes are capable of catalyzing 1-electron oxidations [69]. Now, it is possible to add 2-electron oxidations as a catalytic property of DNA and RNA.

We have demonstrated that G-quadruplex-heme complexes are capable of catalyzing the 2-electron oxidation of a variety of substrates. In particular, we thoroughly studied the G-quadruplex-forming *in vitro* selected oligonucleotide, PS2.M. The PS2.M-heme complex catalyzed 2-electron oxidations of thioanisole, indole and styrene. The oxidation of thioanisole resulted in the production of thioanisole sulfoxide, indole

resulted in the production of a mixture of products, and styrene resulted in the production of styrene oxide, phenylacetaldehyde, and benzaldehyde.

The oxygen atom in the different oxidation products primarily originated from hydrogen peroxide through the Compound I species. However, the mechanism of oxygen transfer has not been resolved for PS2.M-heme catalyzed reactions. The transfer of the oxygen atom from Compound I can proceed *via* the oxygen rebound mechanism or the direct oxygen insertion mechanism. In either case, the origin of the oxygen atom in the oxidation products reveals that the interaction between the reducing substrate and the enzyme (PS2.M-heme) requires the substrate to be bound long enough for oxygen transfer to take place. This may proceed *via* a direct 2-electron oxidation step or through two successive 1-electron oxidations. The latter mechanism results in a radical cation intermediate that is bound to the G-quadruplex-heme complex *via* possible cation-π interactions or stacking interactions.

The investigation of the enantioselectivity of PS2.M-heme for the oxidation of thioanisole revealed a lack of preference for the production of a specific chiral product. In collaboration with Dr. Frédéric Pio, we performed flexible docking simulations using Autodock software to identify the possible heme-binding sites on the NMR-derived solution structure of Bcl-2, a G-quadruplex from the promoter region of *BCL-2* [101]. As seen in Figure 3.14, the heme molecule is stacked on top of G-quartet. Interestingly, a cytidine is positioned directly under the center of the heme molecule, which we postulate to be a possible candidate that may act as an axial ligand to coordinate the iron in the heme molecule [101]. In addition, the distal side of the heme is completely exposed to the solvent and lacks any DNA structure. These insights, in combination with studies

done by Klibanov and colleagues, show that the lack of substrate-, regio- and enatio-selectivity of PS2.M-heme for 1-electron and 2-electron substrates is due to the lack of a structured distal-heme environment [69].

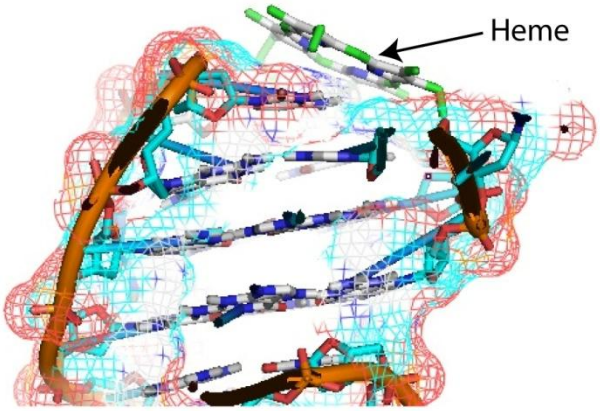

Figure 3.14:The structure of Fe(III) heme docked, using the Autodock program, upon the NMR-derived solution structure of a G-quadruplex formed by the Bcl-2 DNA oligomer.

We have successfully demonstrated that PS2.M-heme can insert an oxygen atom into electron-rich molecules, such as molecules containing heteroatoms or molecules that have a large degree of conjugation. The ultimate gold standard of cytochrome P450 monooxygenase ability would be to oxidize an unactivated carbon, such as those in adamantane or camphor. The ability of PS2.M-heme to hydroxylate unactivated carbons is an ongoing interest in the Sen Laboratory.

4: Conclusion and outlook

The discovery of the catalytic capability of nucleic acids continues to inspire us in our pursuit to understand the catalytic mechanisms and the full catalytic potential of ribozymes. In this work, we sought to uncover the structural features of PS2.M, a G-quadruplex-forming oligonucleotide, that allow it to bind to heme and subsequently catalyze peroxidase reactions. In addition, we set out to investigate if the PS2.M-heme complex could perform other functions of heme proteins, such as 2-electron oxidation reactions where an oxygen atom is transferred to the organic substrate to form the oxidation product.

Our studies revealed that PS2.M folds into many different species and the distribution of species is highly dependent on various conditions. PS2.M is capable of folding into G-quadruplex structures that range from unimolecular to tetrameric and from parallel-stranded to anti-parallel-stranded. However, the G-quadruplex species that binds heme and catalyzes oxidation reactions is most likely a parallel G-quadruplex. The CD spectra of PS2.M are indicative of a primarily parallel-stranded mixture of species.

Furthermore, the addition of hemin to the PS2.M solution causes a decrease in the amount of anti-parallel G-quadruplexes in the mixture. Along with other groups, these results suggest that heme may even cause the switching of anti-parallel stranded G-quadruplexes to parallel stranded G-quadruplexes.

Once heme was bound to PS2.M and the other examined G-quaduplexes, there was an enhancement of the peroxidative ability of heme. A common mechanism employed by G-quadruplexes to enhance the peroxidative ability of heme is to increase the pK_a of the water-heme complex. This causes a shift in the alkaline transition to disfavour the formation of the hydroxide-heme complex at physiological pH. The hydroxide-heme complex interferes with the formation of Compound I, which is the active heme species.

Since PS2.M aids in the formation of Compound I, and Compound I is a common intermediate species for peroxidases and monooxygenases that contain heme, we wanted to explore PS2.M-heme's ability to perform 2-electron oxidation reactions. The use of H_2O_2 to oxidize Fe(III) heme to form Compound I is the same for both the 1-electron and 2-electron oxidation reactions. Once PS2.M-heme complex has formed Compound I, we have demonstrated that PS2.M-heme complex is capable of catalyzing 2-electron oxidations of electron-rich substrates by transferring the ferryl-oxygen to the substrate.

Our studies included a variety of substrates that allowed us to test the ability of PS2.M-heme to oxidize heteroatoms, hydroxylate unsaturated carbons, and epoxidate alkenes. In many cases, the ability of PS2.M-heme to oxygenate the tested substrates was comparable to protein peroxidases, but not as efficient as monooxygenases. However, unlike the majority of classical peroxidases, PS2.M-heme does not seem to be regio- or enantio-selective. This may suggest that the active site of PS2.M-heme is less restrictive than their protein counterparts are. Furthermore, we demonstrated that the ability to catalyze oxygen transfer reactions is not limited to the artificial PS2.M G-quadruplex, but a more general property of G-quadruplexes that can bind heme.

From the results of several of our studies, I propose the following PS2.M-heme structure in Figure 4.1. This structure has similar features to the Autodock-simulated structure of heme bound to Bcl-2 DNA oligomer in Figure 3.14. The heme molecule most likely stacks on top of a G-quartet in the folded PS2.M structure. As demonstrated by our studies and those of other groups, the active species of PS2.M is most likely a parallel G-quadruplex; therefore, my proposed PS2.M folded structure only contains strands parallel to each other. The axial ligand that is needed to coordinate the heme molecule is most likely one of residues in the linkers/loops of the PS2.M-G-quadruplex. I have proposed T2 as a possible candidate for the axial ligand. Finally, like the Bcl-2-heme simulated-structure, the distal side of PS2.M-heme is completely exposed to the solvent environment. The open nature of the distal environment of PS2.M-heme most likely causes the lack of substrate-, regio-, and enantio-selectivity by the enzyme.

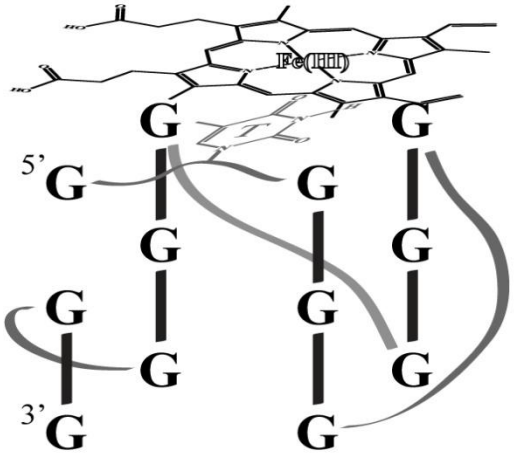

Figure 4.1: A proposed structure of the complex formed by heme binding to PS2.M.

While our studies have provided a great deal of insight on the structure and the catalytic potential of G-quadruplex-heme complexes, it is evident that much more can be

done. One of the ongoing goals in our laboratory is to obtain a high resolution structure of PS2.M. Without this data, it is difficult to conclude how PS2.M binds heme and how PS2.M enhances the 1-electron abstraction and oxygen transfer ability of heme. However, the highly polymorphic folding of PS2.M makes nuclear magnetic resonance spectroscopy and X-ray crystallography studies difficult. Gel based assays can still be an excellent method for investigating the active structure of PS2.M. An ongoing experiment in our laboratory is to use an *in situ* peroxidase assay with diaminobenzidine to identify the active species in either a non-denaturing polyacrylamide or agarose gel.

Aside from structural studies of PS2.M, it would also be interesting to further investigate the mechanism of the newly discovered oxygen transfer ability of G-quadruplex-heme complexes. For instance, the contribution of molecular oxygen to the oxidation of styrene can be investigated with ^{18}O labelled molecular oxygen. Also, it would be interesting to discern the mechanisms involved in indole oxidation that result in a large mixture of products. Since not all the products of indole oxidation were identified, it is important to identify all the unknown peaks especially the ones that did not appear in the mixture of indole oxidation products by cytochrome P450. These studies into the mechanism of oxidation by G-quadruplex-heme could help us understand the potential catalytic contribution of *in vivo* G-quadruplexes.

Furthermore, the potential of PS2.M-heme as an industrial catalyst is very intriguing due to its small size and robustness to various environmental conditions. We have demonstrated that several substrates can be oxygenated by PS2.M-heme; however, it has not been possible to oxidize a saturated carbon. Also, G-quadruplex-heme complexes lack regio- and enantio-selectivity, which is not ideal for the synthesis of most

pharmaceuticals. However, a DNAzyme could be evolved from the G-quadruplex scaffold to oxidize a specific position in a substrate. Our laboratory is actively looking into all these avenues of research.

Reference List

1. Stanley, W.M., *Isolation of a crystalline protein possessing the properties of tobacco-mosaic virus.* Science, 1935. **81**(2113): p. 644-645.

2. Downie, A.W., *Pneumococcal transformation - backward view. Fourth Griffith Memorial Lecture.* J. Gen. Microbiol., 1972. **73**(1): p. 1-11.

3. Avery, O.T., C.M. MacLeod, and M. McCarty, *Studies on the Chemical Nature of the Substance Inducing Transformation of Pneumococcal Types: Induction of Transformation by a Desoxyribonucleic Acid Fraction Isolated from Pneumococcus Type III.* J. Exp. Med.79 (2): 137–158., 1944. **79**(2): p. 137-158.

4. Watson, J.D. and F.H.C. Crick, *A Structure for Deoxyribose Nucleic Acid.* Nature, 1953. **171**(4356): p. 737-738.

5. *The 2009 Nobel Prize in Physiology or Medicine - Press Release*. [cited 2011 6 May]; Available from: http://nobelprize.org/nobel_prizes/medicine/laureates/2009/press.html.

6. Blackburn, E.H. and J.G. Gall, *A tandemly repeated sequence at the termini of the extrachromosomal ribosomal RNA genes in Tetrahymena.* J. Mol. Biol., 1978. **120**(1): p. 33-53.

7. Harley, C.B. and B. Villeponteau, *Telomeres and telomerase in aging and cancer.* Curr. Opin. Genet. Dev., 1995. **5**: p. 249-255.

8. Sen, D. and W. Gilbert, *Formation of parallel four-stranded complexes by guanine-rich motifs in DNA and its implications for meiosis.* Nature, 1988. **334**: p. 364 - 366.

9. Sen, D. and W. Gilbert, *A sodium-potassium switch in the formation of four-stranded G4-DNA.* Nature, 1990. **344**: p. 410-414.

10. Huppert, J. and S. Balasubramanian, *G-quadruplexes in promoters throughout the human genome.* Nucleic Acids Res., 2006. **35**(2): p. 406-413.

11. Balasubramanian, S., L.H. Hurley, and S. Neidle, *Targeting G-quadruplexes in gene promoters: a novel anticancer strategy?* Nat. Rev. Drug Discovery, 2011. **10**: p. 261-275.

12. Huppert, J. and S. Balasubramanian, *Prevalence of quadruplexes in the human genome.* Nucleic Acids Res., 2005. **33**(9): p. 2908-2916.

13. Siddiqui-Jain, A., et al., *Direct evidence for a G-quadruplex in a promoter region and its targeting with a small molecule to repress c-MYC transcription.* Proc. Natl. Acad. Sci., 2002. **99**(18): p. 11593-11598.

14. Gellert, M., M.N. Lipsett, and D.R. Davies, *Helix formation by guanylic acid.* Proc. Natl. Acad. Sci., 1962. **48**(12): p. 2013-2018.

15. Arnott, S., K. Chandrasekaran, and C.M. Marttila, *Structures for polyinosinic acid and polyguanylic acid.* Biochem. J., 1974. **141**(2): p. 537-543.

16. Patel, D.J., A.T. Phan, and V. Kuryavyi, *Human telomere, oncogenic promoter and 5'-UTR G-quadruplexes: diverse higher order DNA and RNA targets for cancer therapeutics.* Nucleic Acids Res., 2007. **35**(22): p. 7429-7455.

17. Tougard, P., J.F. Chantot, and W. Guschlbauer, *Nucleoside conformations: X. An X-ray fiber diffraction study of the gels of guanine nucleosides.* Biochim. Biophys. Acta., 1973. **308**(1): p. 9-16.

18. Zimmerman, S.B., G.H. Cohen, and D.R. Davies, *X-ray fiber diffraction and model-building study of polyguanylic acid and polyinosinic acid.* J. Mol. Biol., 1975. **92**(2): p. 181-184.

19. Friedman, R.A. and B. Honig, *A free energy analysis of nucleic acid base stacking in aqueous solution.* Biophys. J., 1995. **69**(4): p. 1528-1535.

20. Lai, J.S., J. Qu, and E.T. Kool, *Fluorinated DNA Bases as Probes of Electrostatic Effects in DNA Base Stacking.* Angew. Chem. Int. Ed., 2003. **42**: p. 5973-5977.

21. Parkinson, G.N., *Fundamentals of Quadruplex Structures*, in *Quadruplex Nucleic Acids*, S. Neidle and S. Balasubramanian, Editors. 2006, The Royal Society of Chemistry: Cambridge. p. 1-30.

22. Burge, S., et al., *Quadruplex DNA: sequence, topology and structure.* Nucleic Acids Res., 2006. **34**(19): p. 5402-5415.

23. Otero, R., et al., *Guanine Quartet Networks Stabilized by Cooperative Hydrogen Bonds.* Angew. Chem. Int. Ed., 2005. **44**(15): p. 2270-2275.

24. Phan, A.T., V. Kuryavyi, and D.J. Patel, *DNA architecture: from G to Z.* Curr. Opin. Struc. Biol., 2006. **16**: p. 288-298.

25. Hud, N.V. and J. Plavec, *The Role of Cations in Determining Quadruplex Structure and Stability*, in *Quadruplex Nucleic Acids*, S. Neidle and S. Balasubramanian, Editors. 2006, The Royal Society of Chemistry: Cambridge. p. 100-130.

26. Mergny, J.L., A.T. Phan, and L. Lacroix, *Following G-quartet formation by UV-spectroscopy.* FEBS Lett., 1998. **435**: p. 74-78.

27. Hud, N.V., et al., *The Selectivity for K^+ vs. Na^+ in DNA Quadruplexes is Dominated by Relative Free Energies of Hydration: A Thermodynamic Analysis by ^1H NMR.* Biochemistry, 1996. **35**: p. 15383-15390.

28. Dunford, H.B., *Heme Peroxidases*. 1999, New York: John Wiley & Sons, Inc. 88.

29. Dunford, H.B., *Peroxidases & Catalases*. 2010, Hoboken, New Jersey: John Wiley & Sons, Inc.

30. Mansuy, D. and J.-P. Renaud, *Heme-Thiolate Proteins Different from Cytochromes P450 Catalyzing Monooxygenations*, in *Cytochrome P450: Structure, Mechanism, and Biochemistry*, P.R. Ortiz de Montellano, Editor. 1995, Plenum Press: New York. p. 537-574.

31. Matsunaga, I. and Y. Shiro, *Peroxide-utilizing biocatalysts: structural and functional diversity of heme-containing enzymes.* Curr. Opin. Chem. Biol., 2004. **8**: p. 127-132.

32. van Rantwijk, F. and R.A. Sheldon, *Selective oxygen transfer catalysed by heme peroxidases: synthetic and mechanistic aspects.* Curr. Opin. Biotechnol., 2000. **11**(6): p. 554-564.

33. Erman, J.E., et al., *Histidine 52 is a critical residue for rapid formation of cytochrome c peroxiase compound I.* Biochemistry, 1993. **32**: p. 9798-9806.

34. Dawson, J.H., *Probing Structure-Function Relations in Heme-Containing Oxygenases and Peroxidases.* Science, 1988. **240**: p. 433-439.

35. Harris, D.L., *High-valent intermediates of heme proteins and model compounds.* Curr. Opin. Chem. Biol., 2001. **5**: p. 724-735.

36. Adachi, S., et al., *Roles of proximal ligand in heme proteins: Replacement of proximal histidine of human myoglobin with cysteine and tyrosine by site-directed mutagenesis as models for P-450, chloroperoxidase, and catalase.* Biochemistry, 1993. **32**: p. 241-252.

37. Yi, X., et al., *Replacement of the proximal heme thiolate ligand in chloroperoxidase with a histidine residue.* Proc. Natl. Acad. Sci., 1999. **96**: p. 12412-12417.

38. Newmyer, S.L. and P.R.O.d. Montellano, *Histidine catalysis and control of substrate access to the heme iron.* J. Biol. Chem., 1995. **270**: p. 19430-19438.

39. Sundaramoorthy, M., J. Terner, and T.L. Poulos, *Stereochemistry of the chloroperoxidase active site: crystallographic and molecular-modeling studies.* Chem. Biol., 1998. **5**: p. 461-473.

40. Poulos, T.J. and J. Kraut, *The stereochemistry of peroxidase catalyst.* J. Biol. Chem., 1980. **255**: p. 8199-8205.

41. Schlichting, I., et al., *The catalytic pathway of cytochrome p450cam at atomic resolution.* Science, 2000. **287**: p. 1615-1622.

42. Imai, M., et al., *Uncoupling of the cytochrome P-450cam monooxygenase by a single mutation, threonine-252 to alanine or valine: A possible role of the hydroxy amino acid in oxygen activation.* Proc. Natl. Acad. Sci., 1989. **86**: p. 7823-7827.

43. Gerber, N.C. and S.G. Sligar, *Catalytic mechanism of cytochrome P-450: Evidence for a distal charge relay.* J. Am. Chem. Soc., 1992. **114**: p. 8742-8743.

44. Raag, R., et al., *Crystal structure of the cytochrome P450cam active site mutant Thr252Ala.* Biochemistry, 1991. **30**: p. 11420-11429.

45. Poulos, T.J., *Cytochrome P450.* Curr. Opin. Struc. Biol., 1995. **5**: p. 767-774.

46. Raag, R. and T.J. Poulos, *X-ray crystallographic structural studies on cytochrome P450cam: factors controlling substrate metabolism.* Front Biotransfrom, 1992. **7**: p. 1-43.

47. Poulos, T.J., B.C. Finzel, and A.J. Howard, *Crystal structure of substrate-free P. putida cytochrome P450.* Biochemistry, 1986. **32**: p. 9798-9806.

48. Raag, R., et al., *Inhibitor-induced conformational change in cytochrome P450$_{cam}$.* Biochemistry, 1993. **32**: p. 4571-4578.

49. Ravichandran, K.G., et al., *Crystal structure of hemoprotein domain of P450$_{BM-3}$, a prototype for microsomal P450s.* Science, 1993. **261**: p. 731-736.

50. Picot, D., P.J. Loll, and M. Garavito, *The X-ray crystal structure of the membrane protein prostaglandin H2 synthase-1.* Nature, 1994. **367**: p. 243-249.

51. Ortiz de Montellano, P.R. and M.A. Correia, *Inhibition of Cytochrome P450 Enzymes*, in *Cytochrome P450: Structure, Mechanism, and Biochemistry*, P.R. Ortiz de Montellano, Editor. 1995, Plenum Press: New York. p. 305-366.

52. Ortiz de Montellano, P.R., *Catalytic sites of hemoprotein peroxidases.* Annu. Rev. Pharmacol. Toxicol., 1992. **32**: p. 89-107.

53. Raag, R., et al., *Formation, crystal structure, and rearrangement of a cytochrome P-450cam iron-phenyl complex.* Biochemistry, 1990. **29**: p. 8119-8126.

54. Harris, D.L., S.L. Newmyer, and P.R. Ortiz de Montellano, *Horseradish peroxidase-catalyzed two-electron oxidations. Oxidation of iodide, thioanisoles, and phenols at distinct sites.* J. Biol. Chem., 1993. **268**: p. 1637-1645.

55. Miller, V.P., et al., *Monooxygenase activity of cytochrome c peroxidase.* J. Biol. Chem., 1992. **267**: p. 8936-8942.

56. Ozaki, S. and P.R. Ortiz de Montellano, *Molecular Engineering of Horseradish Peroxidase: Thioether Sulfoxidation and Styrene Epoxidation by Phe-41 Leucine and Threonine Mutants.* J. Am. Chem. Soc., 1995. **117**: p. 7056-7064.

57. Shokat, K.M. and P.G. Schultz, *Catalytic Antibodies.* Annu. Rev. Immunol., 1990. **8**: p. 335-363.

58. Cochran, A.G. and P.G. Schultz, *Antibody-Catalyzed Porphyrin Metallation.* Science, 1990. **249**: p. 781-783.

59. Cochran, A.G. and P.G. Schultz, *Peroxidase Activity of an Antibody-Heme Complex.* J. Am. Chem. Soc., 1990. **112**: p. 9414-9415.

60. Gilbert, W., *The RNA world.* Nature, 1986. **319**: p. 618.

61. Eddy, S.R., *Non-coding RNA genes and the modern RNA world.* Nat. Rev. Genet., 2001. **2**: p. 919-929.

62. Travascio, P., Y. Li, and D. Sen, *DNA-enhanced peroxidase activity of a DNA aptamer-hemin complex.* Chem. Biol., 1998. **5**: p. 505-517.

63. Li, Y., C.R. Geyer, and D. Sen, *Recognition of Anionic Porphyrins by DNA Aptamers.* Biochemistry, 1996. **35**: p. 6911-6922.

64. Li, Y. and D. Sen, *A catalytic DNA for porphyrin metallation.* Nat. Struct. Biol., 1996. **3**: p. 743-747.

65. Li, Y. and D. Sen, *Toward an Efficient DNAzyme.* Biochemistry, 1997. **36**: p. 5589-5599.

66. Travascio, P., et al., *A ribozyme and a catalytic DNA with peroxidase activity: active sites versus cofactor-binding sites.* Chem. Biol., 1999. **6**(11): p. 779-787.

67. Travascio, P., D. Sen, and A.J. Bennet, *DNA and RNA enzymes with peroxidase activity - An investigation into the mechanism of action.* Can. J. Chem., 2006. **84**: p. 613-619.

68. Travascio, P., et al., *The Peroxidase Activity of a Hemin-DNA Oligonucleotide Complex: Free Radical Damage to Specific Guanine Bases of the DNA.* J. Am. Chem. Soc., 2001. **123**: p. 1337-1348.

69. Rojas, A.M., et al., *Specificity of DNA-based (DNAzyme) peroxidative biocatalyst.* Biotechnol. Lett., 2007. **29**(2): p. 227-232.

70. Lee, H.W., D.J.F. Chinnapen, and D. Sen, *Structure-function investigation of a deoxyribozyme with dual chelatase and peroxidase activities.* Pure Appl. Chem., 2004. **76**: p. 1537-1545.

71. Elbaz, J., B. Shlyahovsky, and I. Willner, *A DNAzyme cascade for the amplified detection of Pb(2+) ions or L-histidine.* Chem. Commun., 2008. **7**(13): p. 1569-1571.

72. Pavlov, V., et al., *Amplified Chemiluminescence Surface Detection of DNA and Telomerase Acitivty Using Catalytic Nucleic Acid Labels.* Anal. Chem., 2004. **76**: p. 2152-2156.

73. Xiao, Y., et al., J. Am. Chem. Soc., 2004. **126**: p. 7430-7431.

74. Niazov, T., et al., *DNAzyme-Functionalized Au Nanoparticles for the Amplified Detection of DNA or Telomerase Activity.* Nano Lett., 2004. **4**(9): p. 1683-1687.

75. Xiao, Y., et al., *Lighting Up Biochemiluminescence by the Surface Self-Assembly of DNA-Hemin Complexes.* ChemBioChem, 2004. **5**: p. 374-379.

76. Thirstrup, D. and G.S. Baird, *Histochemical Application Of A Peroxidase DNAzyme with a Covalently Attached Hemin Cofactor.* Anal. Chem., 2010. **82**(6): p. 2498-2504.

77. He, Y., Y. Tian, and C. Mao, *Human telomeric DNA sequences have a peroxidase apoenzyme activity.* Mol. Biosyst., 2009. **5**: p. 238-240.

78. Kong, D.-M., et al., *Structure-function study of peroxidase-like G-quadruplex-hemin complexes.* Analyst, 2010. **135**: p. 321-326.

79. Cheng, X., et al., *General Peroxidase Activity of G-Quadruplex-Hemin Complexes and Its Application in Ligand Screening.* Biochemistry, 2009. **48**: p. 7817-7823.

80. Li, T., S. Dong, and E. Wang, *G-quadruplex aptamers with Peroxidase-Like DNAzyme Functions: Which Is the Best and How Does it Work?* Chem. Asian J., 2009. **4**(6): p. 918-922.

81. Majhi, P.R. and R.H. Shafer, *Characterization of an Unusual Folding Pattern in a Catalytically Active Guanine Quadruplex Structure.* Biopolymers, 2006. **82**: p. 558-569.

82. Kong, D.-M., et al., *Peroxidase activity-structure relationship of the intermolecular four-stranded G-quadruplex-hemin complexes and their application in Hg^{2+} ion detection.* Talanta, 2009. **80**: p. 459-465.

83. Bloomfield, V.A., D.M. Crothers, and I. Tinoco, Jr., *Nucleic Acids: Structures, Properties, Functions*. 2000, Sausalito, CA: University Science Books.

84. Wang, Y., K. Hamasaki, and R.R. Rando, *Specificity of Aminoglycoside Binding to RNA Constructs Derived from the 16S rRNA Decoding Region and the HIV-RRE Activator Region.* Biochemistry, 1997. **36**(4): p. 768-779.

85. Kaushik, M., et al., *Possibility of an Antiparallel (Tetramer) Quadruplex Exhibited by the Double Repeat of the Human Telomere* Biochemistry, 2007. **46**: p. 7119-7131.

86. Prislan, I., et al., *Kinetically governed polymorphism of $d(G_4T_4G_3)$ quadruplexes in K^+ solutions.* Nucleic Acids Res., 2011. **39**(5): p. 1933-1942.

87. Gray, D.M., et al., *Measured and Calculated CD Spectra of G-Quartets Stacked with the Same or Opposite Polarities.* Chirality, 2008. **20**: p. 431-440.

88. Luu, K.N., et al., *Structure of the human telomere in K+ solution: An intramolecular (3+1) G-quadruplex scaffold.* J. Am. Chem. Soc., 2006. **128**: p. 9963– 9970.

89. Lin, C.-T., et al., *Structural Conversion of Intramolecular and Intermolecular G-Quadruplexes of bcl2mid: The Effect of Potassium Concentration and Ion Exchange.* J.Phys. Chem. B, 2011. **115**(10): p. 2360-2370.

90. Vorlickova, M., et al., *Guanine tetraplex topology of human telomere DNA is governed by the number o(TTAGGG) repeats.* Nucleic Acids Res., 2005. **33**: p. 5851–5860.

91. Viglasky, V., L. Bauer, and K. Tluckova, *Structural Features of Intra- and Intermolecular G-Quadruplexes Derived from Telomeric Repeats.* Biochemistry, 2010. **49**: p. 2110-2120.

92. Wang, Y. and D.J. Patel, *Solution structure of the human telomeric repeat d[AG3(T2AG3)3] G-tetraplex.* Structure, 1993. **1**(4): p. 263-282.

93. Parkinson, G.N., M.P. Lee, and S. Neidle, *Crystal structure of parallel quadruplexes from human telomeric DNA.* Nature, 2002. **417**: p. 876-880.

94. Hazel, P., et al., *Loop-length-dependent folding of G-quadruplexes.* J. Am. Chem. Soc., 2004. **126**: p. 16405-16415.

95. Balagurumoorthy, P., et al., *Hairpin and parallel quartet structures for telomeric sequences.* Nucleic Acids Res., 1992. **20**(15): p. 4061-4067.

96. Cao, W., et al., *Water Penetration and Binding to Ferric Myoglobin.* Biochemistry, 2001. **40**: p. 5728-5737.

97. Goldbeck, R.A., et al., *Water and ligand entry in myoglobin: Assessing the speed and extent of heme hydration after CO photodissociation.* Proc. Natl. Acad. Sci., 2006. **103**(5): p. 1254-1259.

98. Job, D. and H.B. Dunford, *Horseradish peroxidase. XXVIII. Formation and reactivity of the alkaline form. Evidence for an enzyme-substrate complex in Compound I formation.* Can. J. Chem., 1978. **56**: p. 1327-1334.

99. Marnett, L.J. and T.A. Kennedy, *Comparison of the Peroxidase Activity of Hemoproteins and Cytochrome P450,* in *Cytochrome P450: Structure, Mechanism, and Biochemistry* P.R. Ortiz de Montellano, Editor. 1995, Plenum Press: New York. p. 49-80.

100. Bröring, M., *Organic Reactions Catalyzed by Heme Proteins*, in *Iron Catalysis in Organic Chemistry*, B. Plietker, Editor. 2008, WILEY-VCH Verlag GmbH & Co. KGaA: Weinheim. p. 48-72.

101. Poon, L.C.-H., et al., *Guanine-Rich RNAs and DNAs That Bind Heme Robustly Catalyze Oxygen Transfer Reactions.* J. Am. Chem. Soc., 2011. **133**: p. 1877-1884.

102. Fruetel, J., et al., *Thioanisole Sulfoxidation by Cytochrome P450cam (CYP101): Experimental and Calculated Absolute Stereochemistries.* J. Am. Chem. Soc., 1994. **116**: p. 11643-11648.

103. Isaacs, N., *Physical Organic Chemistry*. 1996, New Jersey: Prentice Hall.

104. Deorge, D.R., *Oxygenation of organosulfur compounds by peroxidases: evidence of an electron transfer mechanism for lactoperoxidase.* Arch. Biochem. Biophys., 1986. **244**(2): p. 678-685.

105. Savenkova, M.I., S.L. Newmyer, and P.R. Ortiz de Montellano, *Rescue of His-42 --> Ala horseradish peroxidase by a Phe-41 --> His mutation. Engineering of a surrogate catalytic histidine.* J. Biol. Chem., 1996. **271**(40): p. 24598-24603.

106. Kobayashi, S., et al., *On the Mechanism of the Peroxidase-Catalyzed Oxygen-Transfer Reaction.* Biochemistry, 1987. **26**: p. 5019-5022.

107. Capeillère-Blandin, C., et al., *Sulphoxidation reaction catalysed by myeloperoxidase from human leucocytes.* Biochem. J., 1998. **335**: p. 27-33.

108. Blée, E. and F. Schuber, *Mechanism of S-Oxidation Reactions Catalyzed by a Soybean Hydroperoxide-Dependent Oxygenase.* Biochemistry, 1989. **28**: p. 4962-4967.

109. Tuynman, A., et al., *The sulphoxidation of thioanisole catalysed by lactoperoxidase and Coprinus cinereus peroxidase: Evidence for an oxygen-rebound mechanism.* Eur. J. Biochem., 1998. **258**: p. 906-913.

110. Tuynman, A., H.E. Schoemaker, and R. Wever, *Enantioselective sulfoxidations catalyzed by horseradish peroxidase, manganese peroxidase, and myeloperoxidase.* Monatsh. Chem., 2000. **131**(6): p. 687-695.

111. Ricoux, R., et al., *New activities of a catalytic antibody with a peroxidase activity: formation of Fe(II)-RNO complexes and stereoselective oxidation of sulfides.* Eur. J. Biochem., 271, 1277-1283., 2004. **271**: p. 1277-1283.

112. Lipps, H.J. and D. Rhodes, *G-quadruplex structures: in vivo evidence and function.* Trends Cell Biol., 2009. **19**(8): p. 414-422.

113. Gillam, E.M.J., et al., *Oxidation of Indole by Cytochrome P450 Enzymes.* Biochemistry, 2000. **39**: p. 13817-13824.

114. Corbett, M.D. and B.R. Chipko, *Peroxide Oxidation of Indole to Oxindole by Chloroperoxidase Catalysis.* Biochem. J., 1979. **183**: p. 269-276.

115. Tuynman, A., et al., *Enantioselective epoxidation and carbon-carbon bond cleavage catalyzed by Coprinus cinereus peroxidase and myeloperoxidase.* J. Biol. Chem., 2000. **275**(5): p. 3025-3030.

116. Ortiz de Montellano, P.R., et al., *Structure-mechanism relationships in hemoproteins. Oxygenations catalyzed by chloroperoxidase and horseradish peroxidase.* J. Biol. Chem., 1987. **262**(24): p. 11641-11646.

117. Ortiz de Montellano, P.R. and L.A. Grab, *Cooxidation of styrene by horseradish peroxidase and phenols: a biochemical model for protein-mediated cooxidation.* Biochemistry, 1987. **26**(17): p. 5310-5314.